European Commission
Research Programme of the Research Fund for Coal and Steel

ANGELHY

Innovative solutions for design and strengthening of telecommunications and transmission lattice towers using large angles from high strength steel and hybrid techniques of angles with FRP strips

WORK PACKAGE 2 – DELIVERABLE 2.5

Report on full scale experimental tests for complete towers

Coordinator:

National Technical University of Athens - NTUA, Greece

Beneficiaries:

ArcelorMittal Belval & Differdange SA - AMBD, Luxembourg

Universite de Liege - ULG, Belgium

COSMOTE Kinites Tilepikoinonies AE - COSMOTE, Greece

Centre Technique Industriel de la Construction Metallique - CTICM, France

SIKA France SAS - SIKA, France

Grant Agreement Number: 753993

AUTHORS:

NATIONAL TECHNICAL UNIVERSITY OF ATHENS

Institute of Steel Structures

Iroon Polytechniou 9, 15780 Athens, Greece

Authors: Ioannis Vayas, Konstantinos Vlachakis, Georgios Palantzas, Xenophon Lignos

SIKA France SAS

84 rue Edouard Vaillant, 93350 Le Bourget, France

Authors: Yvon Giquel, Sébastien Reygner

TABLE OF CONTENTS

1 Introduction

Task 2.5 of work package WP2 of ANGELHY project includes six (6) experimental full-scale tests on cell network telecommunication lattice towers. The towers will be subjected to pushover loading, i.e. to horizontal forces at their tops that will increase gradually until failure. In fact, loading is displacement controlled in order to study the structural response up to and beyond failure. The purpose of the tests is to give an insight to failure mechanisms, buckling lengths for legs and braces as a function of the bracing configuration and the connection conditions, the relevant buckling axes for legs and braces, the slope of the unloading branch and other important design data under realistic conditions. The selection procedure of the specimens, the details about the experimental campaign such as measurements before and during the tests, as well as the test results, are presented in the current report. The test campaign was realized at the Laboratory of the Institute of Steel Structures NTUA.

2 Description of test specimens

The dimensions of the test specimens were specified taking into account the lay-out of the reaction frame and the dimensions of the strong floor of the Laboratory of Steel Structures, NTUA, where the tests were performed. Accordingly, the overall dimensions of the towers were 1.440x1.440x6.822 m, Fig. 2.1. The first figures, 1.440 m, refer to the external dimensions in plan. The axial distance between centroids of the tower legs is 1.40 m. The tower is subdivided in 4 levels, each with height of 1.70 m. The legs, beams and bracing members of the towers were composed of single angle members, as well as the horizontal members used for triangulation of the platforms at all levels.

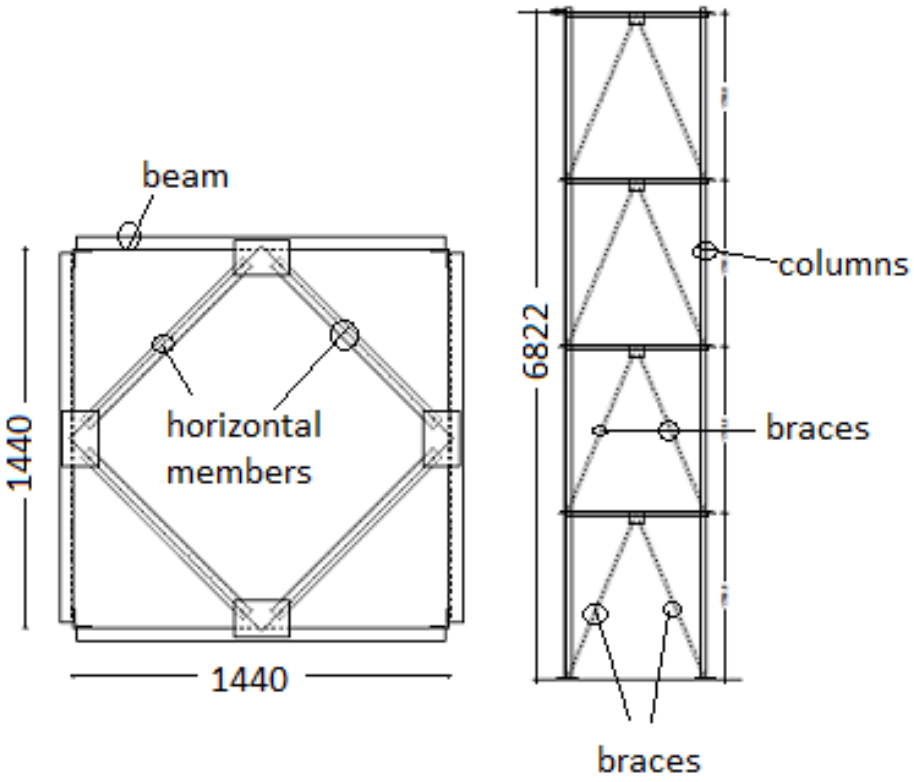

Figure 2.1: Tower dimensions in plan and side view (in different scales)

In total six tests were performed out of which three (3) were subjected to orthogonal loading and three (3) to diagonal loading as shown in Fig. 2.2 and Table 2.1. Out of the three specimens for each loading configurations, two had all steel cross sections and served as reference tests. In the third test the members which were expected to fail in the reference tests were strengthened by FRP strips, applied externally to the angle legs.

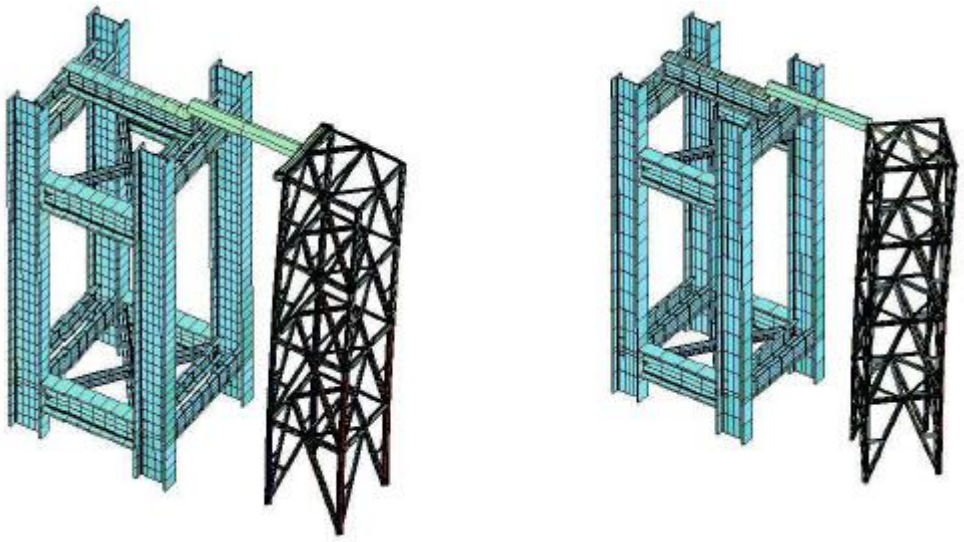

Figure 2.2: Reaction frame and towers of type O, orthogonal loading, and type D, diagonal loading

Table 2.1: Properties of test specimens

No of tower	Designation	Profiles for legs	Profiles for braces	Anticipated failure according to project proposal	Actual failure
1	O-1	L70.70.7	L45.45.5	Braces	Braces
2	O-2	L70.70.7	L65.65.7	Legs	Legs
3	O-1S	L70.70.7	L45.45.5 Strengthened compression braces in all floors	To be investigated	Braces
4	D-1	L70.70.7	L40.40.4	Braces	Braces
5	D-2	L70.70.7	L60.60.6	Legs	Leg
6	D-2S	L70.70.7 strengthened compression leg at two lower floors	L60.60.6 strengthened compression braces at top floor	To be investigated	Leg
Profiles for beams and horizontal members L50.50.5 Strengthening by external FRP strips 50x1.2 mm Bolts M10 to M16 8.8					

The columns run continuously over the height of the towers. The beams, braces and horizontal members were bolted at their ends with one bolt. The beams were bolted directly to the column legs, the braces also directly to the columns at the lower end and to gusset plates 5 mm thick, while the horizontal members to gusset plates 5 mm thick at both ends. All connections were made by 8.8 bolts of different sizes ranging from M10 to M16 according to the recommended size for each profile. The bolt clearance was 1 mm for all bolt sizes. The position of the holes in the legs was as recommended

for angles. Accordingly, the distance of the hole from the heel was 22 mm for L40, 30 mm for L50, 35 mm for L60 and 40 mm for L70. The columns rested on 20 mm thick baseplates that were bolted to the beams of the base structure with 4 bolts, Fig. 2.3.

The steel profiles were delivered by ArcelorMittal, the FRP strips by SIKA France, both partners of ANGELHY. The construction drawings were prepared by NTUA, excerpts are given in Annex A. Fabrication of the tower specimens was done by I. LIAPIS & SONS G.P., Metal constructions, Athens and delivered to the Laboratory at NTUA.

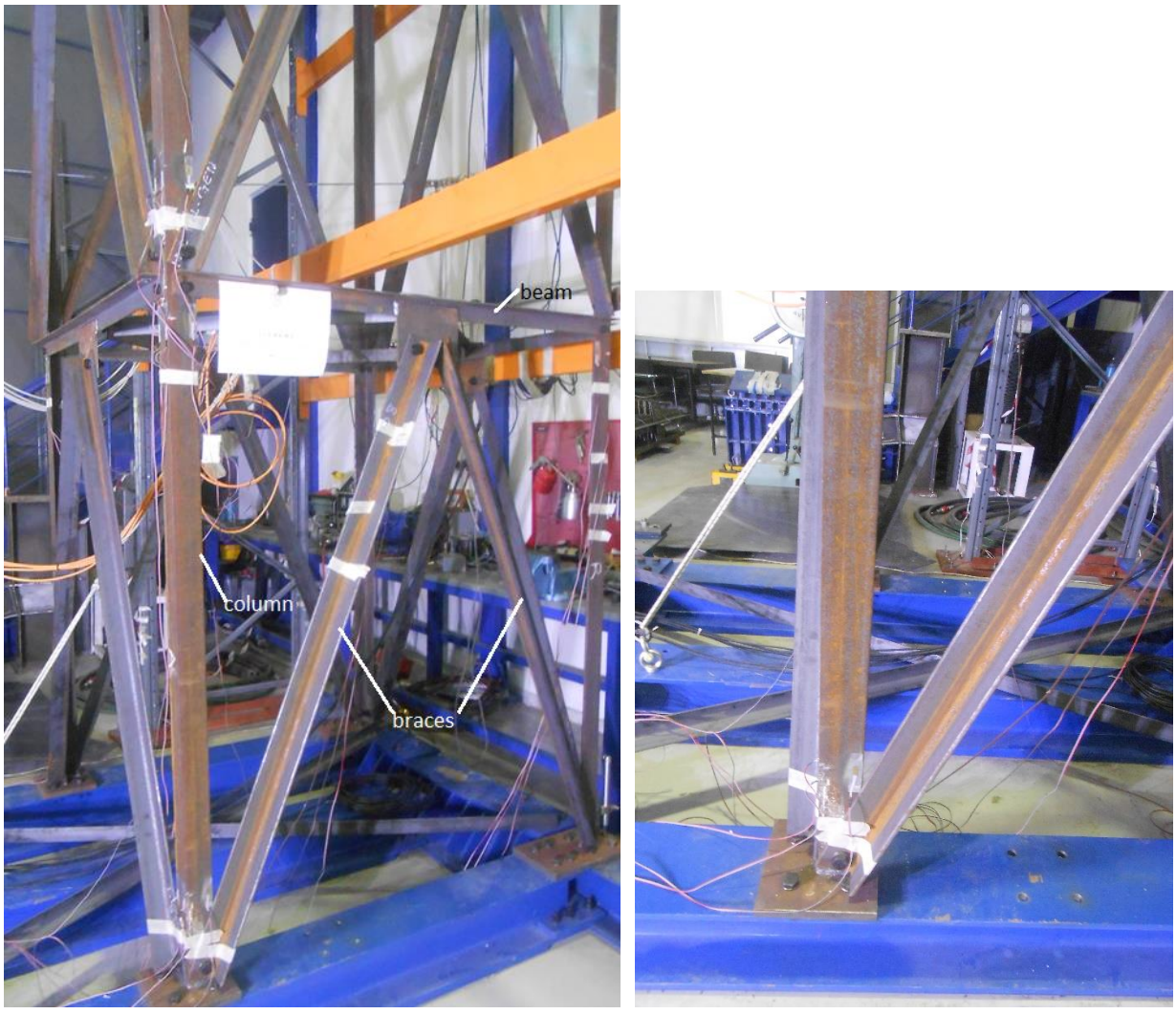

a) **b)**

Figure 2.3: Connections between structural elements, a), and detail of the column base, b)

Strengthening of steel members by FRPs was performed at the Laboratory in NTUA. The steel profiles were sandblasted first. Subsequently FRPS strips were applied using exactly the same procedures as described in Deliverable 2.3. Members were strengthened over the full clear length between bolts. Fig. 2.4 shows pictures of strengthened members. For the strengthened angle sections

L45.45.5 in tower O1-S, the FRP strips were 5 mm wider than the angle leg and accordingly protruded over the angle tips, Fig. 2.5.

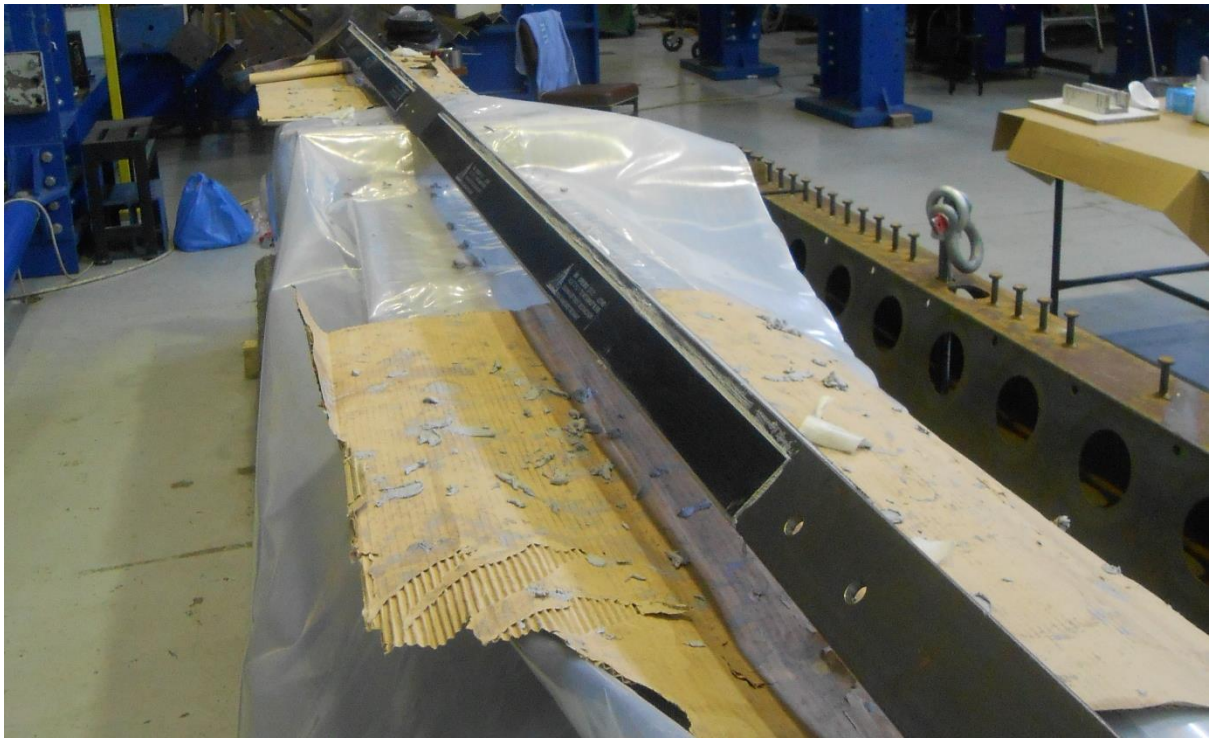

Figure 2.4: Tower braces and legs strengthened by FRPs

Figure 2.5: Outstand for wider FRP than angle leg L45.45.5

3 Material properties

3.1 Steel of angle sections

Coupon tests were performed in order to determine the actual material properties of the structural elements. Coupons were prepared according to the relevant specification, EN ISO 6892-1. The tensile tests were performed in the universal testing machine type INSTRON 300LX. The strain measurements were performed by an extensometer type Instron 2630-113 with a gauge length +50/-5 mm. The test set-up is shown in Figure 3.1. The tests were carried out in accordance with ISO 6892. The resulting stress-strain curves were automatically displayed in the computer and were based on the nominal cross section of the specimen. The resulting stress-strain curves are presented Annex C. Table 3.1 gives the values of the yield and ultimate stress. For the yield stress, the 0,2% conventional yield stress was adopted.

Figure 3.1: Test set-up of the coupon tests

Table 3.1: Measured material properties of the test angle profiles

No	Profile	Yield strength f_y	Tensile strength f_u
1	L70.70.7	308,3 MPa	435,7 MPa
2	L45.45.5	286,7 MPa	416,67 MPa
3	L40.40.4	325,7 MPa	435,37 MPa
4	L60.60.6	280 MPa	403,85 MPa

3.2 FRP plates

The CFRP plates were of type SIKA CARBODUR. The producer provided a certificate of the batch number of the delivered product used in the tests that contained the actual properties of the test material. Table 3.2 gives the values of the nominal and actual material properties. Annex C shows the certificate.

Table 3.2: Nominal and actual material properties of the CFRP plates, SIKA CARBODUR

	Dimensions	Tensile strength	Tensile Strain	Tensile modulus
Nominal	50x1,2	>2800 MPa	>1,7 %	>160 MPa
Actual	50,33x1,2	3187 MPa	1,84 %	174 MPa

4 Test set-up and tower erection

The tests were performed on the strong floor area of the Laboratory. The towers were connected to a base structure which was anchored to the strong floor and were pulled at the top level by an actuator type MALVASIA with a capacity of 600 kN that rested on the top of a rigid reaction frame, Fig. 4.1.

Figure 4.1: Reaction frame (left) and tower specimen (right)

The base structure was designed by NTUA to accommodate both test set-ups with orthogonal and diagonal loading, Fig. 4.2. Since the base structure and the rigid reaction frame were fixed to the strong floor, the tower specimens were turned by 45^0 in order to load them in one direction or the other.

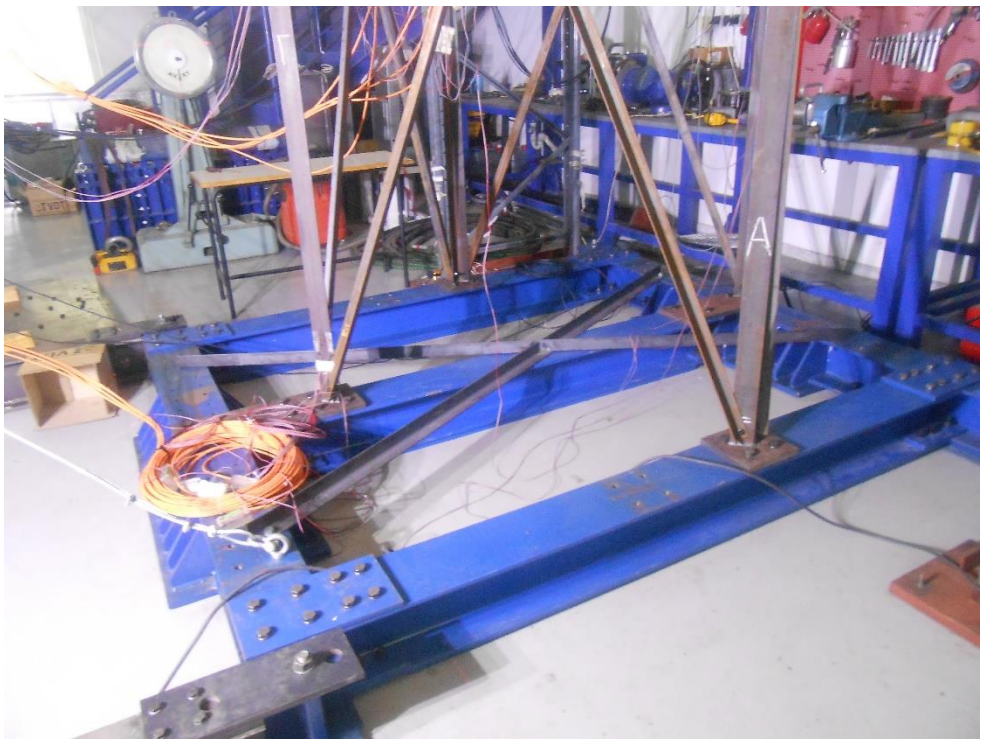

Figure 4.2: Base structure. In the picture tower position for diagonal loading

In order to transfer the horizontal force evenly to the top level, a 6 mm thick steel plate of 100 kg weight acting as diaphragm, was placed on the top level and bolted to all beams of that level. The horizontal force was transferred through a cable that was fastened on one side to the actuator and on the other side to the diaphragm through a pin placed in an eye-bar provided at the diaphragm's protrusion, Fig. 4.3. Construction details of several parts of the test set-up are provided in Annex B.

Figure 4.3: Transfer of the horizontal force for orthogonal and diagonal loading

The erection was carried out by the personnel of the Laboratory from the bottom to the top. It started with the position of the four legs on the base structure. Then the horizontal bars of the first level were bolted to the legs in order to ensure stability. Subsequently two braces were bolted to each beam and the three elements altogether were put in place and bolted to the structure, Fig. 4.4. After the erection was completed, the bolts were tightened by a torque wrench. Bolts between column baseplates and base structure were tightened to a torque resulting in the full preload force, while all other bolts to 50% of the full preload force.

Figure 4.4: Erection of the tower

5 Vibration measurements

5.1 Introduction

The natural frequencies of the towers were measured by a low-cost mpu6050 accelerometer. The accelerometer was placed at the top of each tower before and after the test, Fig. 5.1. Ambient vibrations were produced through application of an impact load, hitting the tower with a simple hammer. Subsequently data were collected for the timeline of the acceleration produced by the tower after each impact and a graph of Acceleration (g) - Time (sec) received. These data were processed using the Fast Fourier Transform (FFT) in order to produce graphs of Amplitude - frequency (Hz) and consequently to estimate the natural frequencies of the towers.

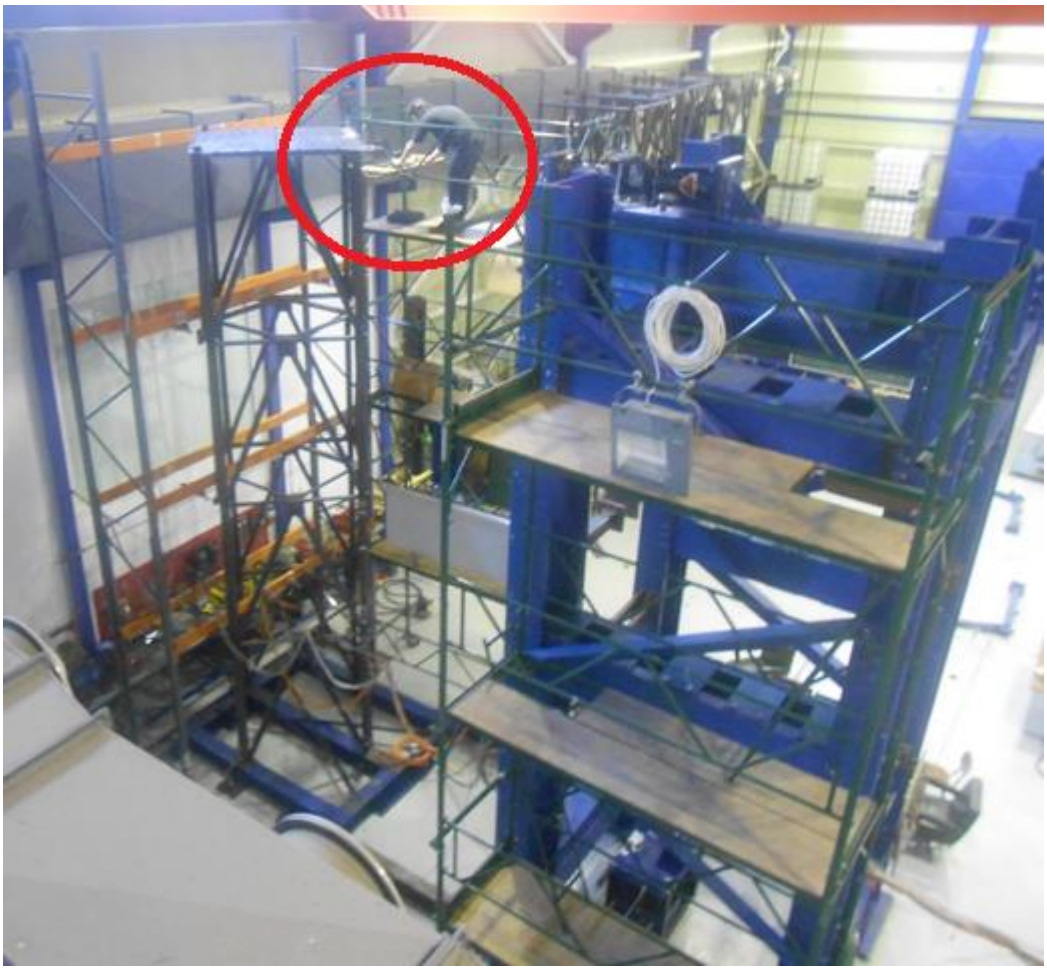

Figure 5.1: Vibration measurements

5.2 Processing Details

Because of the huge volume of the data collected during the tests, the most important frequency values identified in a frequency range of 0-25 Hz were displayed in a single diagram. This range was chosen as the most suitable because the predicted analytical values of eigenfrequencies were within that range, and also in order to have better supervision over the area of the graphs that is the most

important. In further detail the graphs are displaying values of a-f(Hz), where the value a does not refer to the amplitude but is calculated as follows:

$$a(\mathrm{f}) = \frac{\Sigma\left(\frac{A,i(f)}{Amax,i}\right)}{N} \qquad (5.1)$$

where:

A,i(f) is the amplitude depending on the frequency from the FFT performed on each of the acceleration data i

A_{max},i is the maximum amplitude value calculated for each data i and

N is the number of different data obtained from each measurement

This seemed to be the most effective way to combine the information of the data acquired that also gives the reader a complete overview of the data and the results for each tower.

To make things simpler the a-value indicates how often a frequency appeared as important in our data and how important it was. For example, if for a frequency a value a = 1 is calculated, this specific frequency appears as important in every FFT graph calculated for the data and has always the highest amplitude.

It should be also noted that because of the randomness of the implemented input loads (simple hammer strikes) this seemed to be the only effective way to compare the data results with each other.

5.3 Vibration test results

5.3.1 Results for Tower 1 (O-1)

In the following figures the graphs of a-f(Hz) and the frequencies that appeared as important in the data are displayed. Fig. 5.2 shows the results before and Fig. 5.3 before and after the experiment.

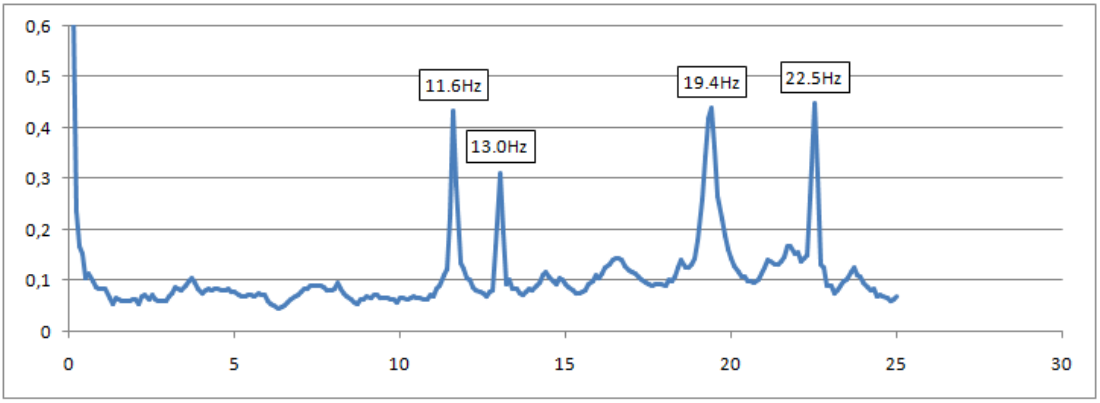

Figure 5.2: a-f(Hz) graph for tower 1 before the experiment

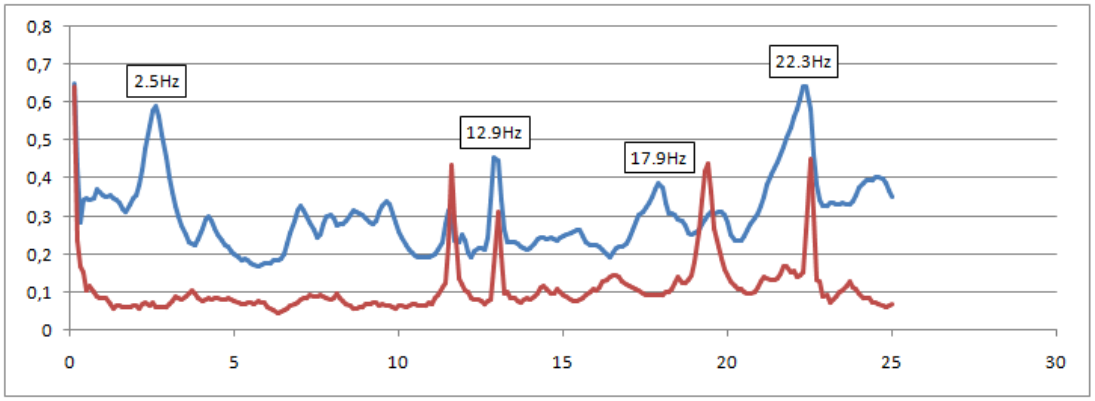

Figure 5.3: *a*-f(Hz) graph for tower 1 before (red) and after (blue) the experiment

It seems that we can't draw safe conclusions over which of these values refer to the translational natural frequency and which to a torsional, a higher mode or even a frequency referring to the vibration of a singular element, although some values consistently appeared in both graphs.

5.3.2 Results for Tower 2 (O-2)

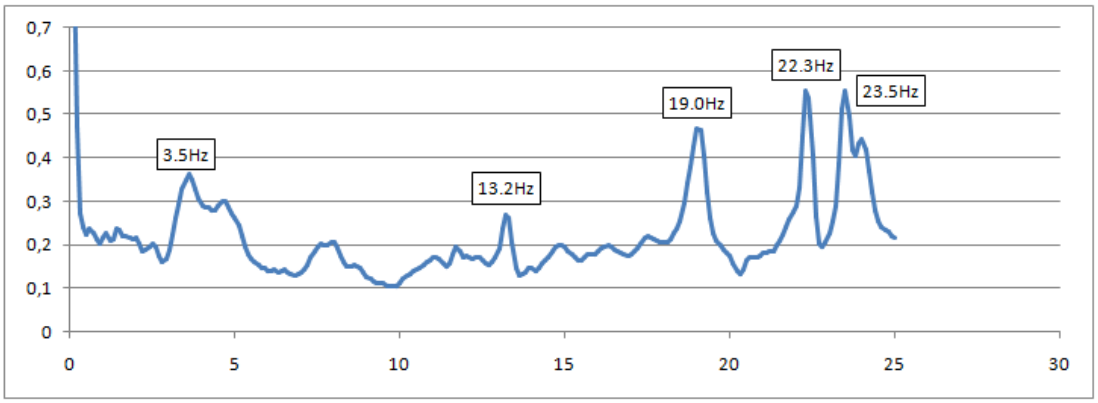

Figure 5.4: *a*-f(Hz) graph for tower 2 before the experiment

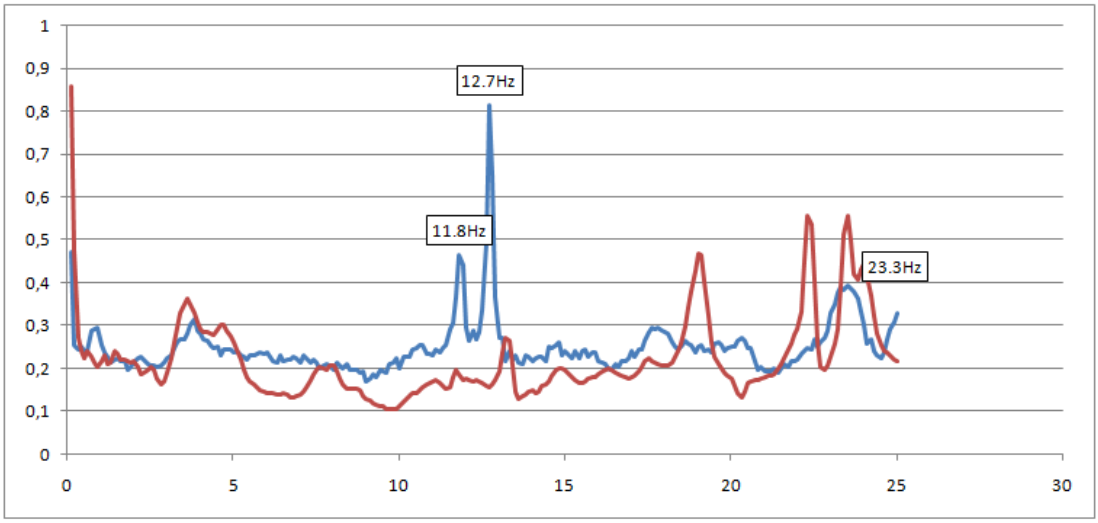

Figure 5.5: *a*-f(Hz) graph for tower 2 before (red) and after (blue) the experiment

It seems that especially before the experiment we had similar results with the first tower, but after the experiment we can identify a frequency of 12,7Hz with a value of 23,3Hz appearing too.

5.3.3 Results for Tower 3 (O-1S)

This is the first experiment where the CFRP reinforcement was implemented. Because of the schedule of this experiment, only data after the experiment were collected.

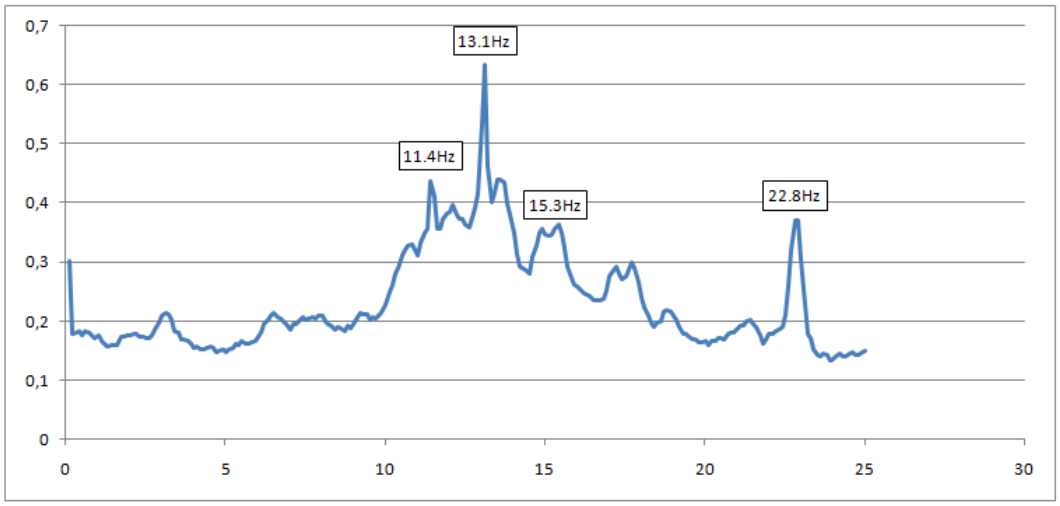

Figure 5.6: *a*-f(Hz) graph for tower 3 after the experiment

In that case a frequency of 13,1Hz seems το appear in most cases with a frequency of 22,8Hz also being a characteristic value appearing in the graph.

5.3.4 Results for Tower 4 (D-1)

The analytical model predicts a frequency value of 15,67Hz for the first mode (and a torsional mode of 22,28Hz).

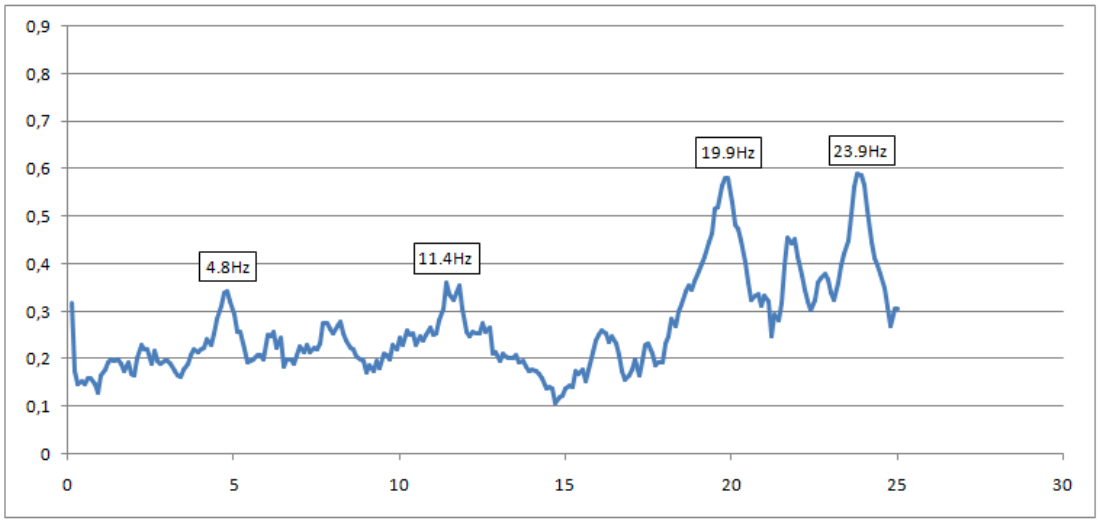

Figure 5.7: *a*-f(Hz) graph for tower 4 before the experiment

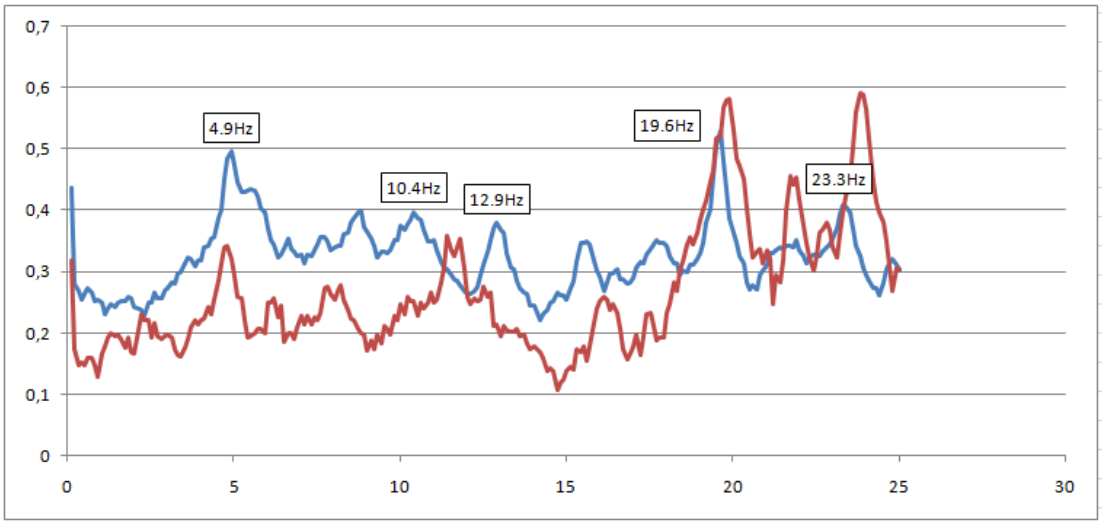

Figure 5.8: *a*-f(Hz) graph for tower 4 before (red) and after (blue) the experiment

In that case it seems that the most consistent value in that of 19,9Hz with a value of 19,6Hz appearing again in the data collected after the experiment.

5.3.5 Results for Tower 5 (D-2)

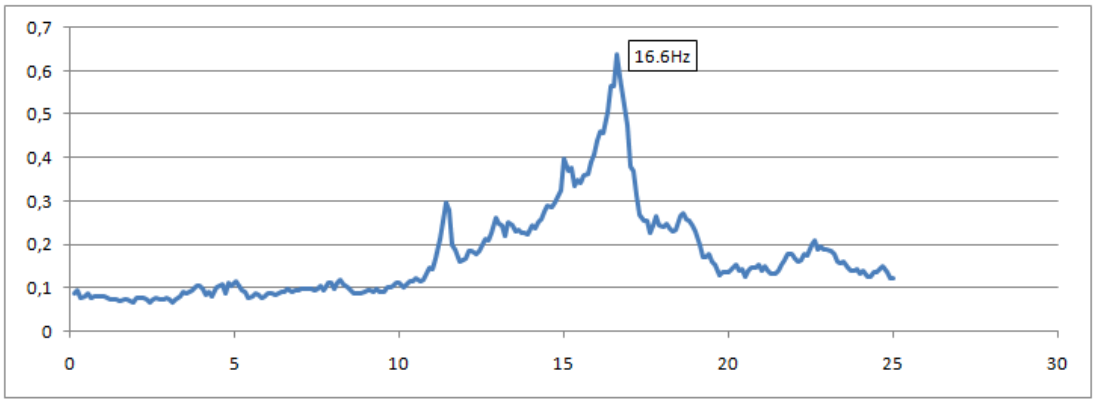

Figure 5.9: *a*-f(Hz) graph for tower 5 before the experiment

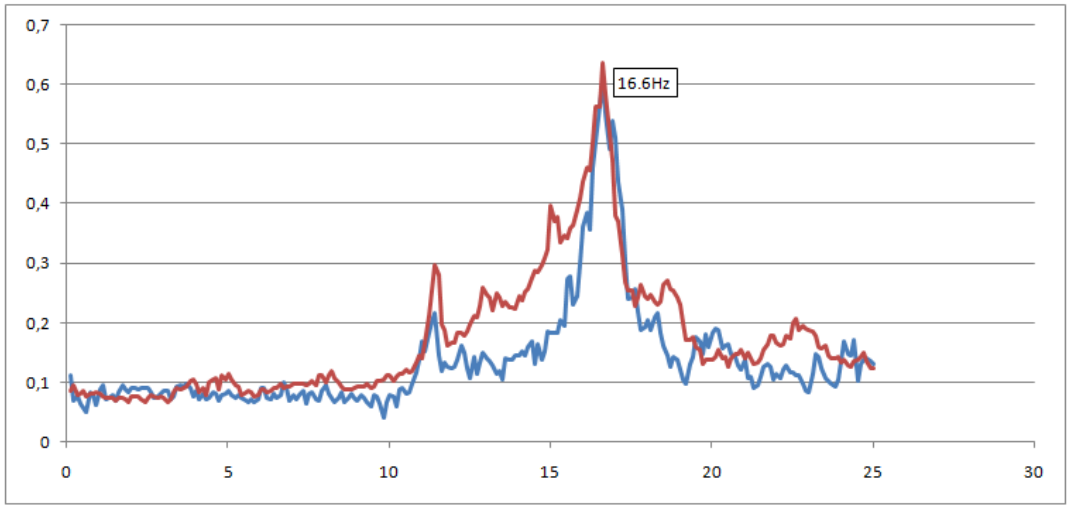

Figure 5.10: *a*-f(Hz) graph for tower 5 before (red) and after (blue) the experiment

In this case we were able to get the most consistent results with both the data before and after the experiment converging to the same value of 16,6Hz.

5.3.6 Results for Tower 6 (D-2S)

This is the second experiment with the CFRP reinforcements, this time data were collected both before and after the experiment.

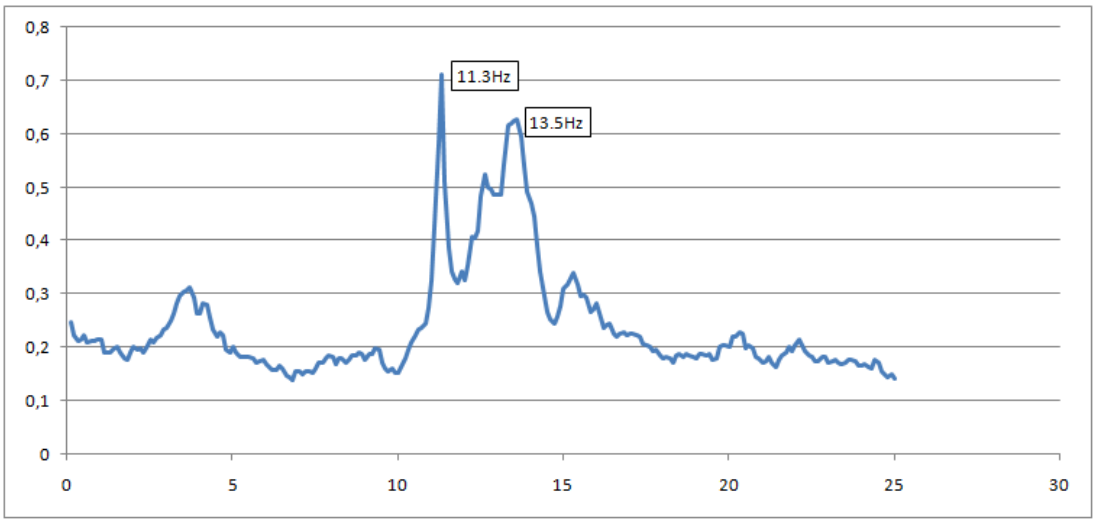

Figure 5.11: *a*-f(Hz) graph for tower 6 before the experiment

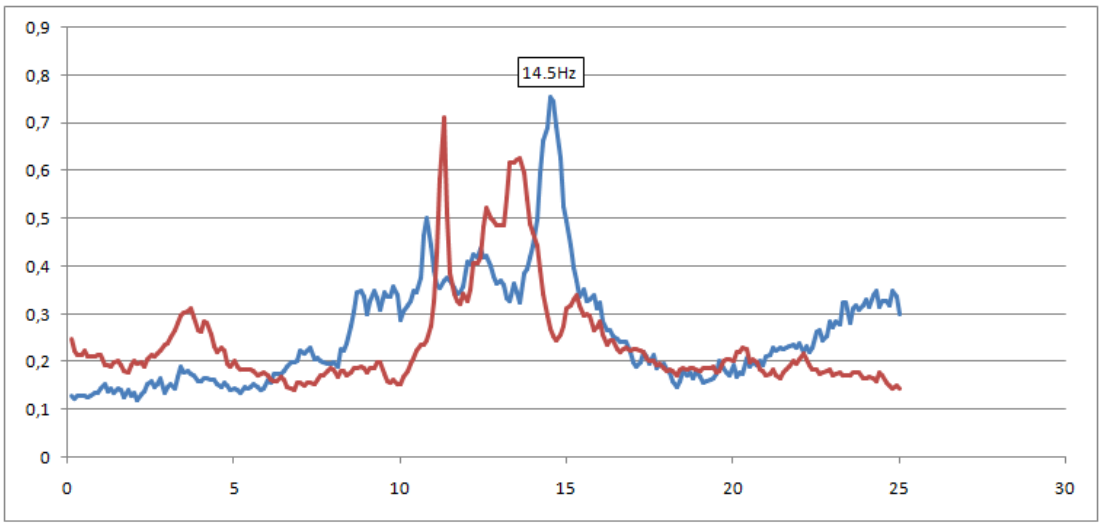

Figure 5.12: *a*-f(Hz) graph for tower 6 before (red) and after (blue) the experiment

For this experiment it seems that the most reliable value is the 14,5Hz even though it refers to the data collected after the experiment as those data were more consistent.

5.3.7 Vibration test results for individual elements

After the end of the experiments to the towers and because of the inconsistency of the results for them, it was decided to perform additional tests this time to individual braces picked at random from various towers to use as a reference to compare the accuracy of the method when used to single elements.

The process used was the same and the results are the following:

- **L40.40.4**, braces with theoretical frequency f=32,13Hz

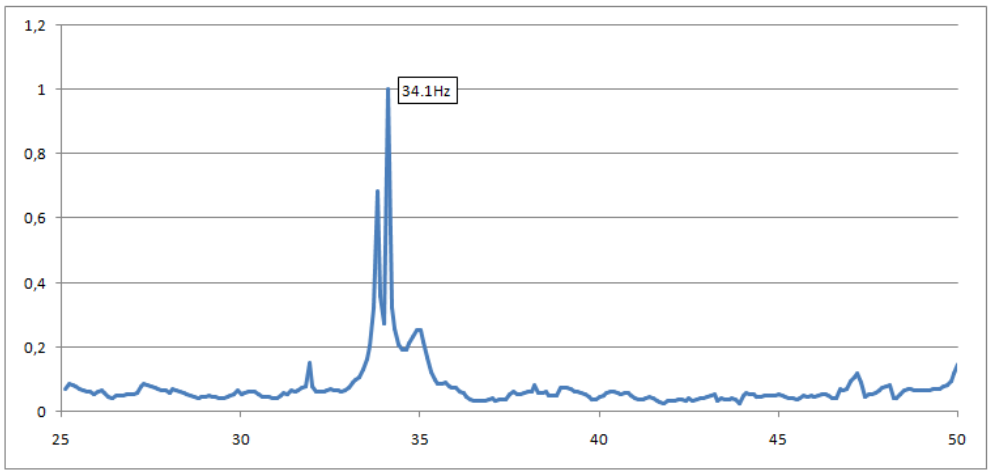

Figure 5.13: *a*-f(Hz) graph for L40.40.4 braces

- **L45.5**, braces with theoretical frequency f=36,00Hz

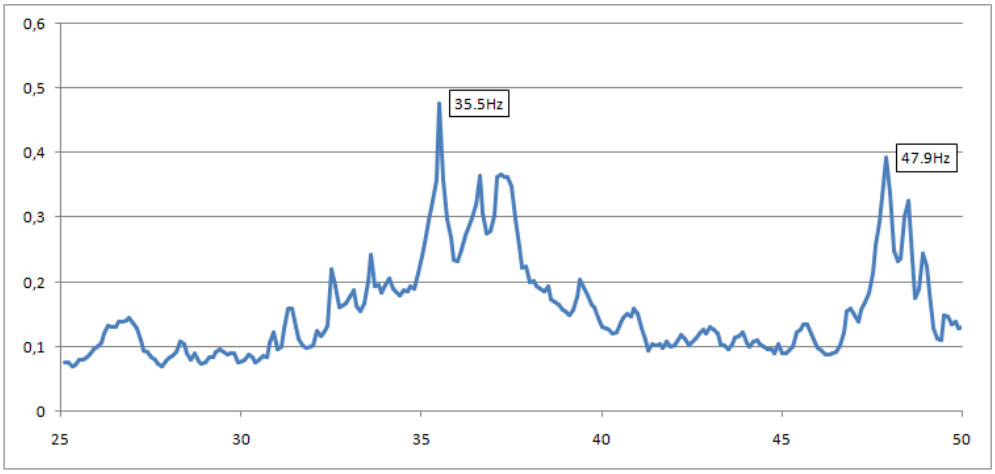

Figure 5.14: *a*-f(Hz) graph for L45.45.5 braces

- **L45.45.5+CFRP** braces with an expected frequency over f=36,00Hz

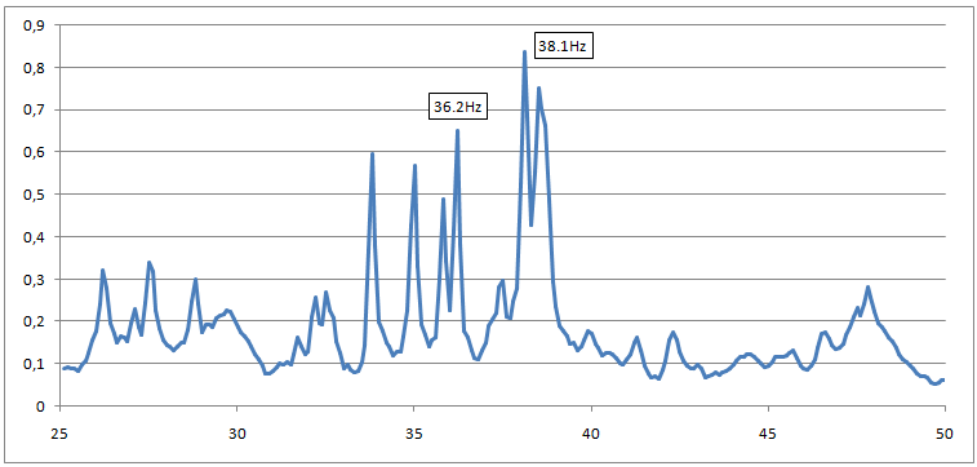

Figure 5.15: *a*-f(Hz) graph for L45.45.5+CFRP braces

- **L60.60.6-1**, braces with theoretical frequency f=48,42Hz

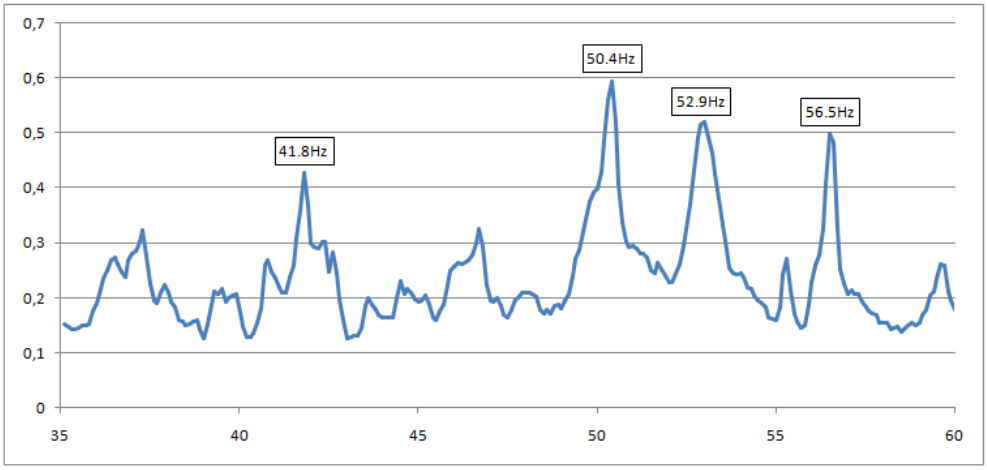

Figure 5.16: *a*-f(Hz) graph for L60.60.6-1 braces

- **L60.60.6-2** braces with theoretical frequency f=48,42Hz

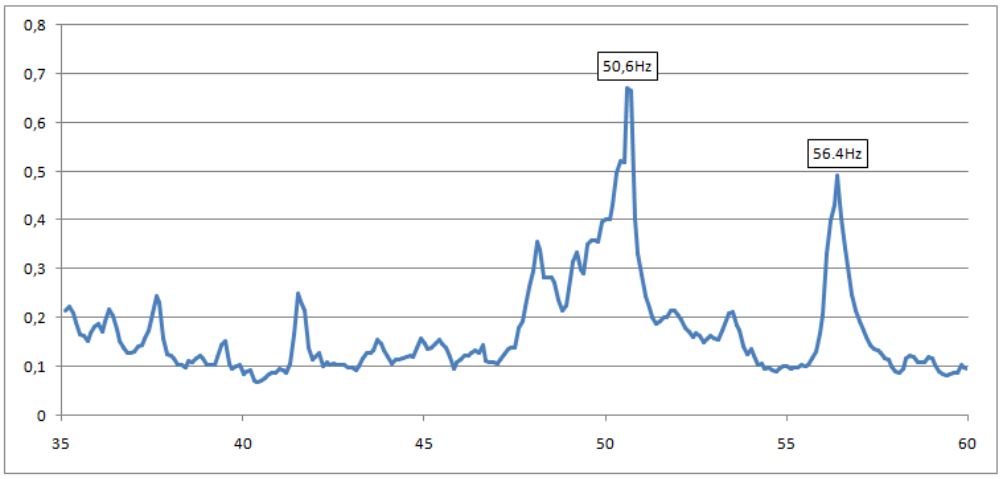

Figure 5.17: *a*-f(Hz) graph for L60.60.6-2 braces

5.4 Summary of results

Table 5.1 illustrates the measured fundamental frequencies for the towers and Table 5.2 for the individual members.

Table 5.1: Measured fundamental frequencies for the towers

Tower	O – 1	O – 2	O – 1S	D – 1	D – 2	D – 2S
Frequency Hz	19,4	19,0	22,8	19,9	16,6	14,5

Table 5.2: Measured fundamental frequencies for individual members

Brace	L40.40.4	L45.45.5	L45.45.5+FRP	L60.60.6-1	L60.60.6-2
Frequency Hz	34,1	35,5	38,1	50,4	50,6

6 Loading procedure and measurements

Loading was imposed in displacement control. The displacement was fed from the computer to the controller, which then displaced the hydraulic actuator to match the demand. The imposed displacement increased linearly with constant velocity illustrated in Table 6.1. As explained later, tower 2 was loaded first up to a load near the failure load, then unloaded and reloaded again up to failure. The loading speed of the initial and the final test was a little different as indicated in Table 6.1.

Table 6.1: Velocity of imposed displacements at tower top

Tower No	1	2		3	4	5	6
Specimen designation	O-1	O-2 Stage 1 loading	O-2 Stage 2 loading	O1-S	D-1	D-2	D-2S
Velocity mm/h	50	75	100	75	75	75	75

The data measured during the tests were the following:

- Displacement of the cylinder piston with an electronic displacement transducer.
- Hydraulic load applied by the cylinder, with the load cell at the end of the piston.
- Horizontal displacements of the towers at all floors. Displacements were measured in the three (3) lower levels with electronic displacement transducers (LVDTs) and at the top level with electronic wires, Fig. 6.1. Measurements were made at two legs. Their average results in the floor displacement resulted, while their difference the floor rotation. The measuring equipment was supported by the back beams of a rack structure that was placed in between the tower, Fig. 6.2, 6.3.
- Vertical displacements of the back-tower legs subjected to tension to record possible uplifting of the base.
- Strains of steel or FRP, for strengthened specimens, at selected cross sections of legs and braces in which failure was anticipated. For the steel towers strains were measured at 8 cross sections, with 3 measurements in each section, i.e. 24 strain gages in total. For the strengthened towers the total number of strain gages was also 24, but with more strain measurements in less cross sections. The position of strain gages in the cross section was at 10 mm from the edge, while the cross sections were at 70 mm distance from the theoretical nodes and 230 mm from the column base, Fig. 6.4.

The measurements for all towers are presented in Annex D.

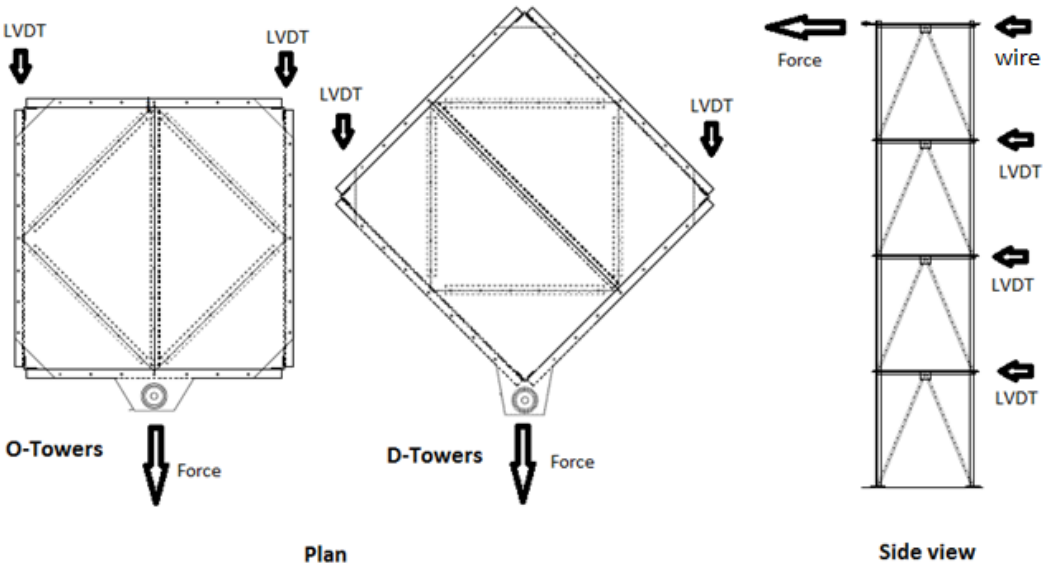

Figure 6.1: Position of LVDTs for horizontal displacements measurements

Figure 6.2: LVDTs measuring the horizontal displacements and supporting rack structure for orthogonal loading

Figure 6.3: LVDTs measuring the horizontal displacements and supporting rack structure for diagonal loading

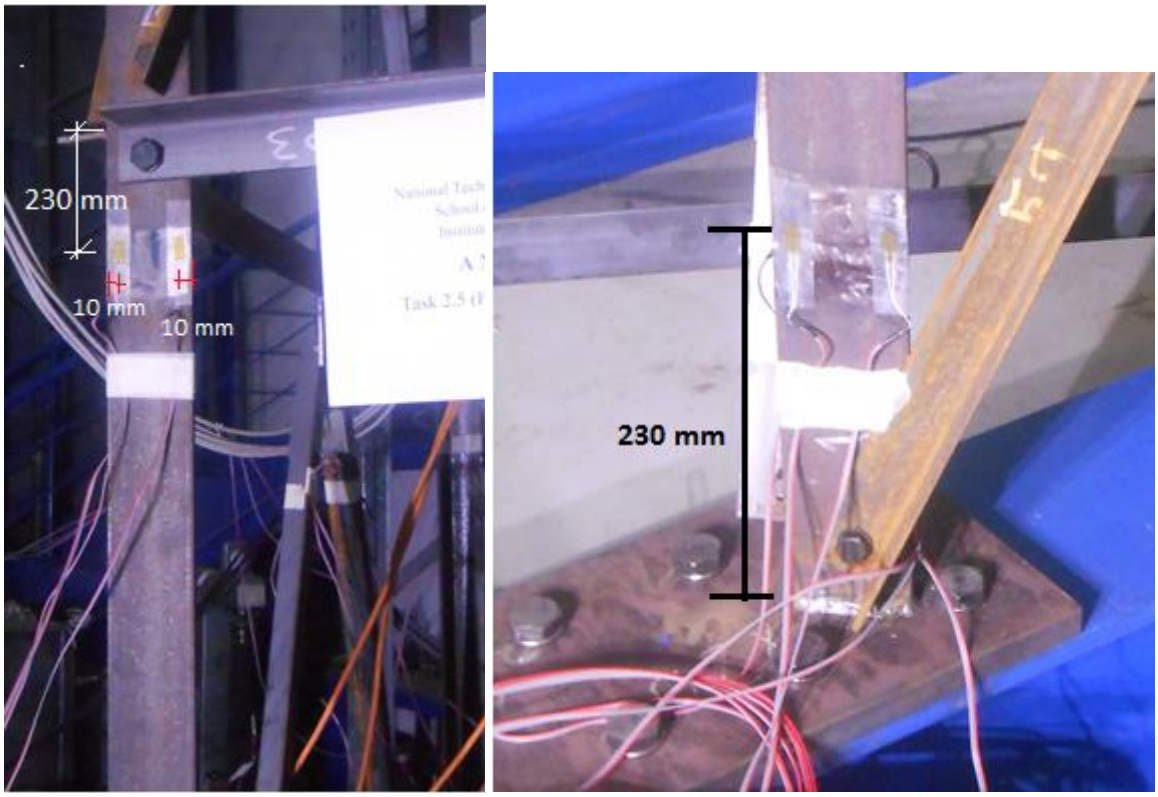

Figure 6.4: Position of strain gages at cross sections

7 Test results

7.1 Tower 1, type O-1

The tower was loaded progressively with a loading speed of 50 mm/h. At the initial stage no deformations were visible. After a load of 15 kN several bangs were heard that kept going until the load reached approximately 20 kN. Subsequently the specimen calmed down and loading increased sharply again. Shortly before the maximum load signs of buckling of the top compression brace at the 4th floor on the stiffer wall of the tower that displaced less than the opposite one was visible. As planned, global failure occurred due to weak axis flexural buckling of the compression braces, Fig. 7.1. The maximum load was reached when a second, 3rd floor diagonal at the same wall of the tower buckled, towards the heel in respect to the weak axis. Subsequently, the load dropped smoothly.

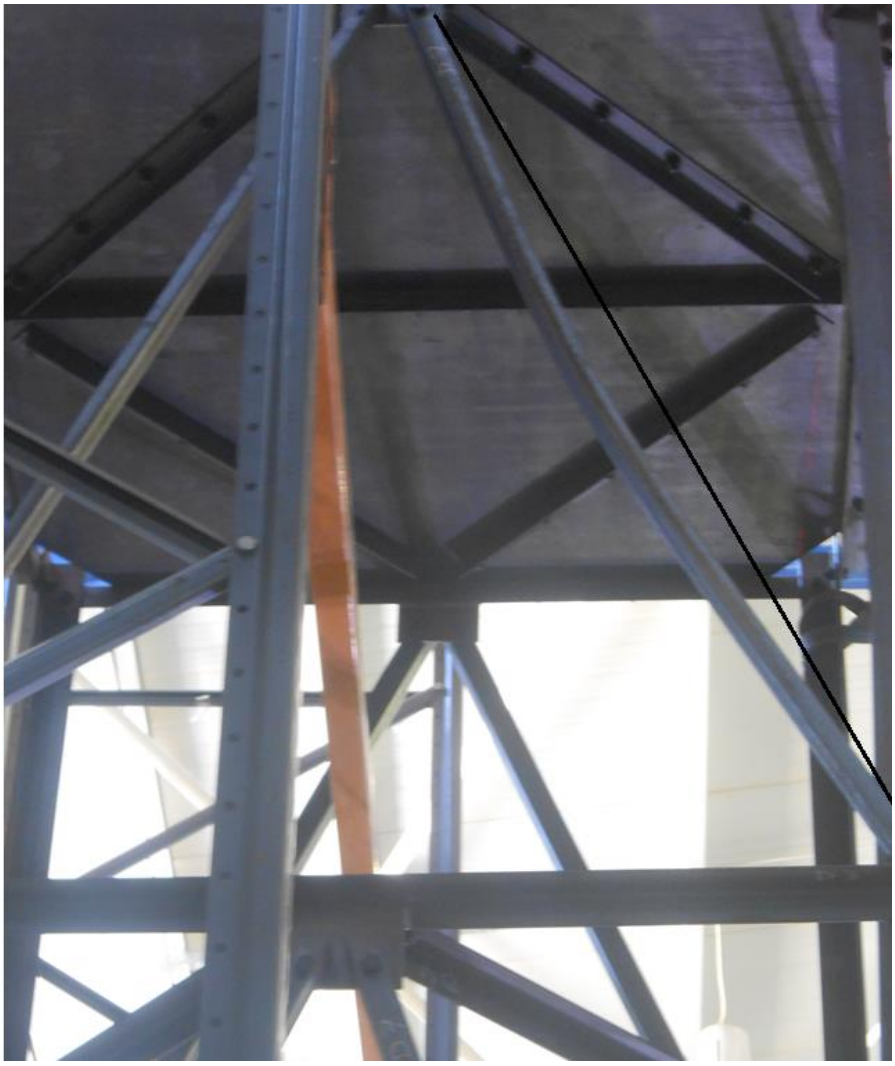

Figure 7.1: Tower O-1. Weak axis flexural buckling of the failed diagonal towards the heel

Fig. 7.2 shows the horizontal floor displacements, while Fig. 7.3 the floor rotations. The former is calculated as the mean value of the measured displacements on the two sides, the latter as their difference divided by the tower width. Fig. 7.4 shows that the tower response may be approximated by a trilinear curve.

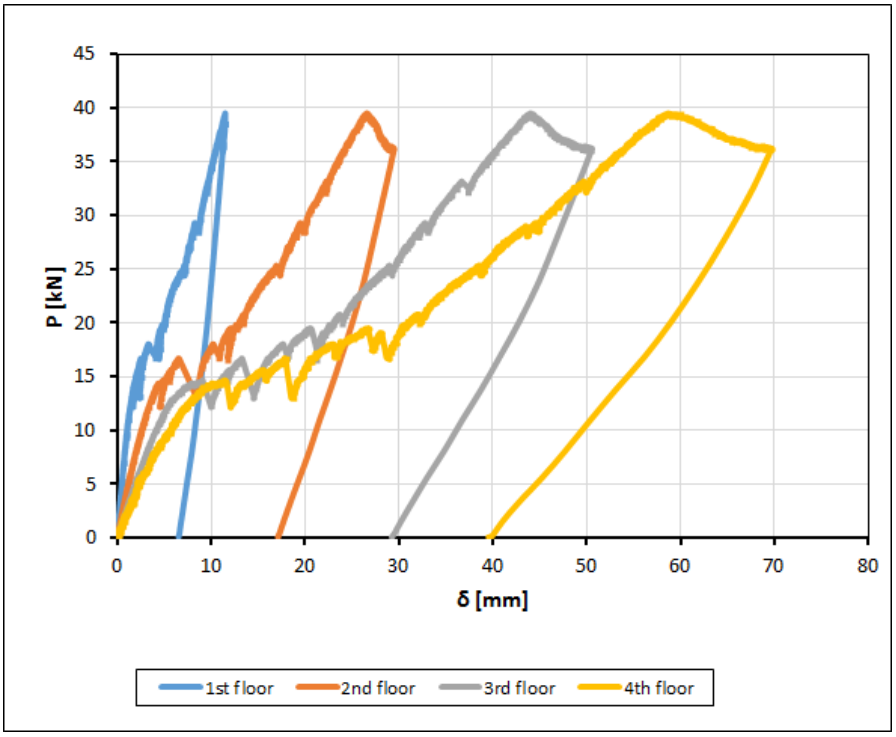

Figure 7.2: Tower O-1. Load- displacement curves

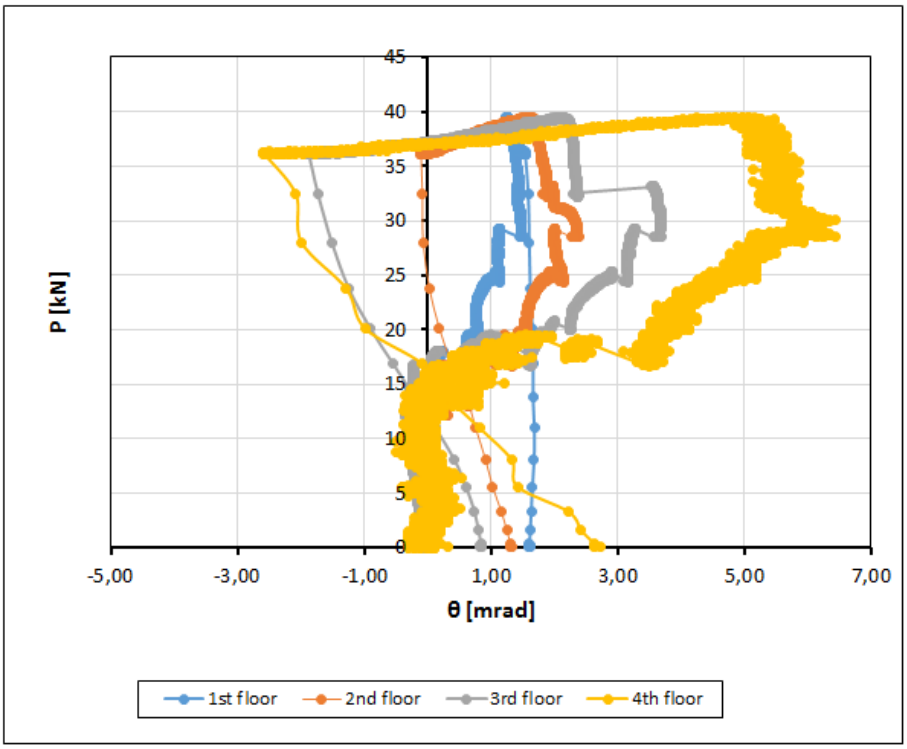

Figure 7.3: Tower O-1. Load- rotation curves

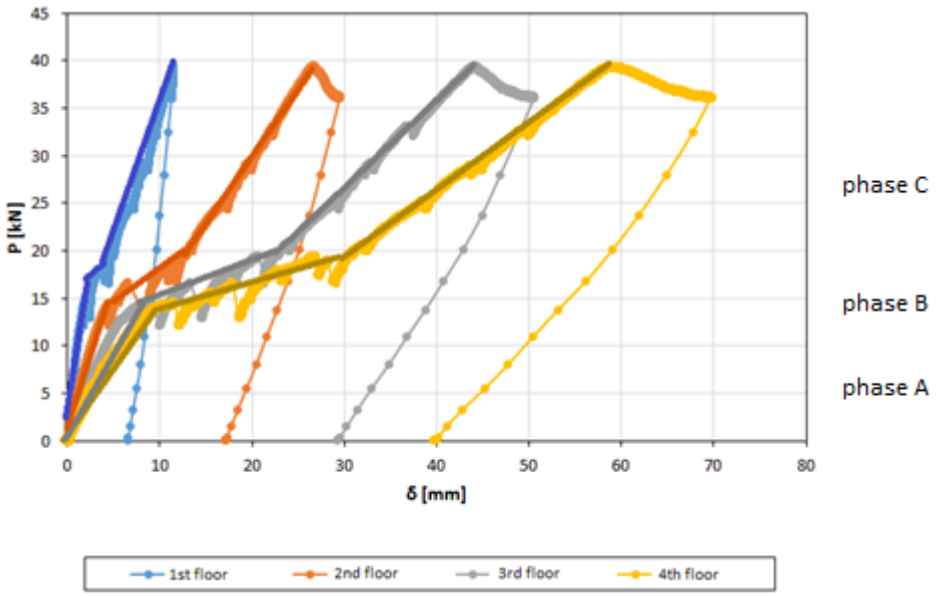

Figure 7.4: Tower O-1. Trilinear approximation of the displacement curves

Accordingly, three phases may be distinguished:

- Phase A is the initial, stiffer, phase where no buckling occurs and the response is linear. Bolts are slip resistance and transfer shear forces through friction. The tower rotation is small and both walls transfer similar forces. This phase ends at different forces for the various floors, with the smaller, 15 kN, for the 4th floor and the larger, 17 kN, the 1st floor.
- Phase B exhibits the softest response due to the fact that slip occurs in the bolts, which one by one came in contact with their bearing surfaces. The tower starts to twist and one wall parallel to the force transfers higher forces than his opposite. This phase ends at 20 kN for the 2nd to 4th floor and 18 kN for the 1st floor. This indicates that the bolts at the 1st floor slipped at external force between 17 and 18 kN.
- Phase C exhibits an intermediate response in which all bolts transfer load through bearing. Rotation does not increase in all floors but the 4th, which continues to rotate up to a certain load and stops. At higher loads, after 30 kN, rotation stops in all floors. After the attainment of the maximum load, rotations of all floors come to zero (0), while the rotation of the 4th floor changes sign. This indicates that the stiffer wall becomes softer after failure due to the fact that two diagonals in that wall remained in the buckled state after failure.

Strain measurements in columns indicate that columns in phase A are subjected mainly to compression, Fig. 7.5. However, significant bending starts in phase B and increases up to the middle of phase C. In the last half of phase C, associated to constant tower's twist, bending is kept constant and only compression increases.

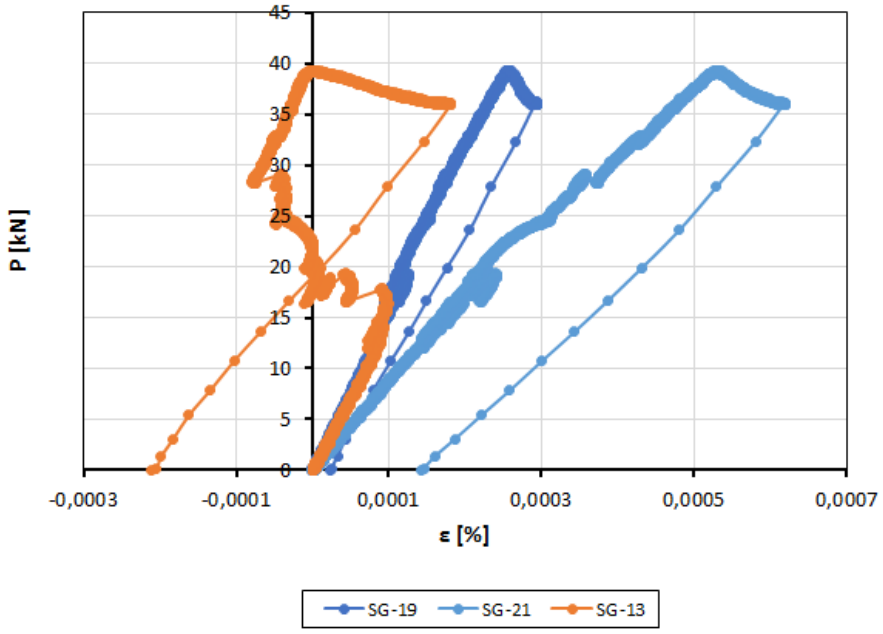

Figure 7.5: Tower O-1. Strains at compression column near the base

Strain measurements in braces indicate that all braces, whether in tension or compression, are subjected to bending besides their axial force, Figs. 7.6, 7.7. This is the result of the eccentric loading through the bolt that connects the brace in one leg.

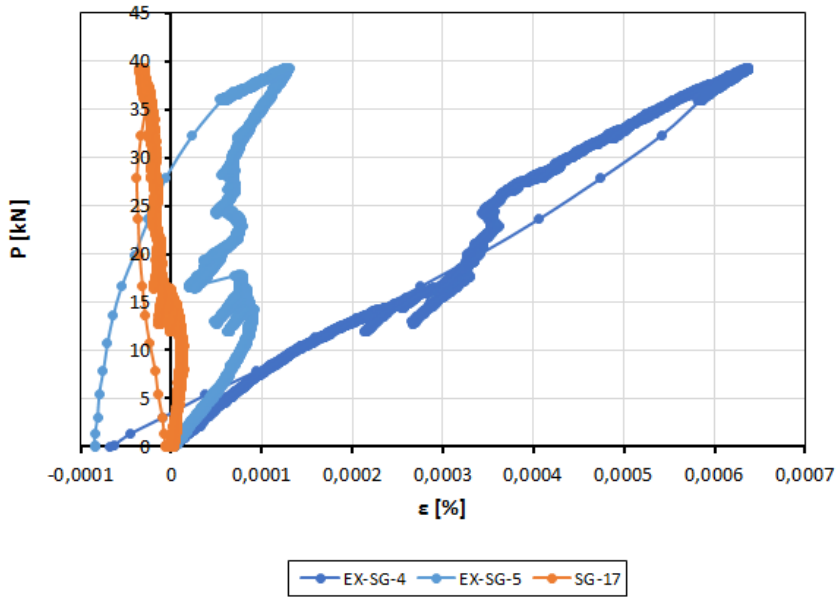

Figure 7.6: Tower O-1. Strains at upper part of 1st floor compression brace

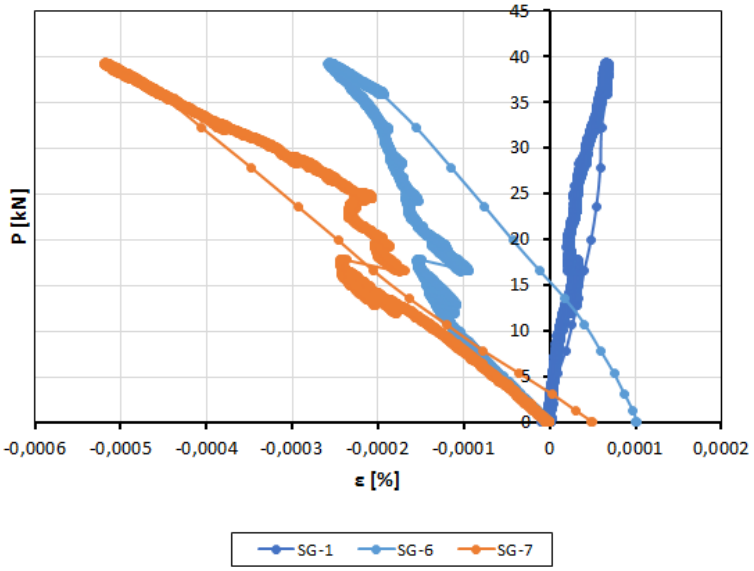

Figure 7.7: Tower O-1. Strains at upper part of 1st floor tension brace

7.2 Tower 2, type O-2

The tower was loaded in 2 stages. In stage 1 the loading speed was 75 mm/h. Like the previous one, tower 2, type O-2 exhibits three phases of response. Fig 7.8. Phase A, associated with slip resistant behaviour of bolts, phase B during which the bolts slide with noisy bangs and phase C where the bolts transfer loads through bearing. This tower also, and especially the 4th floor, is twisting in phase B, Fig. 7.9. The load increased without any sign of failure. At 100 kN load the tower was unloaded due to the fact that the 8.8 anchors of the base structure to the rigid floor were designed for this loading. Loading in stage 2 started after replacement of the 8.8 with 10.9 anchors and was applied with a loading speed of 100 mm/h. Failure occurred at 105 kN, a slightly higher load compared to the load applied in stage 1.

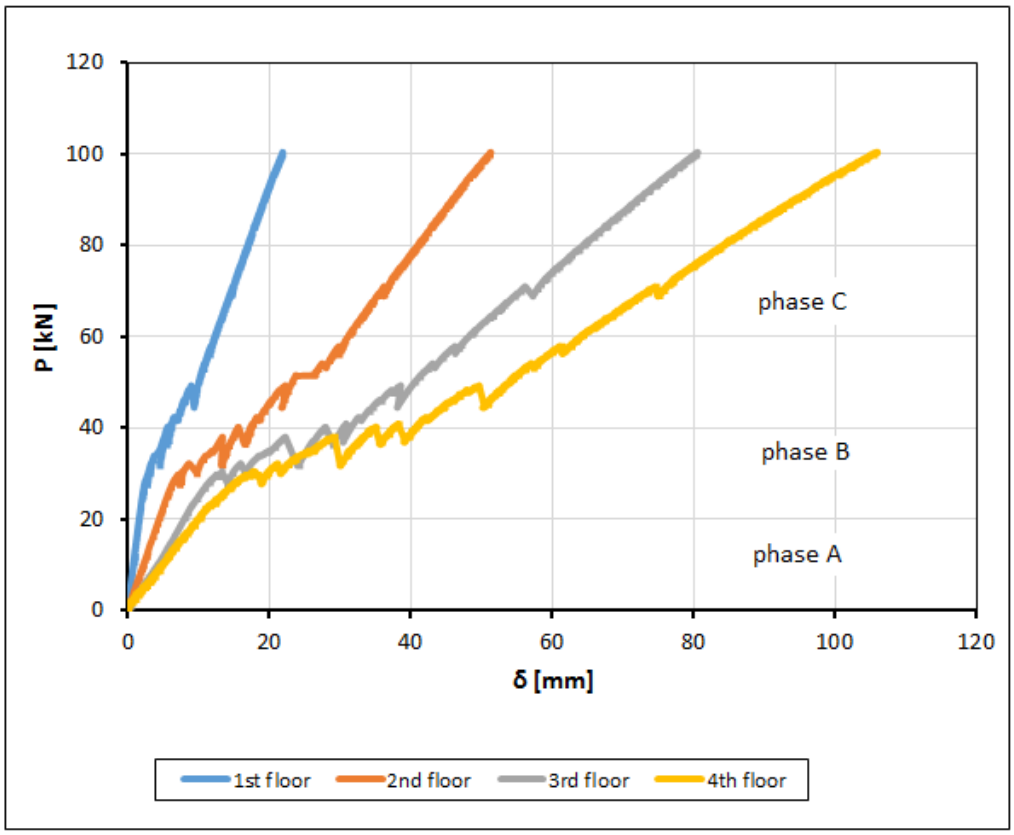

Figure 7.8: Tower O-2. Loading stage 1. Load- displacement curves

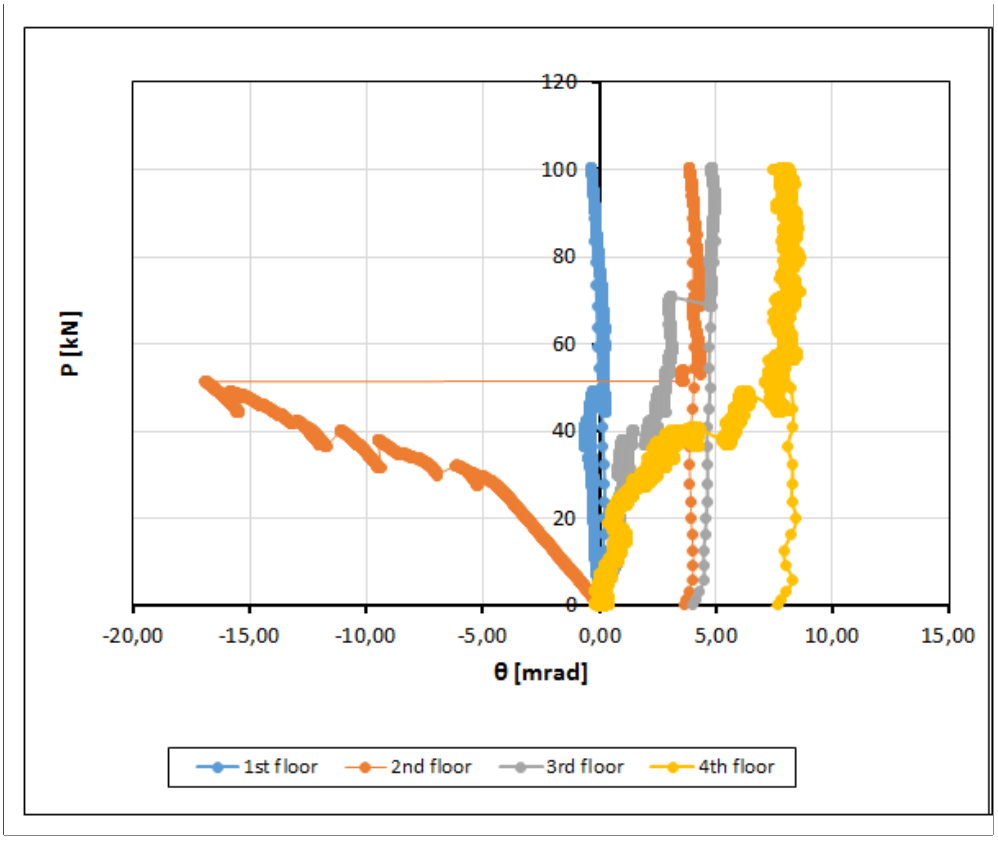

Figure 7.9: Tower O-2. Loading stage 1. Load- rotation curves

At the loading stage 2 the bolts could transfer shear load from the beginning since they were already in contact with the bearing surfaces. Accordingly, there was no slip in the bolts and no bangs and the load-displacement curve was smooth with little non-linear behaviour, Fig. 7.10, while twist was not significant, Fig. 7.11. The stiffness in loading stage 2 was almost equal to the initial stiffness of loading stage 1, Fig. 7.12. Global failure occurred, as planned, due to weak axis flexural buckling of one compression leg at the tower base, Fig. 7.13.

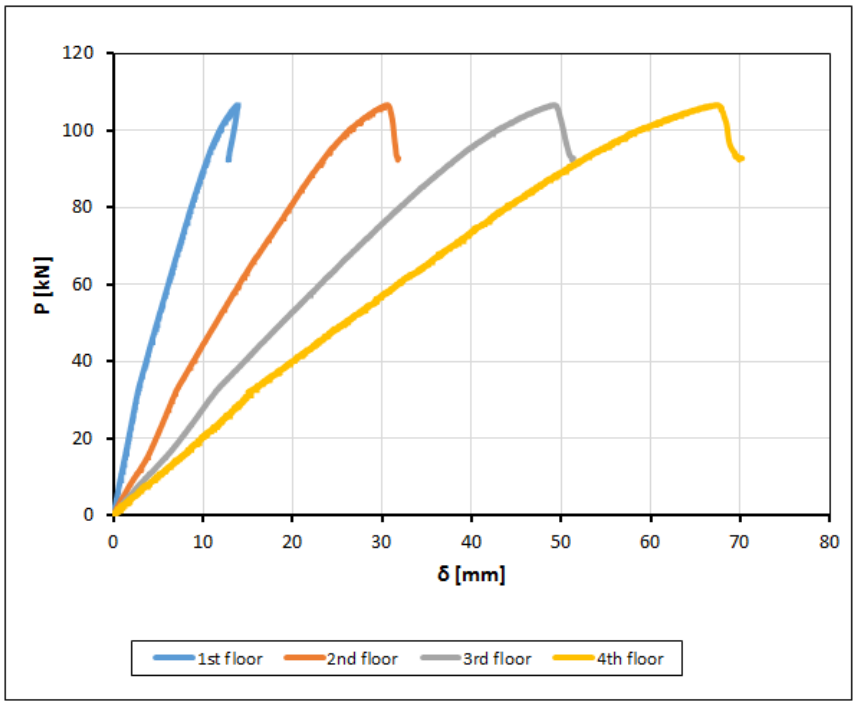

Figure 7.10: Tower O-2. Loading stage 2. Load- displacement curves

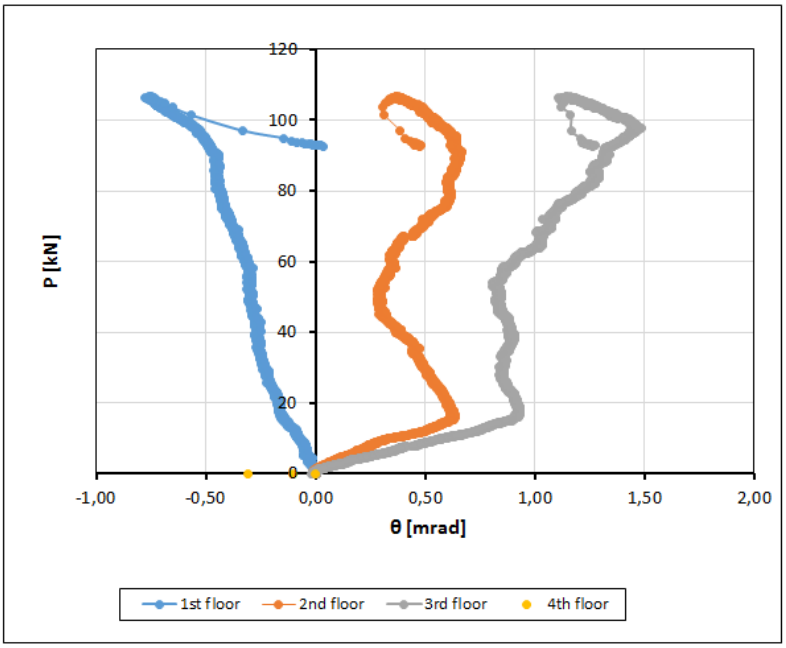

Figure 7.11: Tower O-2. Loading stage 2. Load- rotation curves

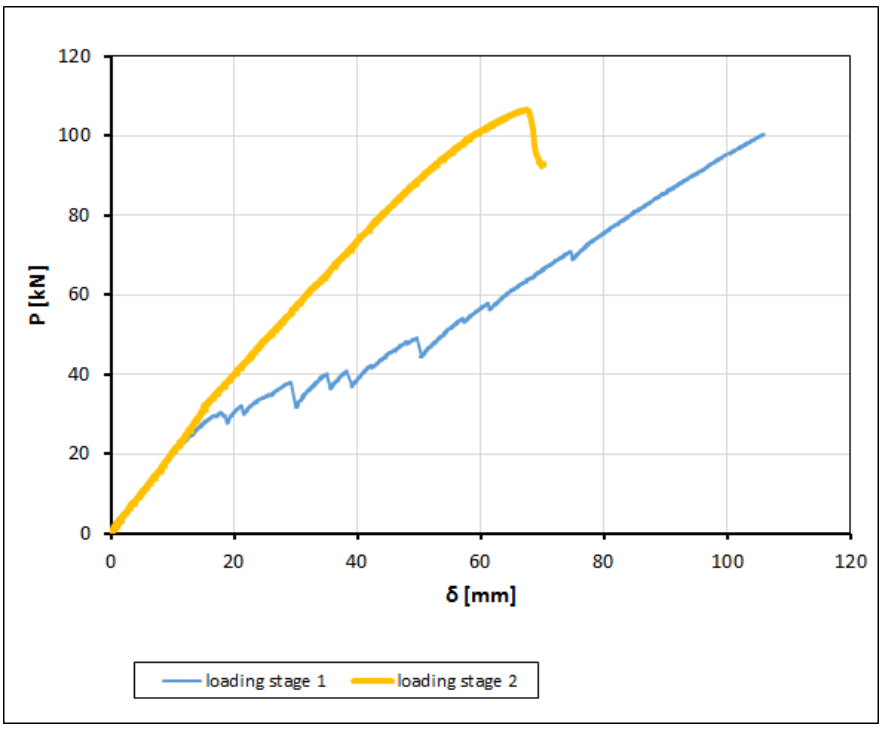

Figure 7.12: Tower O-2. Loading stages 1 and 2. Load- displacement curves

Figure 7.13: Tower O-2. Weak axis flexural buckling of the failed leg towards the lips

Strain measurements indicate little bending in the 1st floor legs, but larger bending in the 2nd floor legs, Figs 7.14, 7.15. Oppositely, the braces are subjected to significant bending due to the eccentric connection, Fig. 7.16.

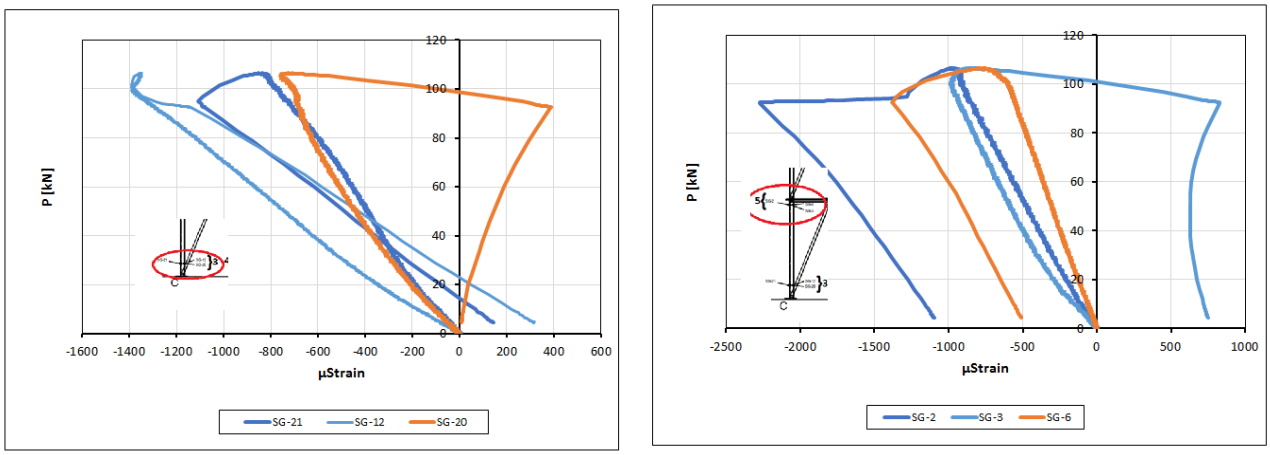

Figure 7.14: Tower O-2. Strains at the bottom and top section of one leg at 1st floor

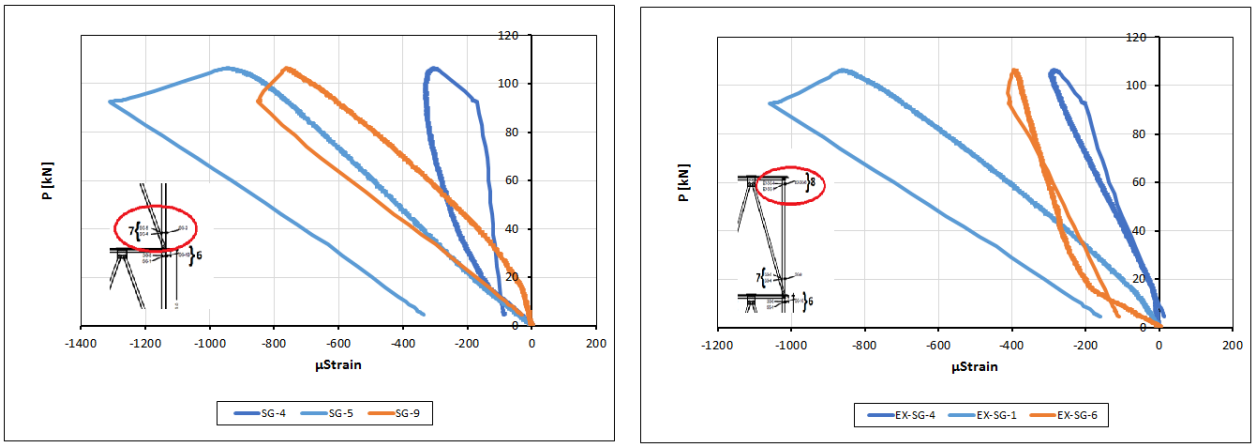

Figure 7.15: Tower O-2. Strains at the bottom and top section of one leg at 2nd floor

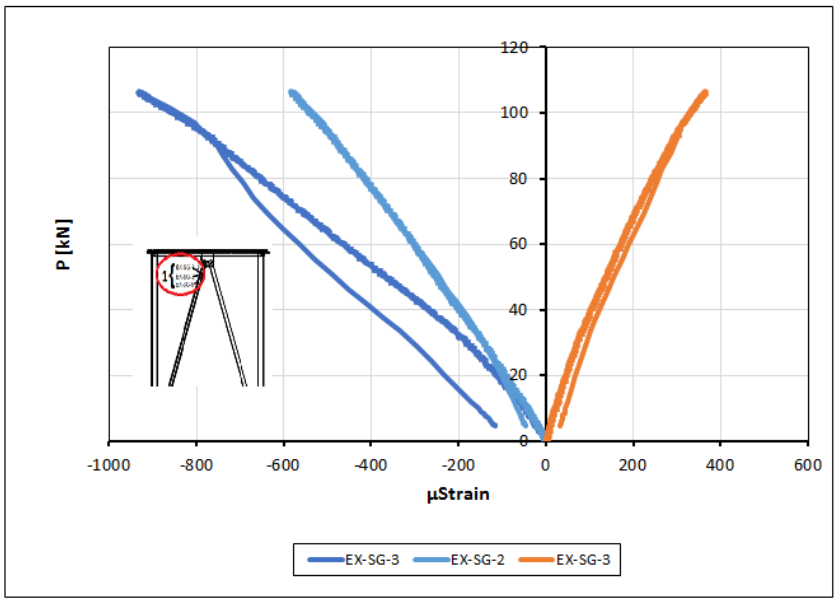

Figure 7.16: Tower O-2. Strains at upper part of 1st floor compression brace

7.3 Tower 3, type O-1S

This tower was identical with tower 1 type O1, with the difference that the compression diagonals were strengthened with FRPS. As in tower 1, three phases of response depending on the way shear forces were transferred by the bolts could be distinguished, Fig. 7.17:

- Phase A where shear forces were transferred through friction,
- Phase B where slip occurred until the bolts reached their bearing surfaces and
- Phase C where shear forces were transferred through bearing.

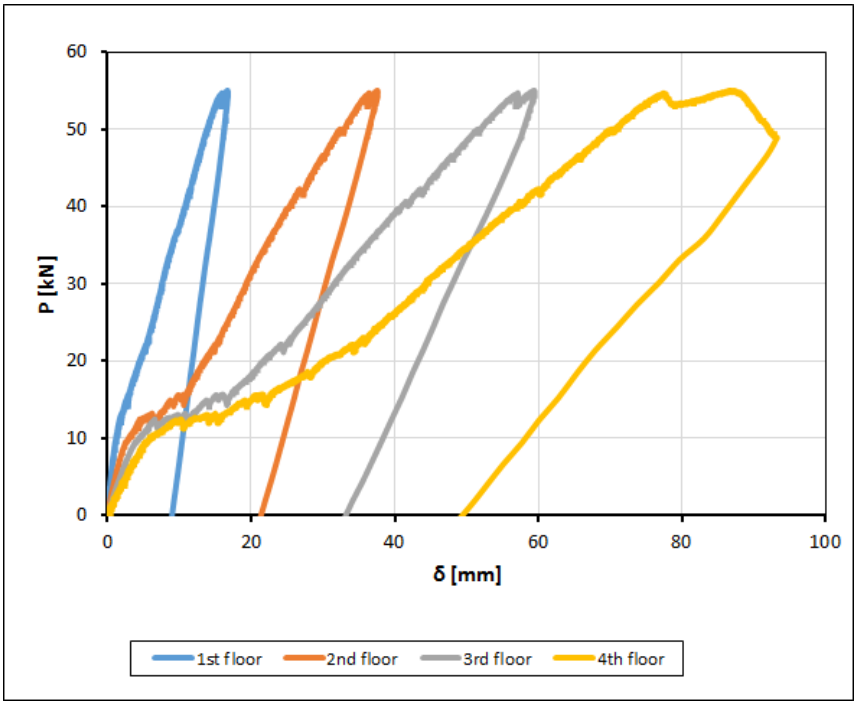

Figure 7.17: Tower O-1S. Load- displacement curves

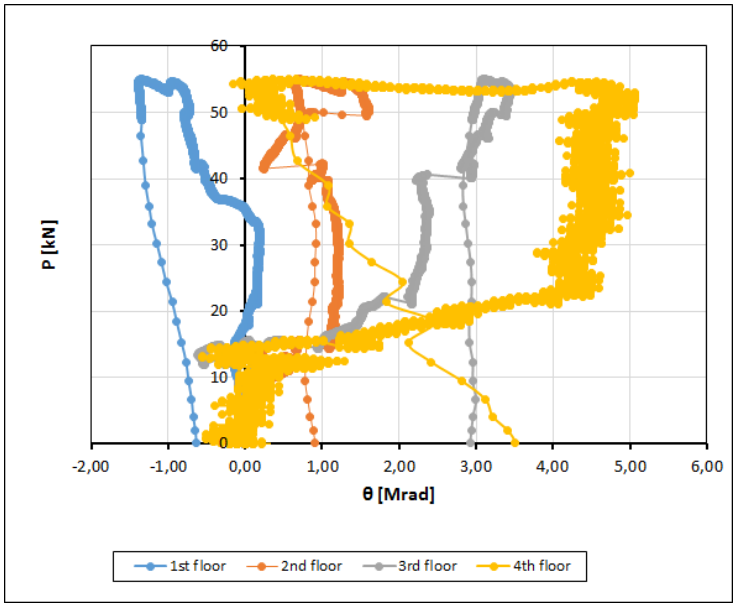

Figure 7.18: Tower O-1S. Load- rotation curves

During phase B the tower, especially its top floor, was subjected to significant twist, Fig. 7.18.

Failure was due to flexural buckling of the two 4th floor compression diagonals, Fig. 7.19.

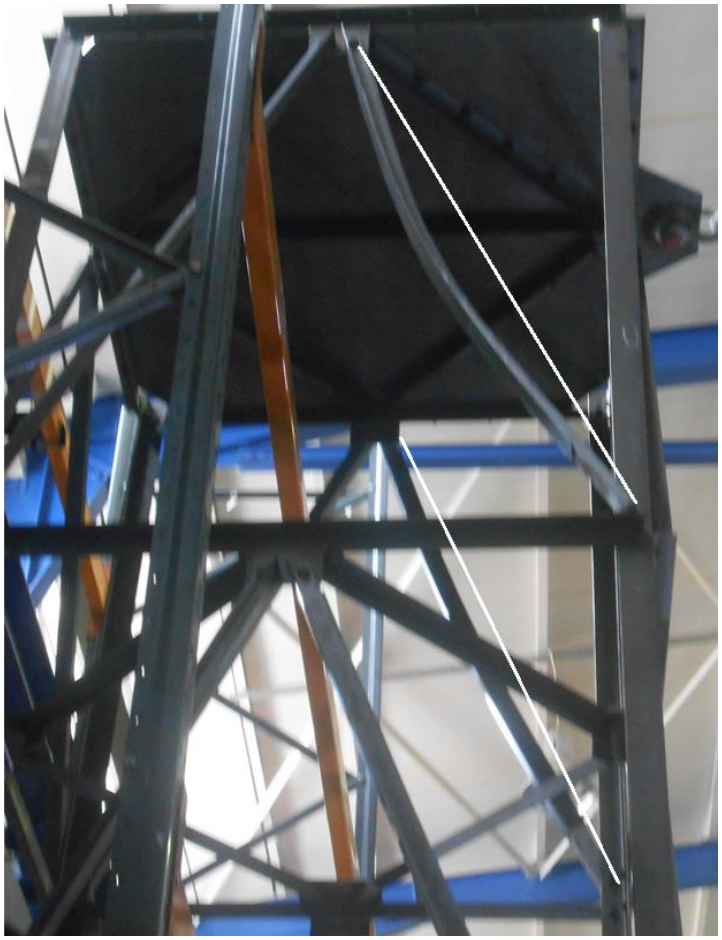

Figure 7.19: Tower O-1S. Weak axis flexural buckling of the failed diagonals towards the lips

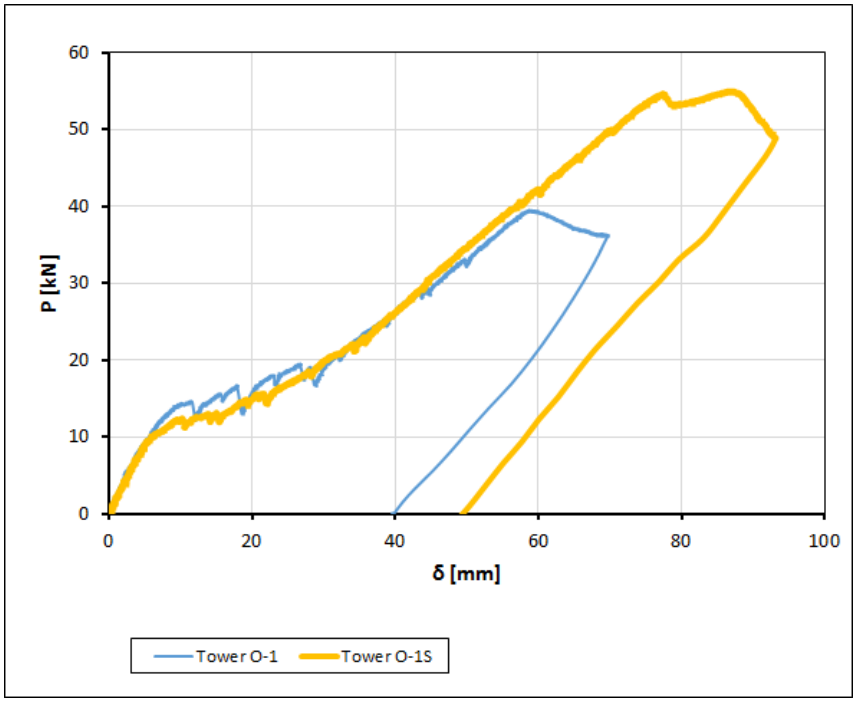

Figure 7.20: Load- displacement curves of tower O-1 and O-1S

The response of the initial and the strengthened towers O-1 and O-1S was very similar, except that the strengthened tower exhibited a 30% increase in capacity, Fig. 7.20.

Strain measurements in the 1st floor strengthened diagonal indicate little local bending of the angle legs, but significant bending due to the eccentric bolted connection, Fig. 7.21. Strains at the loaded angle leg were substantial higher than in the opposite one and larger in the tip than in the heel indicating that the diagonal is bent towards the heel. Strains at the compression leg indicate also substantial bending. However, strains are larger in the heel that in the tips, indicating that the leg is bent towards the tip, Fig. 7.22.

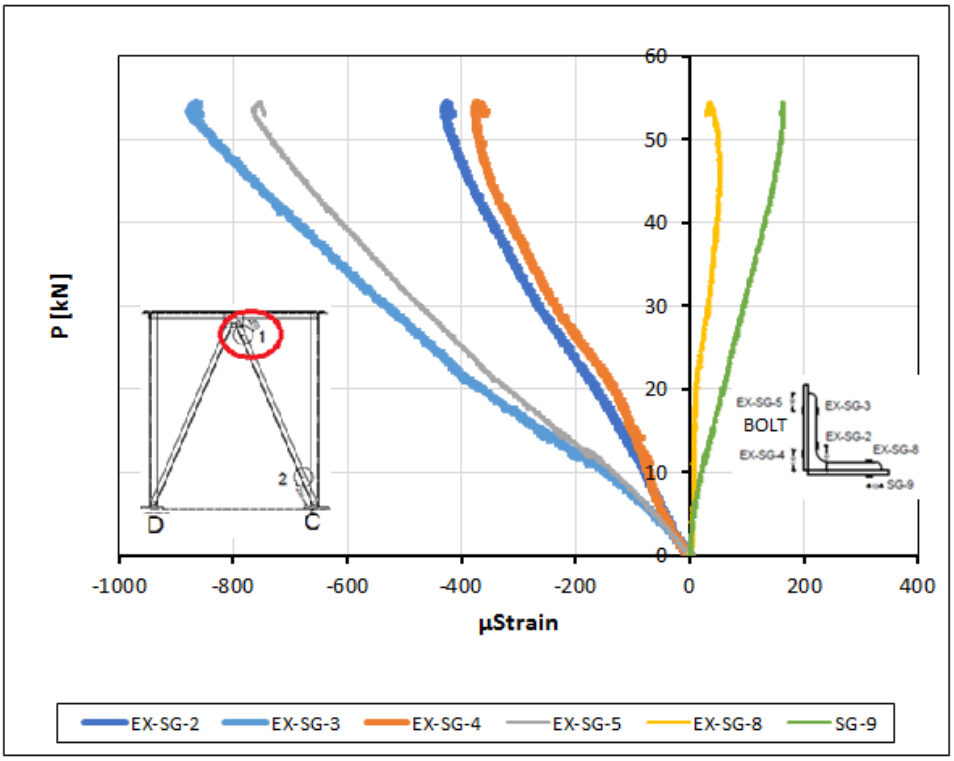

Figure 7.21: Tower O-1S. Strains at upper part of 1st floor compression brace

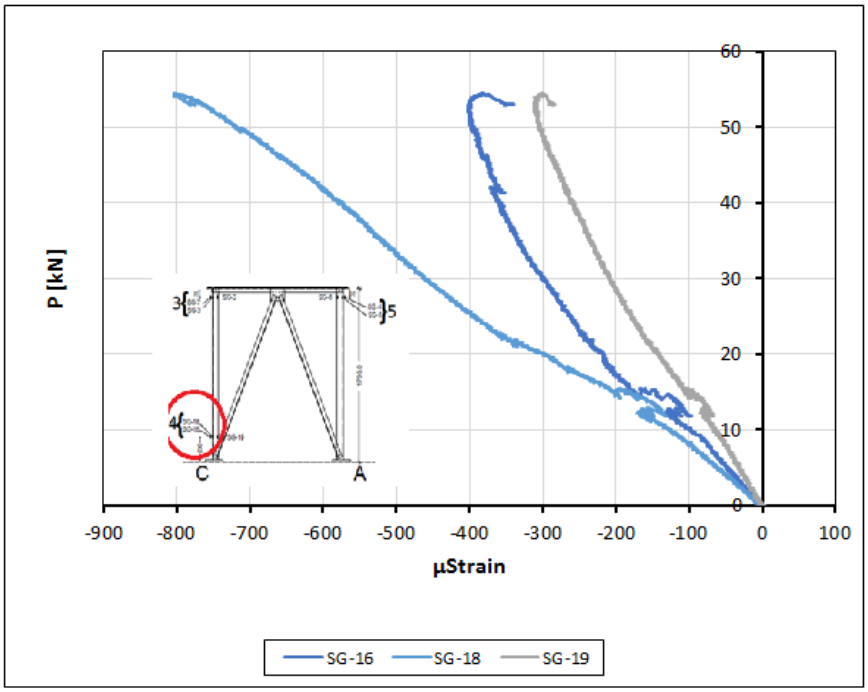

Figure 7.22: Tower O-1S. Strains at lower part of 1st floor compression leg

7.4 Tower 4, type D-1

This tower is similar to tower type O-1, but has smaller braces L40.40.4 because it is loaded along the diagonal and the braces of all the walls are sharing equally the force. Here again, three phases of response as in the other towers may be distinguished, with phase A in which the load transfer of the bolts is through friction, phase B where the bolts slip and phase C where the bolts carry forces through bearing, Fig. 7.23. In phase B the tower is twisting at levels comparable, although a little smaller, to tower type O-1. At failure several diagonals of the top 2 floors buckled in respect of the weak axis towards the lips, Fig. 7.25. The failure load and displacement at this load are similar to those of tower type O-1.

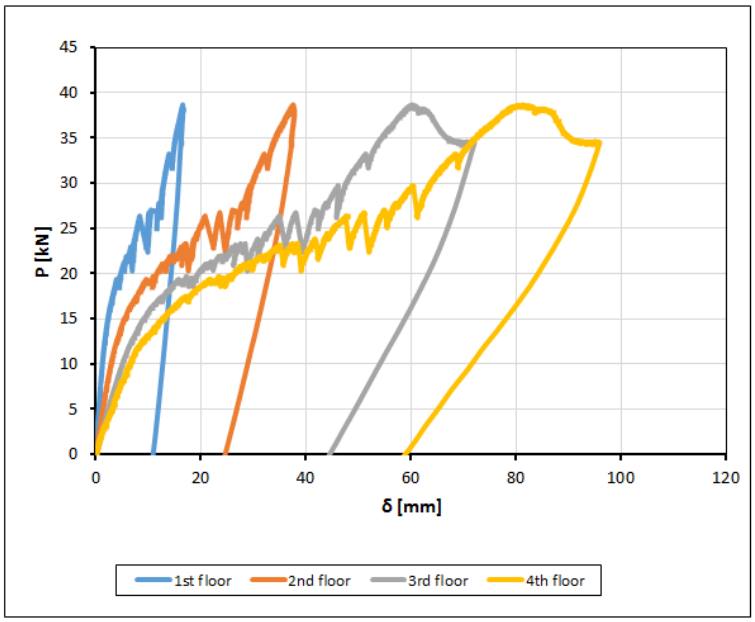

Figure 7.23: Tower D-1. Load- displacement curves

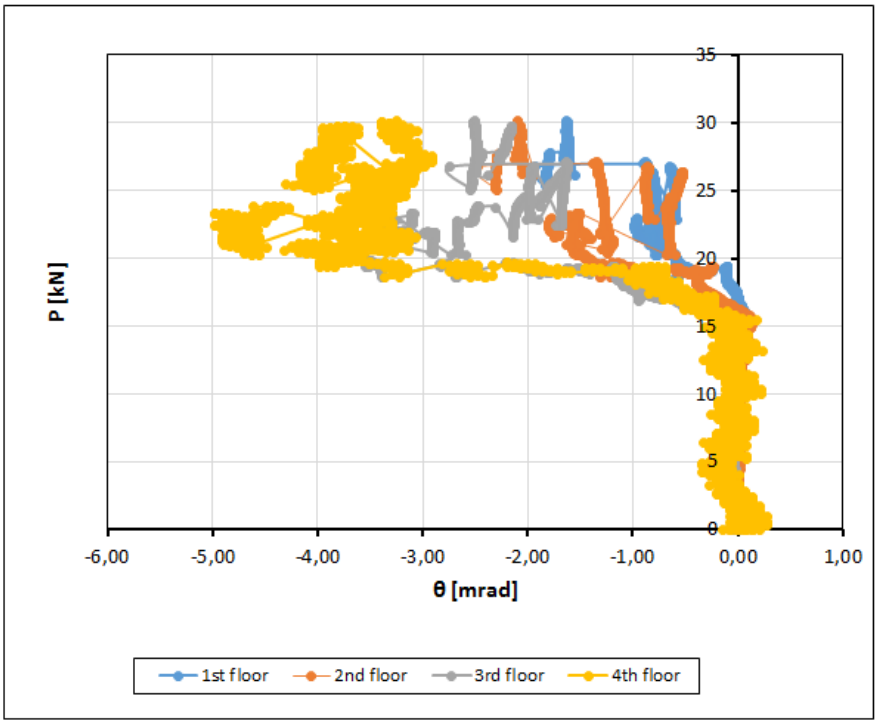

Figure 7.24: Tower D-1. Load- rotation curves

Figure 7.25: Tower D-1. Weak axis flexural buckling of the failed diagonals towards the lips

Strain measurements at the compression diagonals indicate significant bending due to the eccentric bolted connection with strains at the loaded angle leg substantial higher than in the opposite one, Fig. 7.26. The deviations of all measurements show that in fact, bending is bi-axial, with significant strong axis moment. Measured strains show that braces remained elastic near throughout loading. However, the measurements referred to sections near the brace supports and braces in the lower floors, while failure occurred in the upper floors.

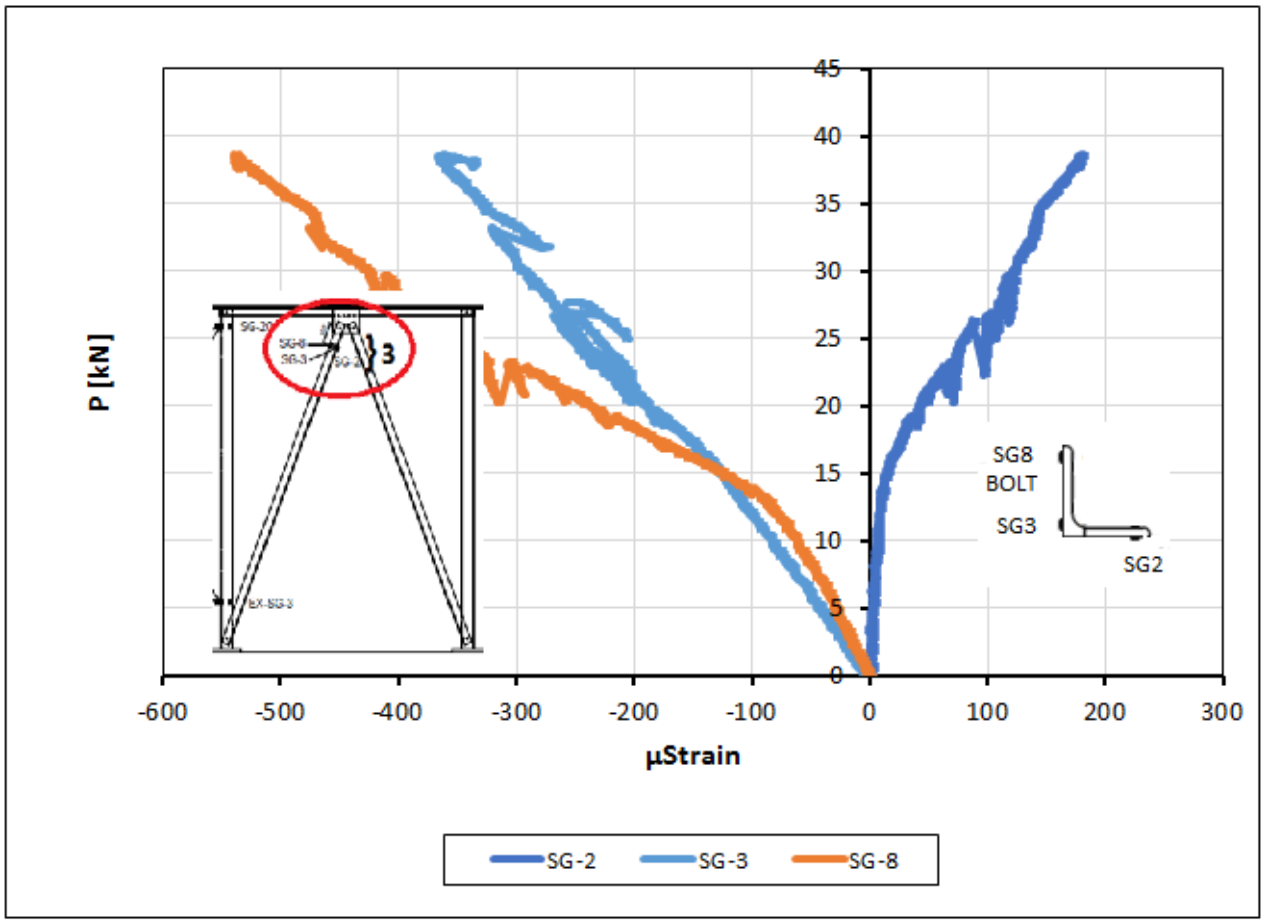

Figure 7.26: Tower D-1. Strains at upper cross section of 1st floor compression brace

7.5 Tower 5, type D-2

This tower has stronger braces compared to tower type D-1 in order to trigger failure in the compression leg. The three phases of response are visible, with phase A shorter and phase C longer compared to tower D-1, Fig. 7.27. Phase B is also longer and the tower twist larger compared to tower D-1, Fig. 7.28. Failure occurred due to flexural buckling of the compression leg. This buckled in respect of the weak axis but, unlike the braces, towards the lips. Fig. 7.29 shows that buckling was restrained in the 1st floor, while in the upper floors the legs did not showed signs of failure. Failure load was significant higher compared to tower D-1.

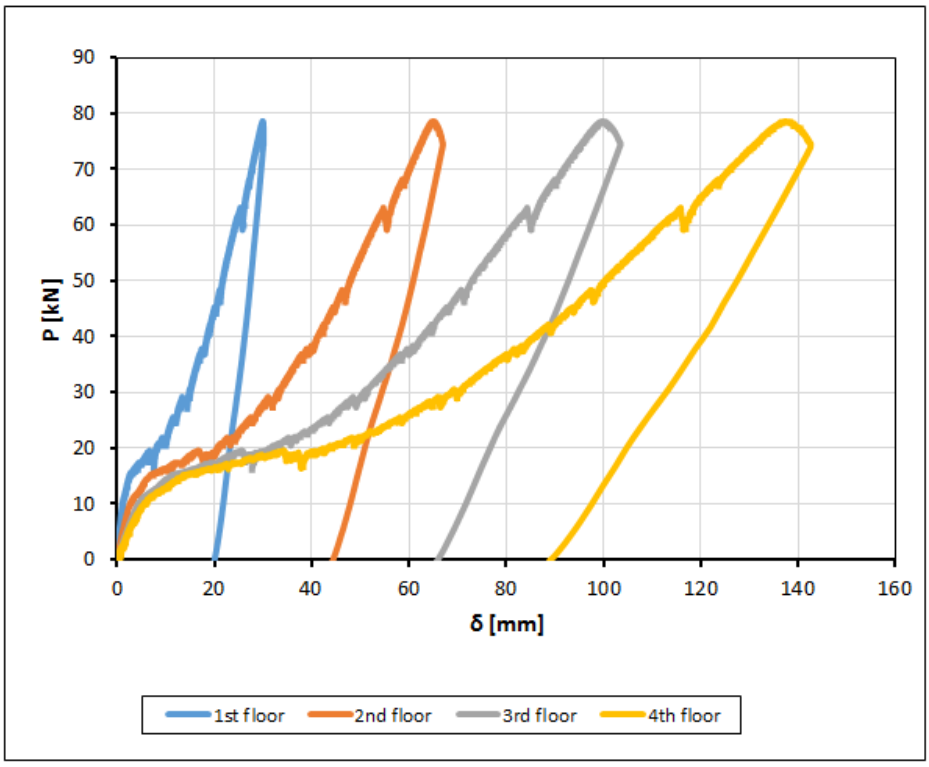

Figure 7.27: Tower D-2. Load- displacement curves

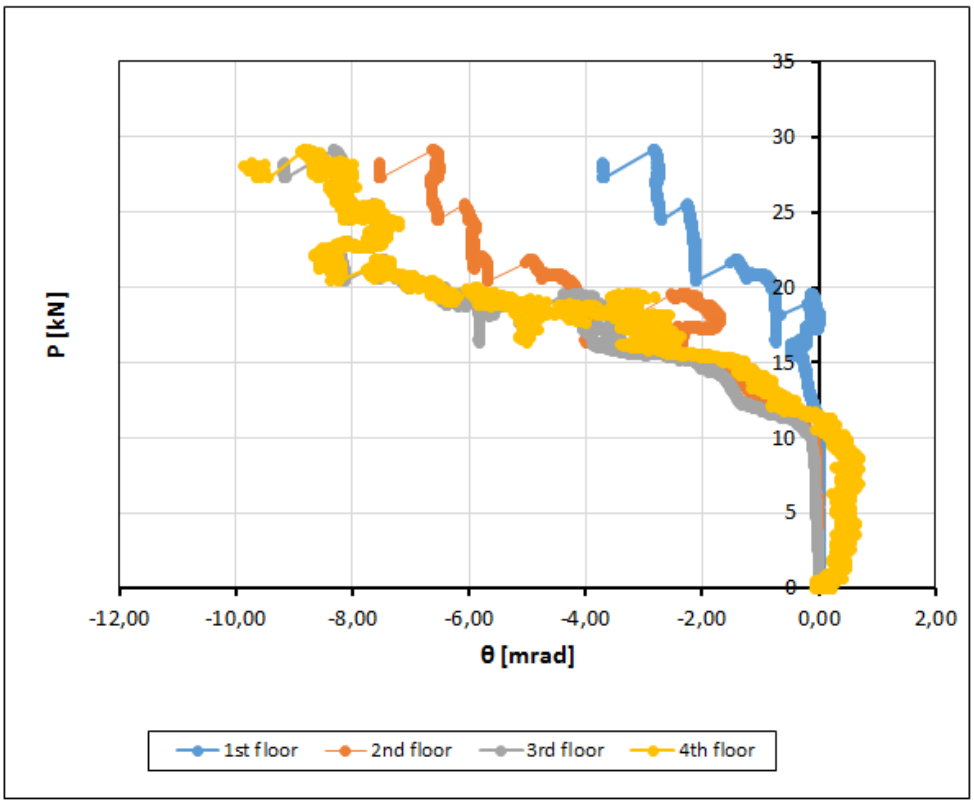

Figure 7.28: Tower D-2. Load-rotation curves

Figure 7.29: Tower D-2. Weak axis flexural buckling of the leg towards the lips

Strain measurements at the basis of the compression leg indicate the leg is subjected to compression in phase A and subsequently bent, Fig. 7.30. Near the failure load a moment develops that leads the lips to higher compression and the heel unloading. Taking into account the failure direction of the

leg, it may be seen that the developing moment at the base of the leg is opposite to the one at mid-span. Similar observations can be made at the top cross section of the same leg that is initially is subjected to compression that turns to compression and bending, Fig. 7.31.

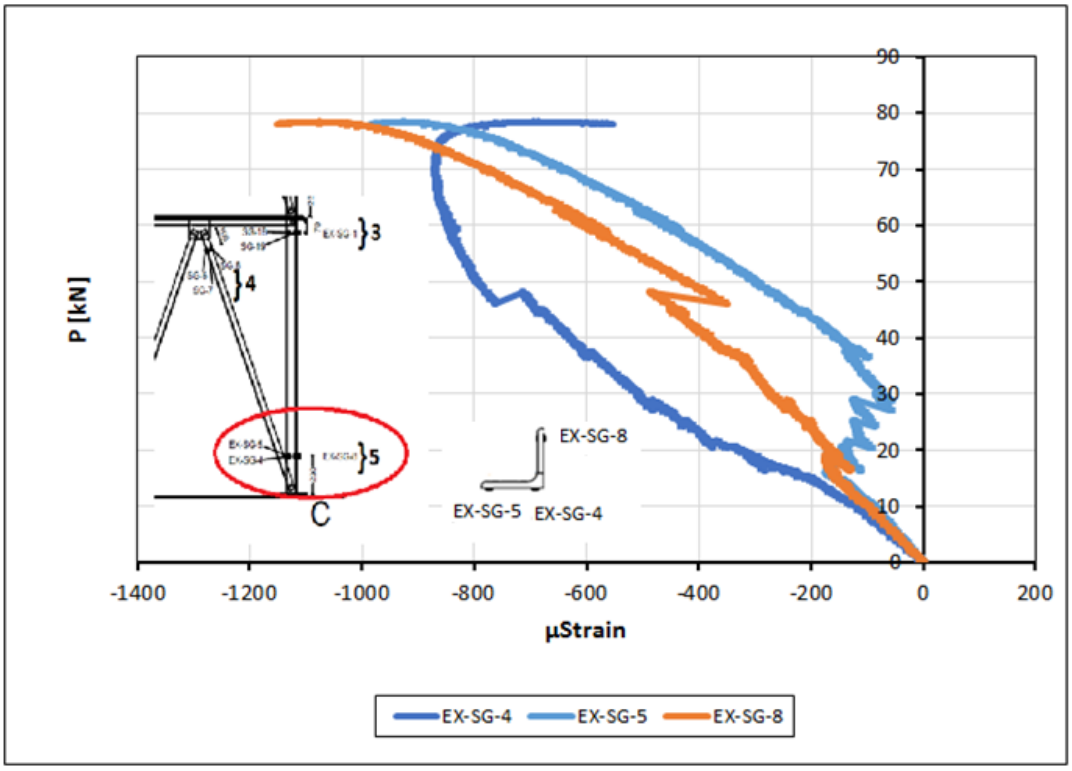

Figure 7.30: Tower D-2. Strains at basis of leg

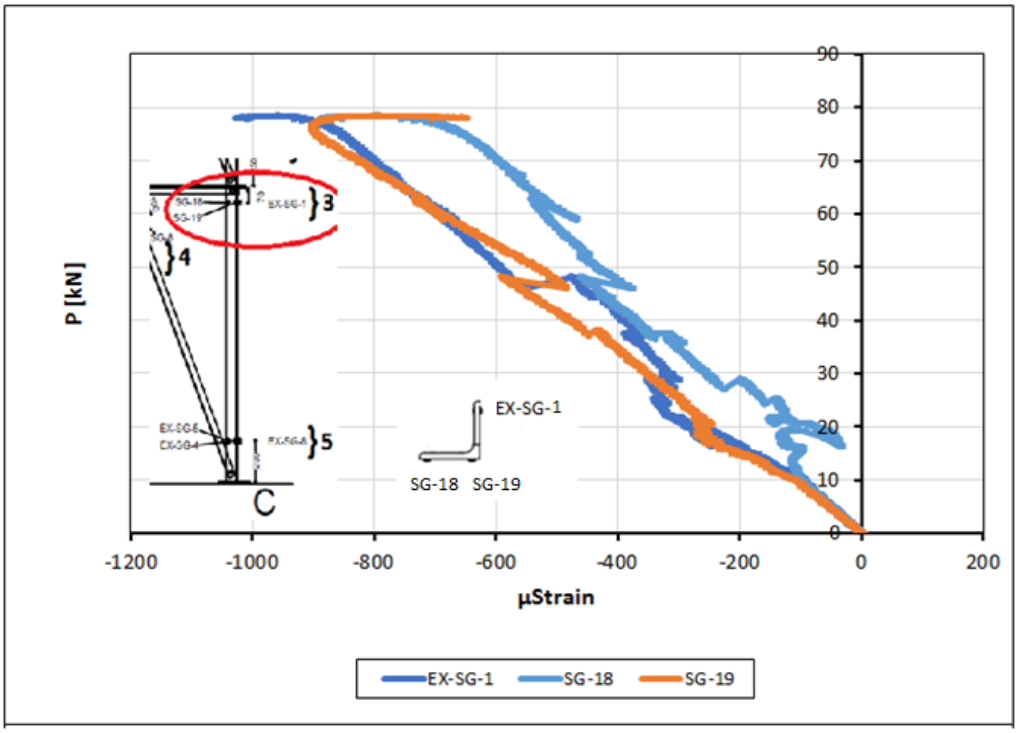

Figure 7.31: Tower D-2. Strains at top section of 1st floor leg

Strains at the compression diagonals indicate again significant bending due to the eccentric bolted connection. Strains at the loaded angle leg substantial higher than in the opposite one, Fig. 7.32. It may be seen that braces remain during the entire loading elastic. Elastic remain also all three (3) legs, but the one which is subjected to compression.

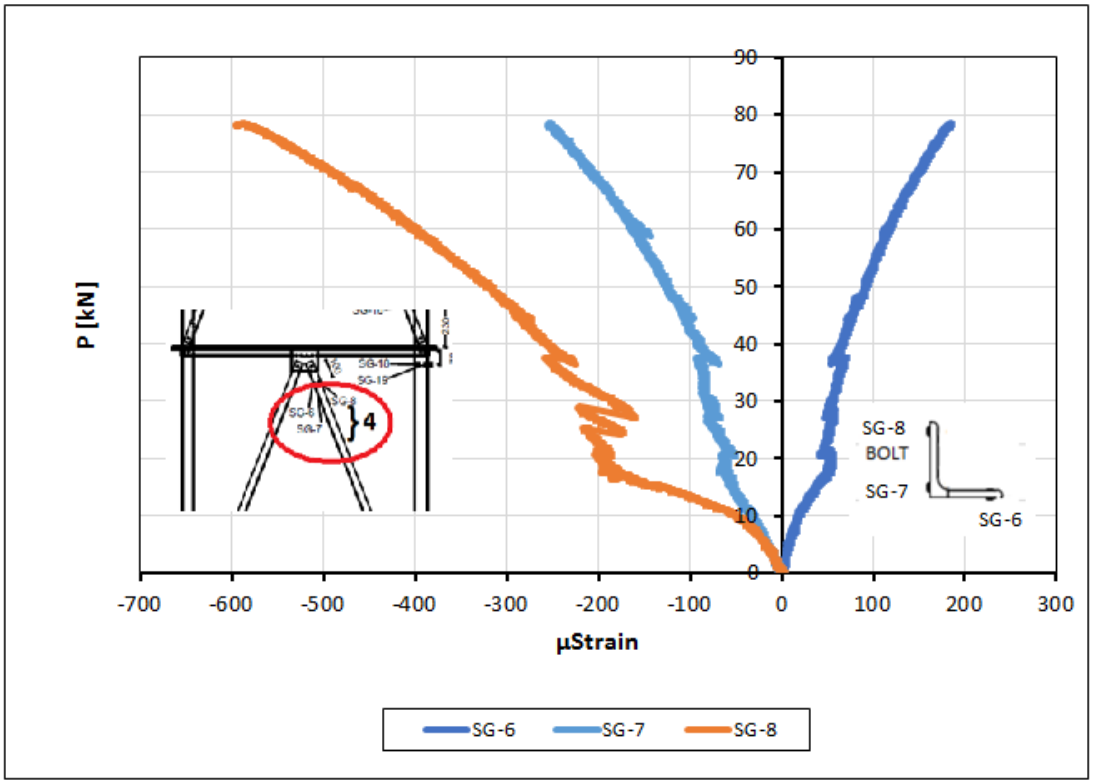

Figure 7.32: Tower D-2. Strains at upper cross section of 1st floor compression brace

7.6 Tower 6, type D-2S

This tower is identical to tower type D-2 with following strengthening measures: a) the compression leg in the first two floors and b) the four compression diagonals in the 4th floor, Fig. 7.33. Strengthening was by FRPs applied externally to the angle legs. As in all tests, the three phases of response are visible, Fig. 7.34. However, this tower was subjected to very large twist in Phase B, Fig. 7.35, which lead to failure at a slightly higher load compared to the un-strengthened tower D-2. Failure occurred due to flexural buckling of the compression leg. This buckled in respect of the weak axis towards the heel. Fig. 7.36 shows that buckling was restrained in the 1st floor, while in the upper floors the compression leg did not showed signs of failure.

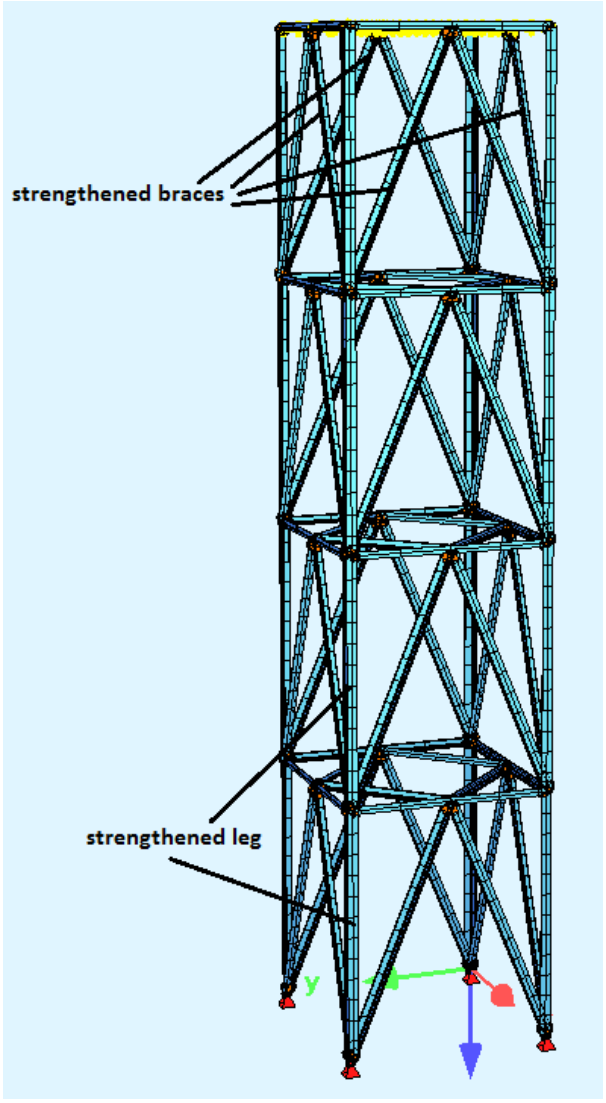

Figure 7.33: Tower D-2S. Strengthened members

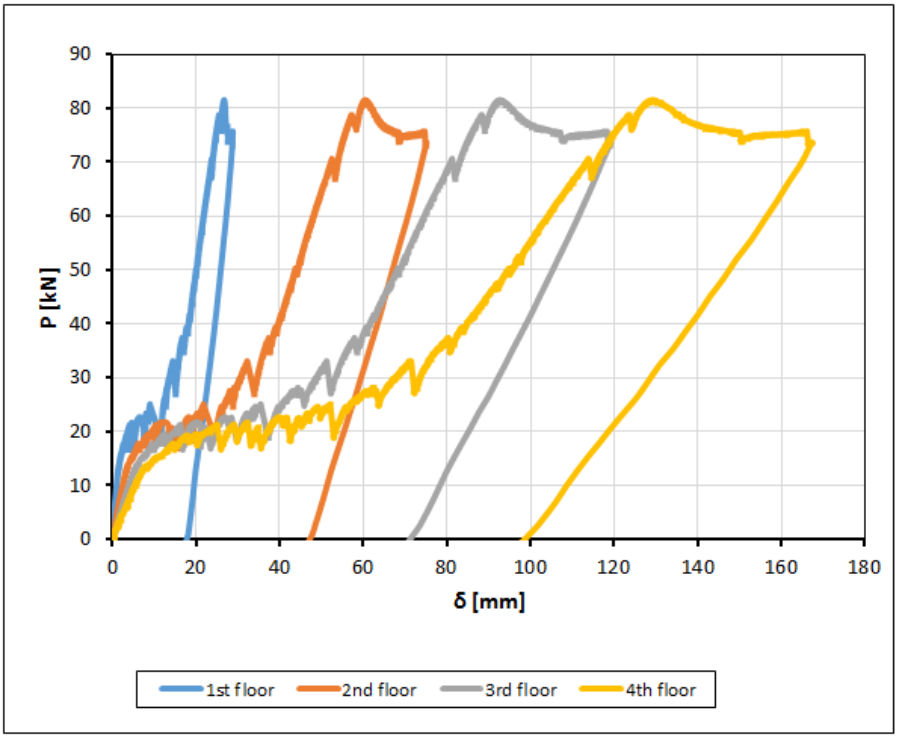

Figure 7.34: Tower D-2S. Load - displacement curves

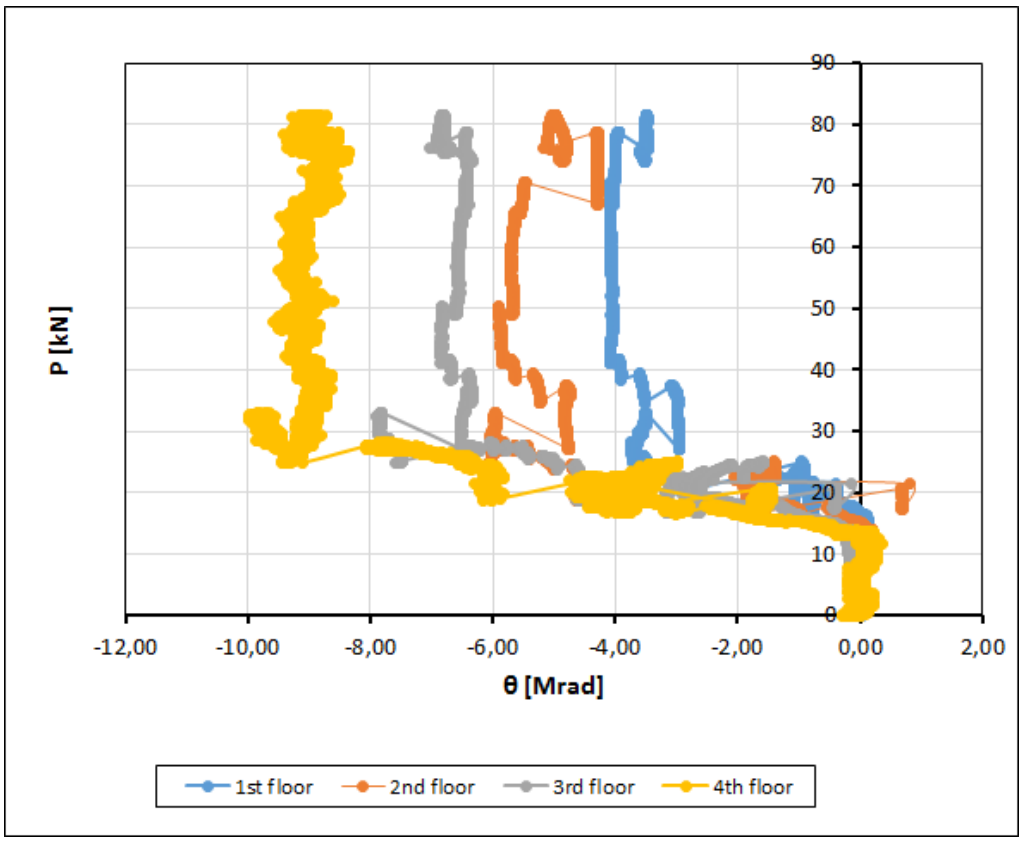

Figure 7.35: Tower D-2S. Load - rotation curves

Figure 7.36: Tower D-2S. Weak axis flexural buckling of the compression leg towards the heel

Strain measurements at the basis of the compression leg indicate the leg is subjected to compression in phase A and bending in Phase B, Fig. 7.37. Near the failure load a minor axis moment develops that leads the lips to higher compression and the heel to unloading. Taking into account the failure direction of the leg, it may be seen that the developing moment at the base of the leg is opposite to the one at mid-span. The conditions are similar at the top cross section of the same leg that is initially is subjected to compression becoming near the failure load compression and bending, Fig. 7.38. Very clear are the conditions at the 2nd floor leg, where strain measurements indicate strong bending around the weak axis starting in Phase B and continuing up to the failure load, Fig. 7.39.

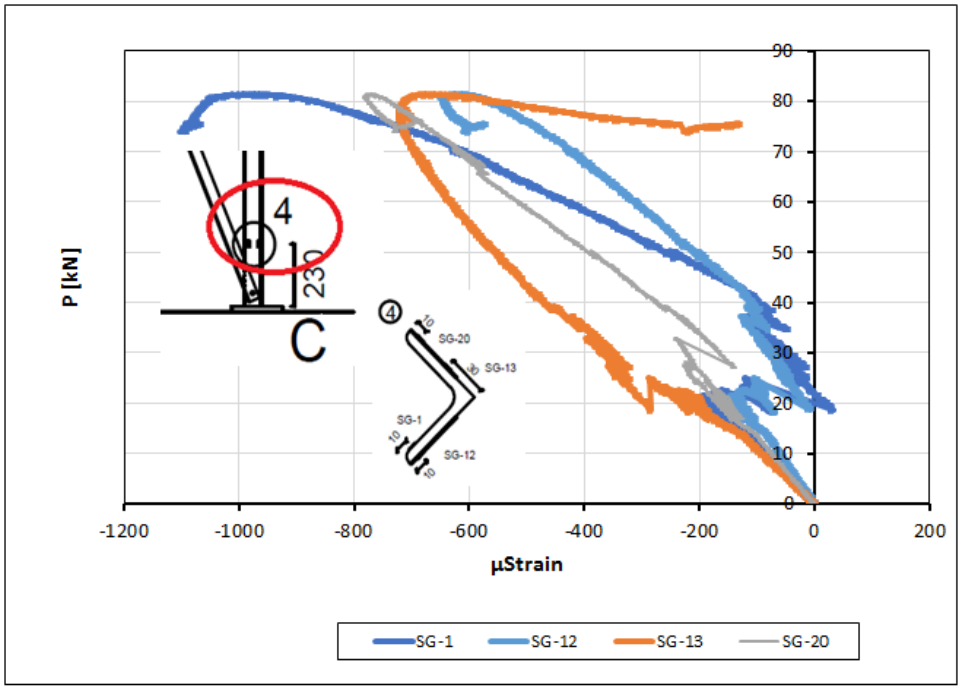

Figure 7.37: Tower D-2S. Strains at basis of leg

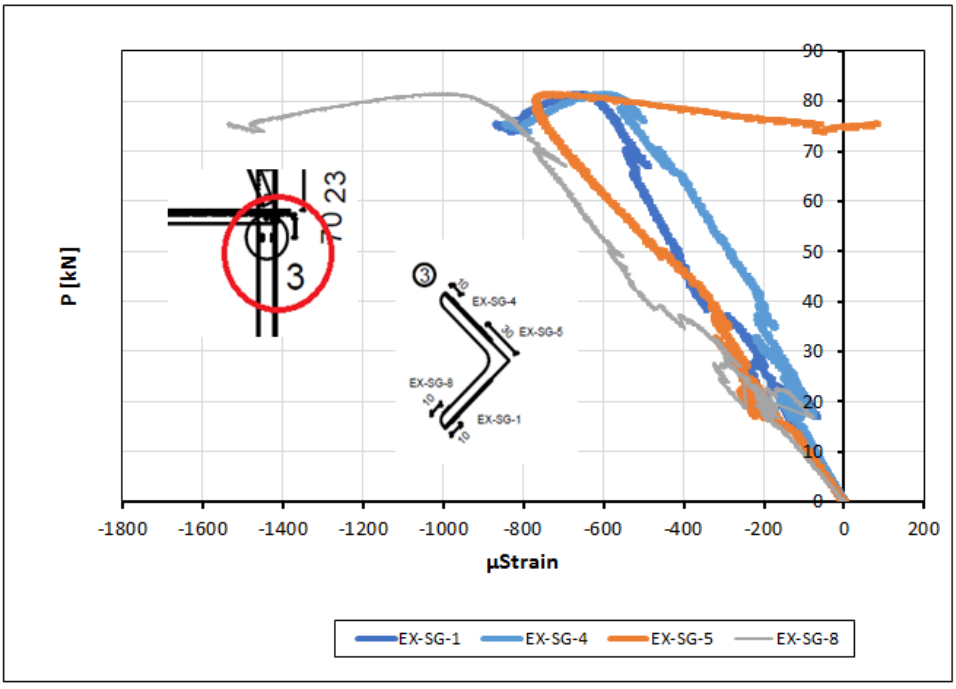

Figure 7.38: Tower D-2S. Strains at top section of 1st floor leg

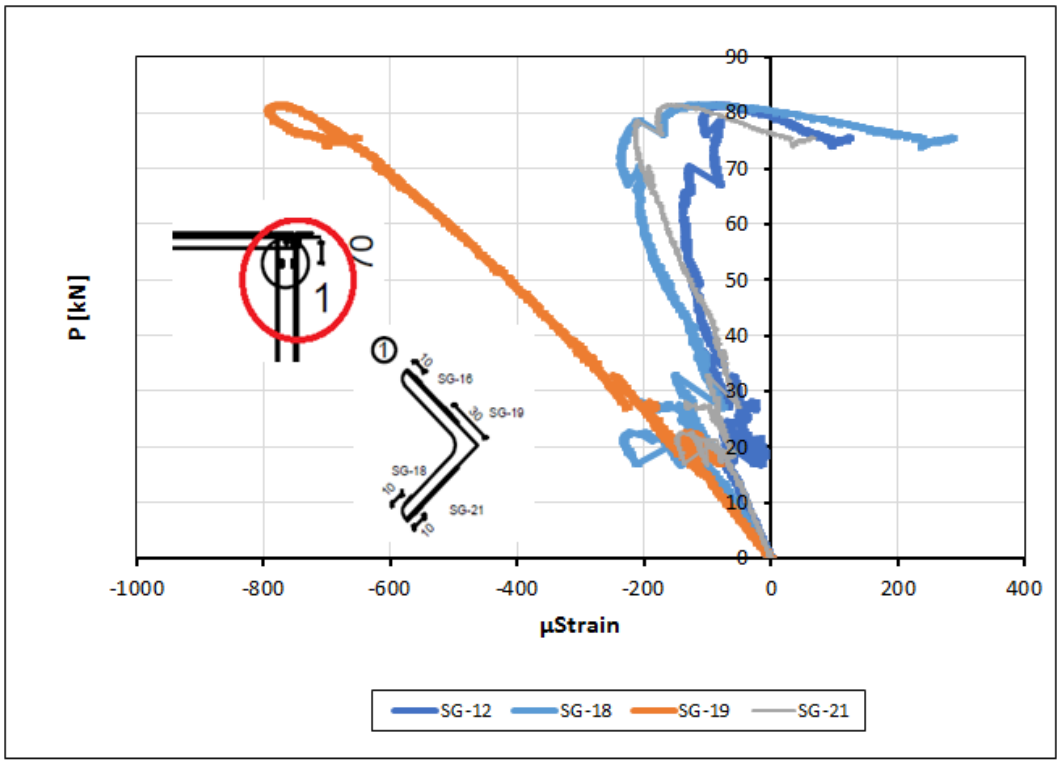

Figure 7.39: Tower D-2S. Strains at top section of 2nd floor leg

Strains at the compression diagonals indicate significant bending quite from the beginning due to the eccentric bolted connection. Strains at the loaded angle leg substantial higher than in the opposite one, Fig. 7.40. The brace remains elastic during the entire loading.

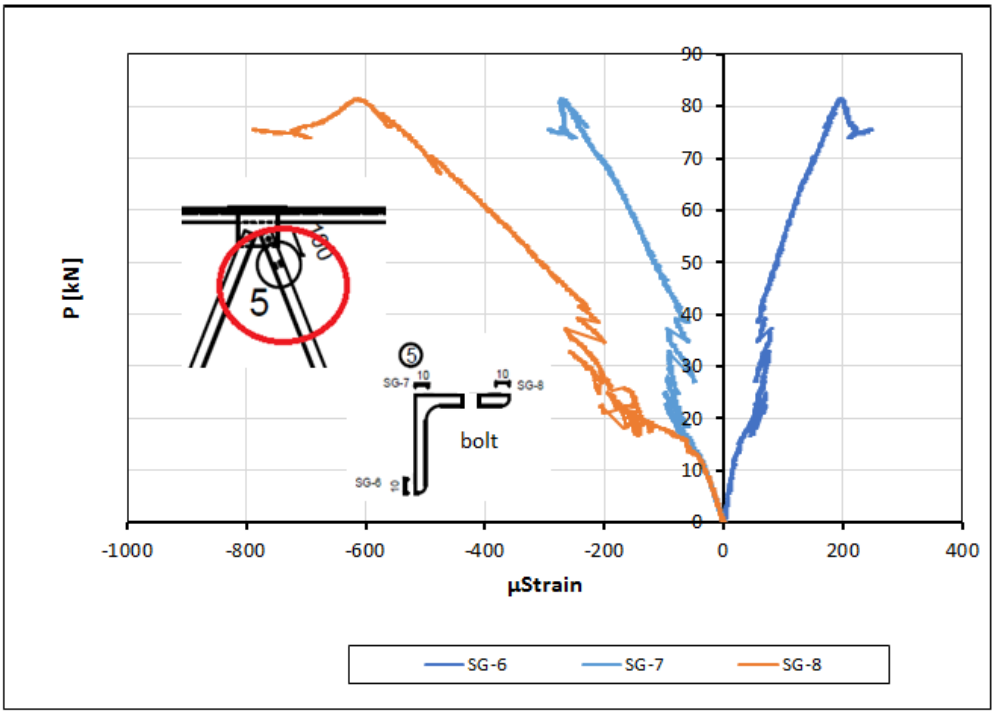

Figure 7.40: Tower D-2S. Strains at top section of 1st floor compression brace

8 Summary and conclusions

Six (6) experimental full-scale tests on angle sections lattice towers were carried out during Task 2.5 of work package WP2 of the ANGELHY project. The test campaign was realized at the Laboratory of the Institute of Steel Structures NTUA. The towers were subjected to pushover loading, i.e. to a horizontal force at their tops that was gradually increased until failure. The members in four (4) tested towers were exclusively from steel, while in two (2) towers some members were strengthened by FRP plates.

Depending on the connection behavior, three phases of response could be distinguished. In phase A bolts transfer shear forces through friction. In phase B slip occurs in the bolts, which come in contact with their bearing surfaces. In phase C all bolts transfer load through bearing. During phase B twist of the towers was recorded. In all tests, failure occurred in members as anticipated. Failure was due to flexural buckling around the weak axis. Braces buckled towards the heel (maximum compression in the lips), legs towards the lips ((maximum compression in the heel).

The results of all tests are summarized in Table 8.1. The load – top displacement curves of all specimens are illustrated in Figure 8.1.

Table 8.1: Summary of results for all tests

Tower No	1	2	3	4	5	6
Specimen designation	O-1	O-2	O1-S	D-1	D-2	D-2S
Failed member	Brace	Leg	Strengthened brace	Brace	Leg	Strengthened leg
Failure mode	Weak axis flexural buckling					
Failure load	39 kN	106,5 kN	54,5 kN	38,5 kN	78,5 kN	81,5 kN
Stiffness phase A kN/m	1422	1611 (1683) in 2nd test	1562	1439	1615	1490
Stiffness phase B kN/m	271	529	398	287	299	195
Stiffness phase C kN/m	714	981	766	575	708	964

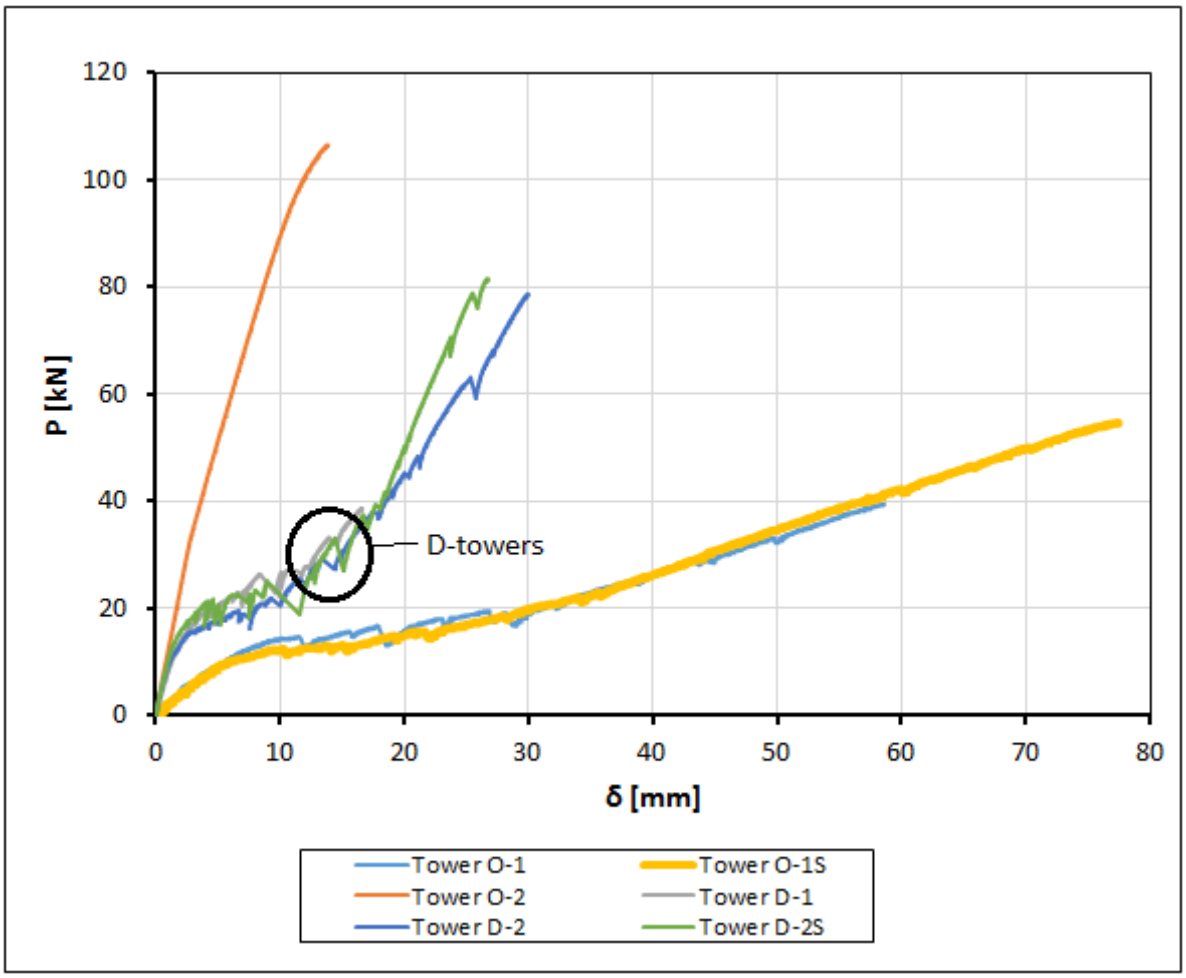

Figure 8.1: Load – top displacement curves for all towers

References

[1] EN ISO 6892-1 (2010) Metallic materials - Tensile testing - Part 1: Method of test at room temperature

List of Figures

List of Tables

Annex A

Construction drawings of specimens

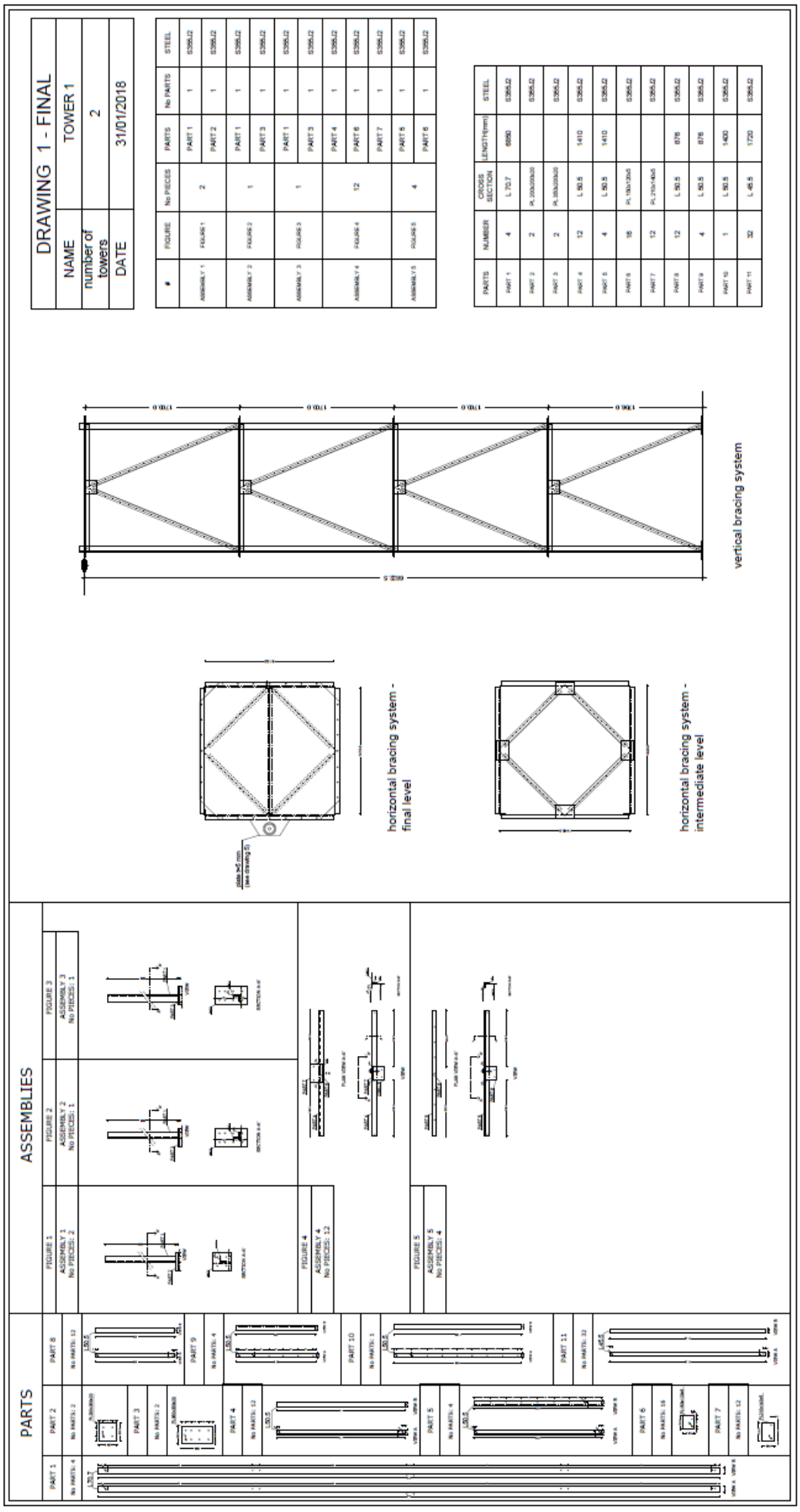
DRAWING 1 - FINAL
NAME
TOWER 1
number of towers
2
DATE
31/01/2018
vertical bracing system
horizontal bracing system - final level
horizontal bracing system - intermediate level
ASSEMBLIES
PARTS

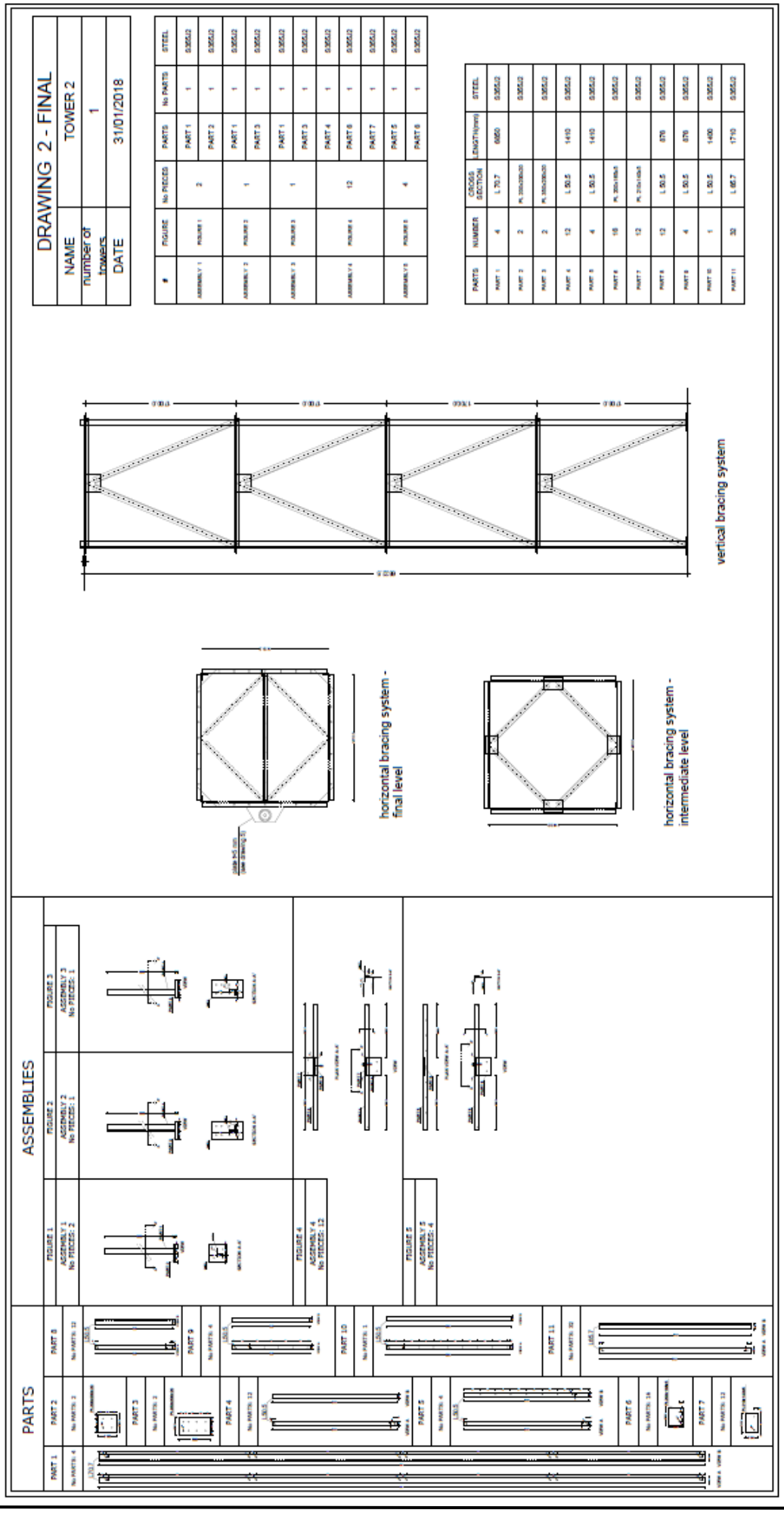
DRAWING 2 - FINAL
NAME
TOWER 2
number of towers
1
DATE
31/01/2018
vertical bracing system
horizontal bracing system - final level
horizontal bracing system - intermediate level
PARTS
ASSEMBLIES

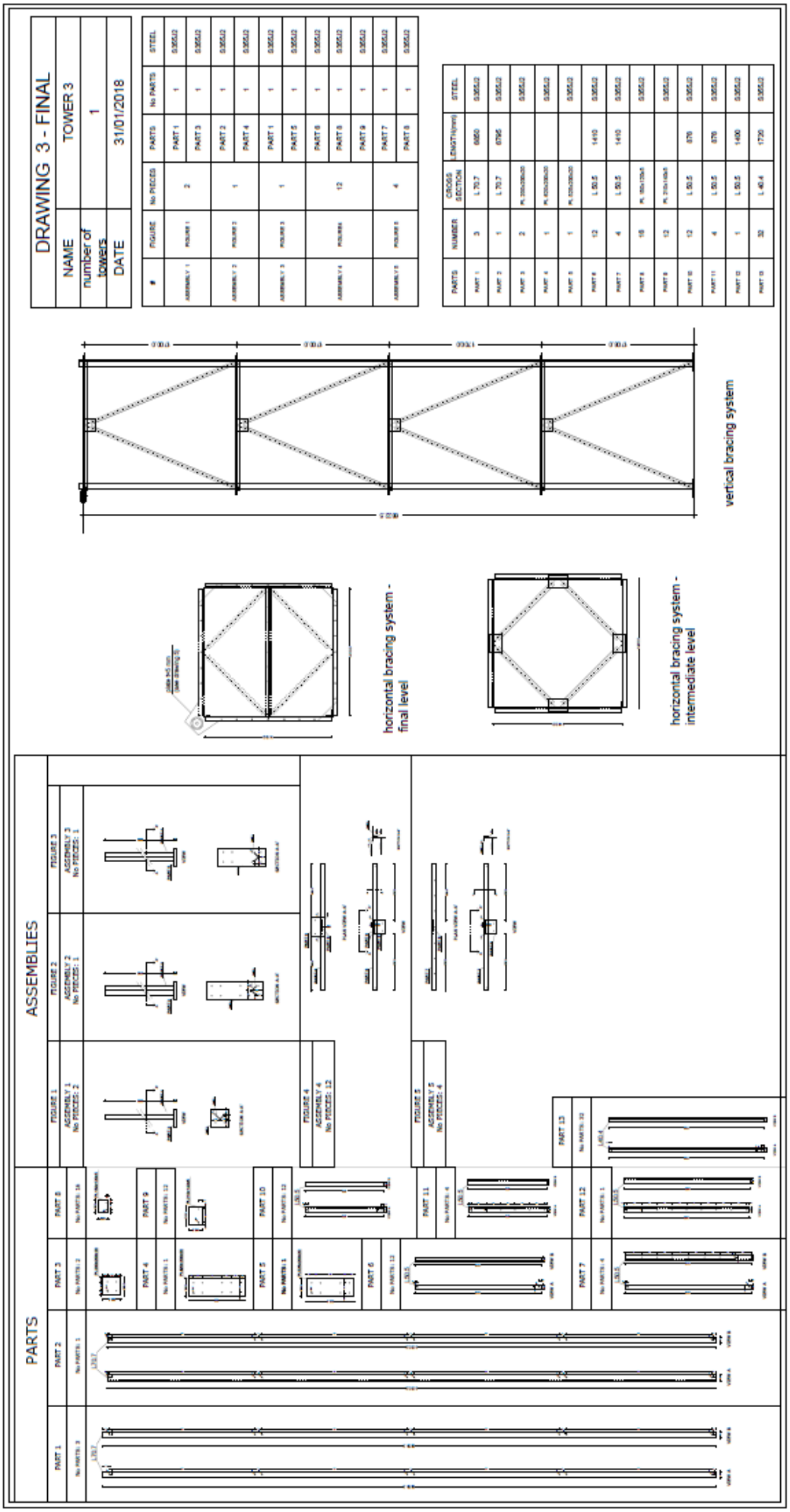
DRAWING 3 - FINAL
NAME
TOWER 3
number of towers
1
DATE
31/01/2018
vertical bracing system
horizontal bracing system - final level
horizontal bracing system - intermediate level
ASSEMBLIES
PARTS

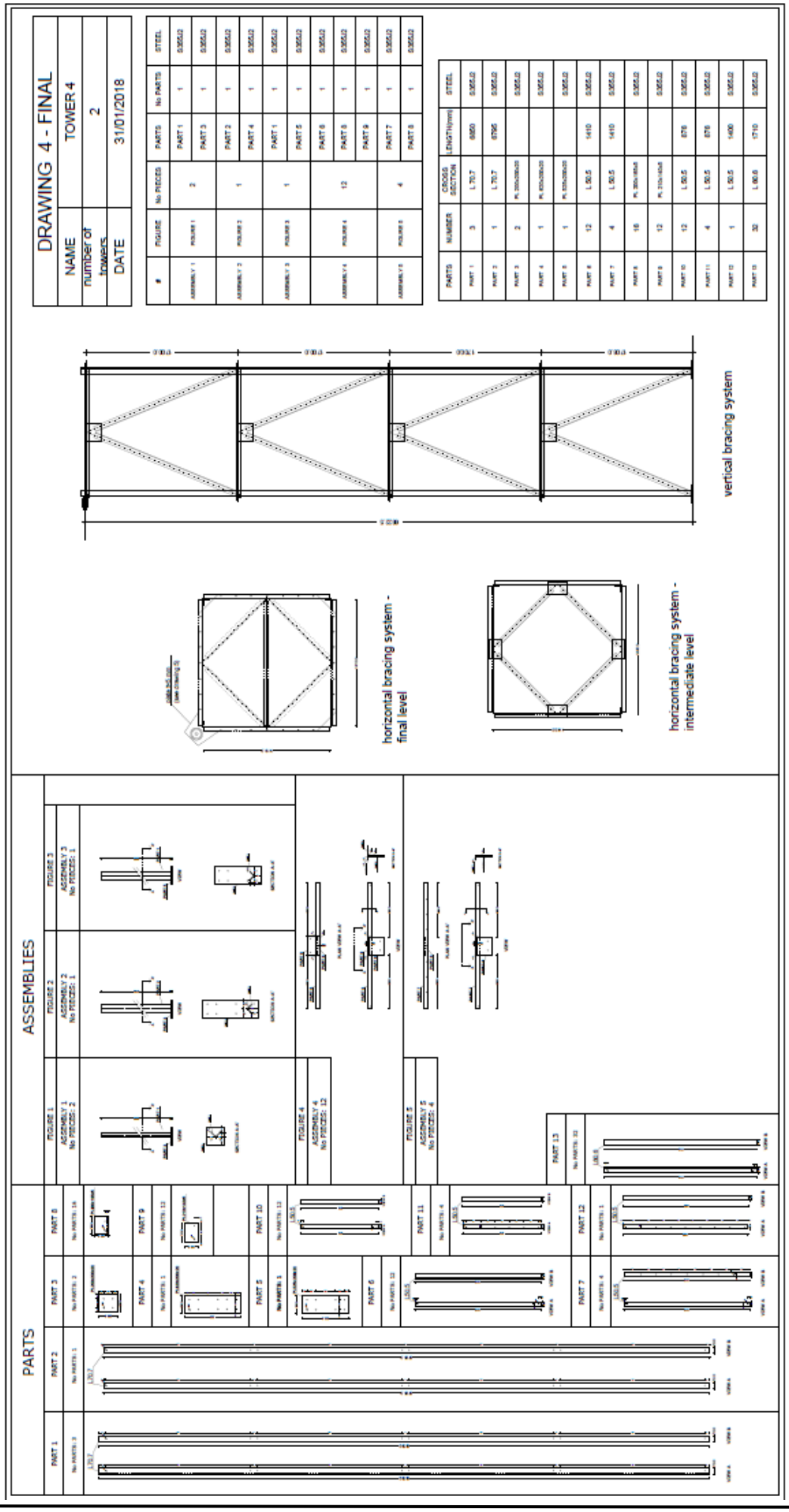
DRAWING 4 - FINAL
NAME
TOWER 4
number of towers
2
DATE
31/01/2018
vertical bracing system
horizontal bracing system - final level
horizontal bracing system - intermediate level
ASSEMBLIES
PARTS

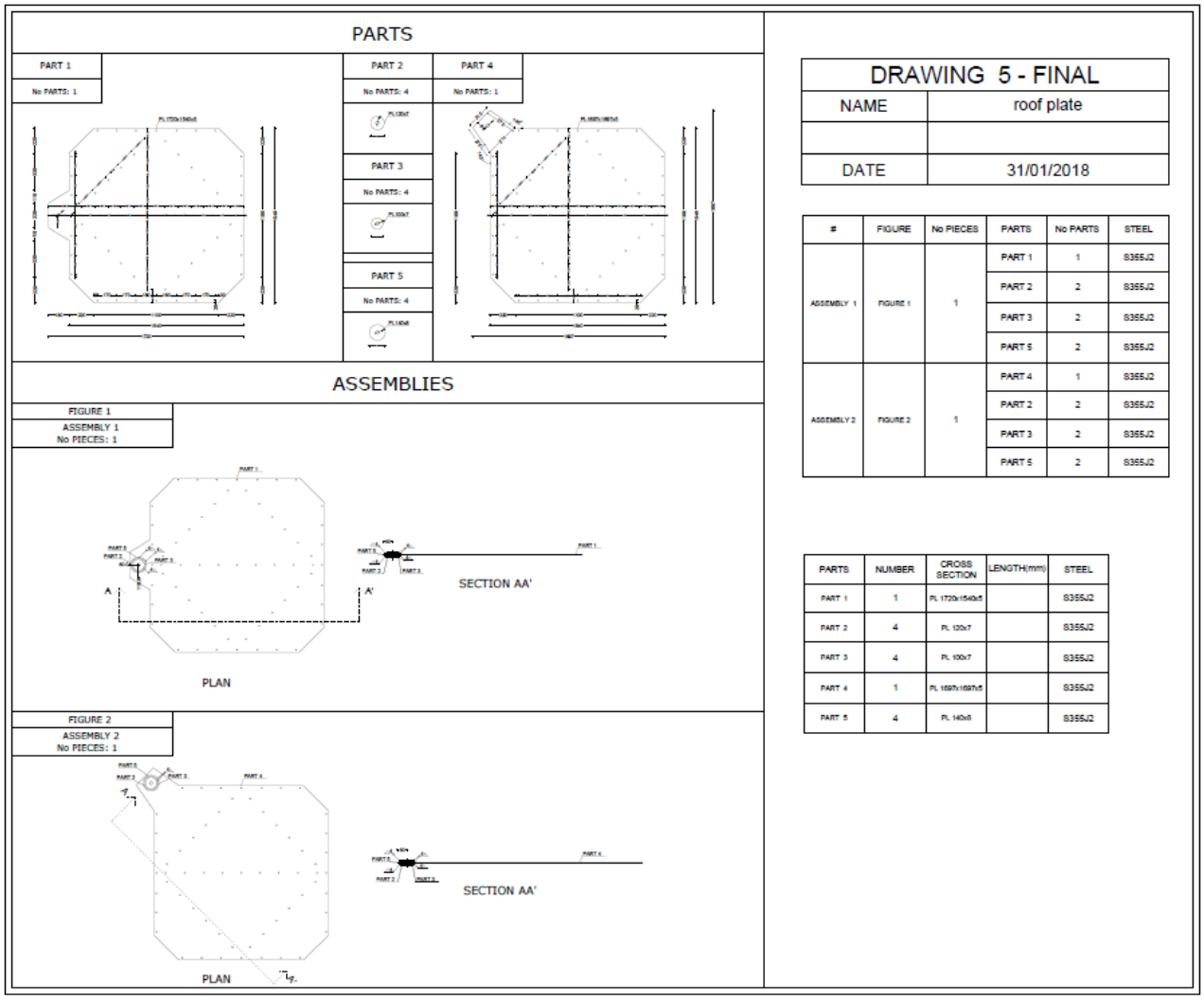

DRAWING 5 - FINAL	
NAME	roof plate
DATE	31/01/2018

#	FIGURE	No PIECES	PARTS	No PARTS	STEEL
ASSEMBLY 1	FIGURE 1	1	PART 1	1	S355J2
			PART 2	2	S355J2
			PART 3	2	S355J2
			PART 5	2	S355J2
ASSEMBLY 2	FIGURE 2	1	PART 4	1	S355J2
			PART 2	2	S355J2
			PART 3	2	S355J2
			PART 5	2	S355J2

PARTS	NUMBER	CROSS SECTION	LENGTH(mm)	STEEL
PART 1	1	PL 1720x1540x5		S355J2
PART 2	4	PL 120x7		S355J2
PART 3	4	PL 100x7		S355J2
PART 4	1	PL 1697x1697x5		S355J2
PART 5	4	PL 140x8		S355J2

Annex B

Construction drawings for base structure

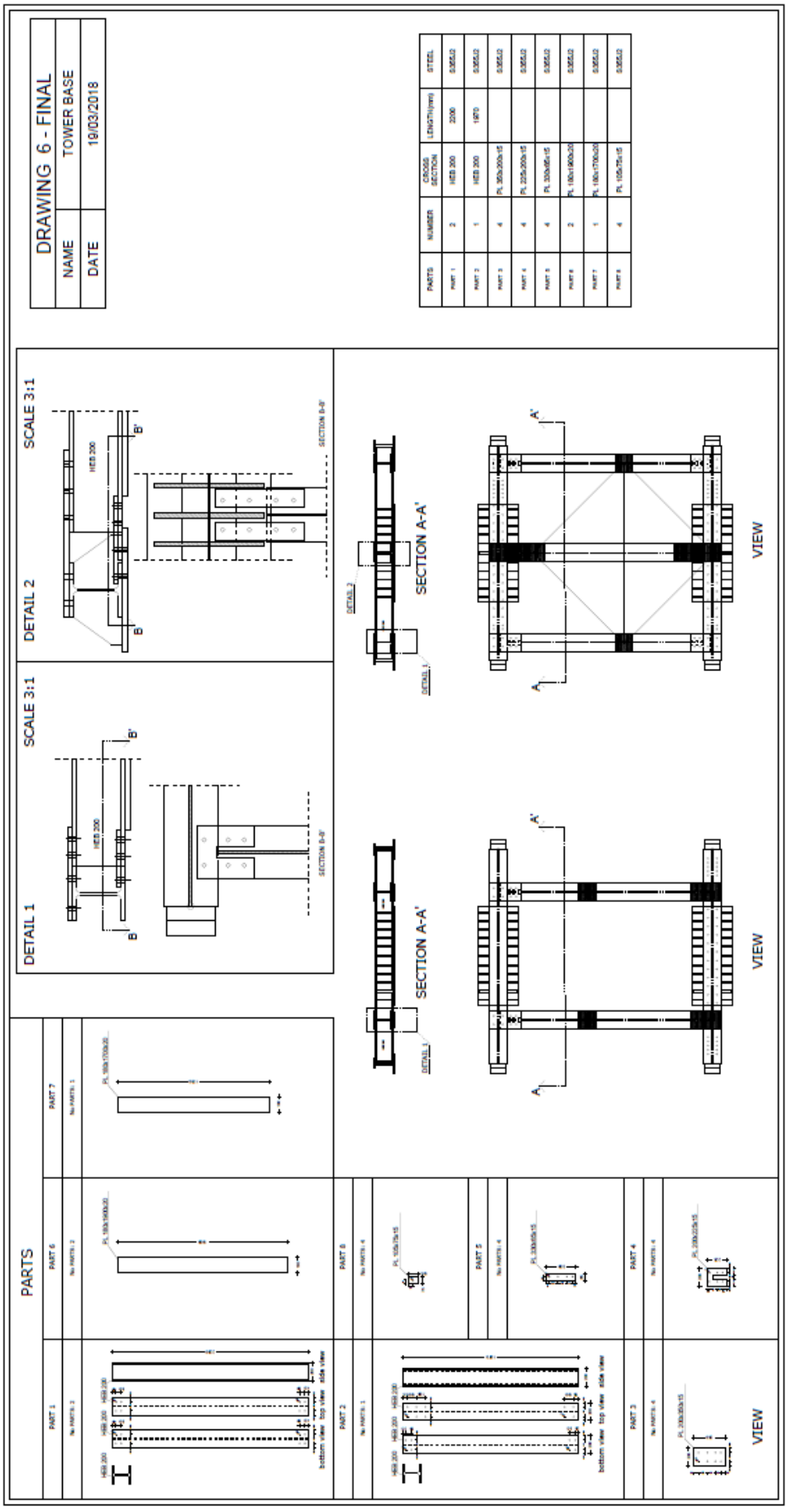

Annex C

Measured material properties

SIKA Certificate for CFRP plates (excerpts)

CERTIFICATE OF COMPLIANCE
FOR SIKA CARBODUR® CFRP PLATES

BUILDING TRUST

CONTACT	Annika Baier	PHONE	+41 58 436 4043
	Corporate Product Engineer	E-MAIL	baier.annika@ch.sika.com
	Structural Bonding	DATE	October 21. 2019

Reference number:	CD_X0870901_S512
Products tested:	Sika CarboDur® S512
Batch number of tested products:	Lot. No. X0870901
Production site:	Sika Construction 1168

Properties	QC specifications	QC test results	Test Method used
Width [mm]	48.5 – 51.5	50.33	EN 2561
Thickness [mm]	1.17 – 1.3	1.20	EN 2561
Glass Transition Temperature [°C]	> 100	119	EN 1006
Tensile Strength [MPa]	> 2800	3187	EN 2561
Tensile strain [%]	> 1.7	1.84	EN 2561
Tensile Modulus [MPa]	> 160	174	EN 2561

Width (mm)	Thickness (mm)	Glass Transition Temperature EN61006 (°C)	Tensile Strength EN2561 (MPa)	Tensile Strain EN2561 (%)	Tensile modulus EN 2561 (GPa) 10 to 50% load	Tensile modulus ISO 527-5 (GPa) 0.05 to 0.25% strain	Tensile modulus ASTM 3039 (Gpa) 0.1 to 0.3% strain
50,33	1,20	119	3187	1,84	174	160	162

Coupon test for section L 70.70.7

Εθνικό Μετσόβιο Πολυτεχνείο
Εργαστήριο Μεταλλικών Κατασκευών
National Technical University of Athens
Institute of Steel Structures

ΔΟΚΙΜΗ ΕΦΕΛΚΥΣΜΟΥ
TENSILE MATERIAL TEST

Εργοδότης / Company: *ANGELHY* | Έργο / Project: *63/2170 ΕΛΕ ΕΜΠ* | Ημερομηνία δοκιμής / Date of testing: 22/10/2019

Κωδικός δοκιμίου / Specimen code	Σχήμα δοκιμίου / Shape of specimen	Πάχος δοκιμίου στα παράλληλα άκρα / Thickness of parallel section			Πλάτος δοκιμίου στα παράλληλα άκρα / Width of parallel section			Μήκος παρά/λων άκρων / Specimen Gage length	Αρχικό εύρος μηκυνσιο-μέτρου / Gage length extension meter	Θερμ/σια δοκιμής / Testing room temp/re	Σχετική υγρασία χώρου δοκιμής / Relative humidity testing room	Ρυθμός φόρτισης / Stress rate	Δειγ/ψία δεδ/ων / Data sampling frequency	Άνω όριο τάσης διαρροής / Upper tensile stress at yield	Άνω όριο ανηγμένη επιμήκ-υνση διαρροής / Upper tensile strain at yield	Κάτω όριο τάσης διαρροής / Lower tensile stress at yield	Κάτω όριο ανηγμένη επιμήκ-υνση διαρροής / Lower tensile strain at yield	Οριακή τάσης / Ultimate tensile stress	Ανηγμένη επιμήκ-υνση οριακής τάσης / Ultimate tensile strain	Μέτρο Ελαστ/τας / Modulus of Elasticity
		min	max	mean	min	max	mean	L_o	L_e	T	RH	R	f	fy, up	εy, up	$f_{y,Low}$	$\varepsilon_{y,Low}$	f_u	ε_u	E
		[mm]	[mm]	[mm]	[mm]	[mm]	[mm]	[mm]	[mm]	[°C]	[%]	[MPa/s]	[Hz]	[MPa]	[%]	[MPa]	[%]	[MPa]	[%]	[GPa]
L70.7 1	*Rectangular*	-	-	*7.13*	-	-	*20.56*	*90*	*50*	*25*	*40*	*1.0*	*11.1*	*308.31*	*0.112*	*297.01*	*2.491*	*435.17*	*21.495*	*207*

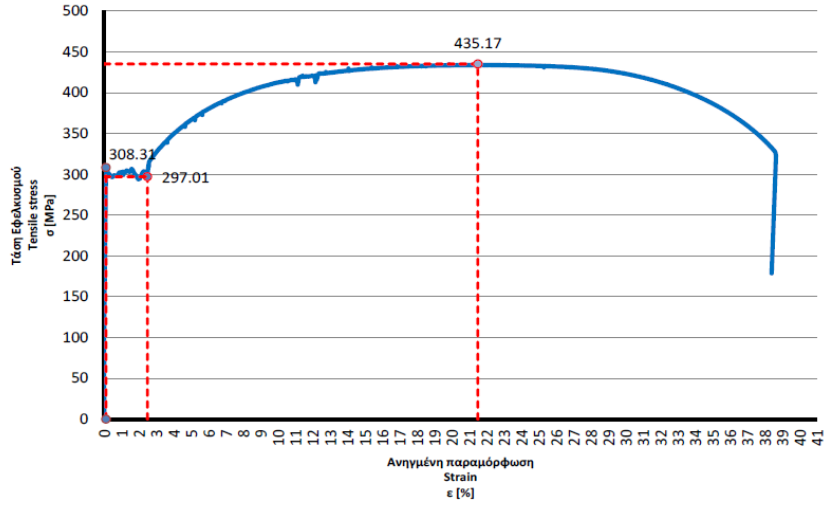

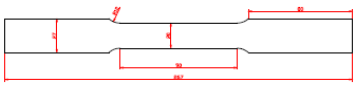

Σχέδιο δοκιμίου σύμφωνα με EN ISO 6892-1
Specimen drawing , in accordance to EEN ISO 6892-1

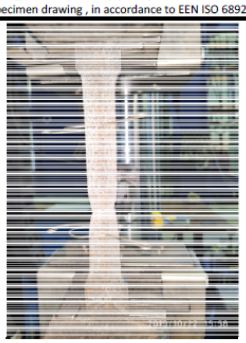

Φωτογραφία αστοχίας δοκιμίου
Photo of specimen failure

Στοιχεία μηχανής δοκιμών / Tensile testing machine	Τύπος Μηχανής δοκιμών / Type of testing machine	300LX Clamping	Τύπος μηκυνσιομέτρου / Type extensometer	*2630-113 clips +50/- B2/0,+70*	Πρότυπο συμμόρφωσης / Reference Standard:	*EN ISO 6892-1*	Υπεύθυνος δοκιμών / Tested by:

Coupon test for section L 60.60.6

Εθνικό Μετσόβιο Πολυτεχνείο
Εργαστήριο Μεταλλικών Κατασκευών
National Technical University of Athens
Institute of Steel Structures

ΔΟΚΙΜΗ ΕΦΕΛΚΥΣΜΟΥ
TENSILE MATERIAL TEST

Εργοδότης / Company: *ANGELHY* | Έργο / Project: *63/2170 ΕΛΕ ΕΜΠ* | Ημερομηνία δοκιμής / Date of testing: 4/11/2019

Κωδικός δοκιμίου / Specimen code	Σχήμα δοκιμίου / Shape of specimen	Πάχος δοκιμίου στα παράλληλα άκρα / Thickness of parallel section			Πλάτος δοκιμίου στα παράλληλα άκρα / Width of parallel section			Μήκος παρά/λων άκρων / Specimen Gage length	Αρχικό εύρος μηκυνσιο-μέτρου / Gage length extension meter	Θερμ/σια δοκιμής / Testing room temp/re	Σχετική υγρασία χώρου δοκιμής / Relative humidity testing room	Ρυθμός φόρτισης / Stress rate	Δειγ/ψία δεδ/ων / Data sampling frequency	Διαρροή στο 0,2% / Yield at 0,2%	Ανηγμένη επιμήκ-υνση στο 0,2% / Strain at 0,2%	Κάτω όριο τάσης διαρροής / Lower tensile stress at yield	Κάτω όριο ανηγμένη επιμήκ-υνση διαρροής / Lower tensile strain at yield	Οριακή τάσης / Ultimate tensile stress	Ανηγμένη επιμήκ-υνση οριακής τάσης / Ultimate tensile strain	Μέτρο Ελαστ/τας / Modulus of Elasticity
		min	max	mean	min	max	mean	L_o	L_e	T	RH	R	f	fy,0.2%	εy,0.2%	$f_{y,Low}$	$\varepsilon_{y,Low}$	f_u	ε_u	E
		[mm]	[mm]	[mm]	[mm]	[mm]	[mm]	[mm]	[mm]	[°C]	[%]	[MPa/s]	[Hz]	[MPa]	[%]	[MPa]	[%]	[MPa]	[%]	[GPa]
L 60.6 1	*Rectangular*	-	-	*6.22*	-	-	*20.62*	*90*	*50*	*22*	*66*	*0,7*	*11,1*	*280,30*	*0,427*	*279,70*	*0,943*	*403,85*	*21,240*	*209*

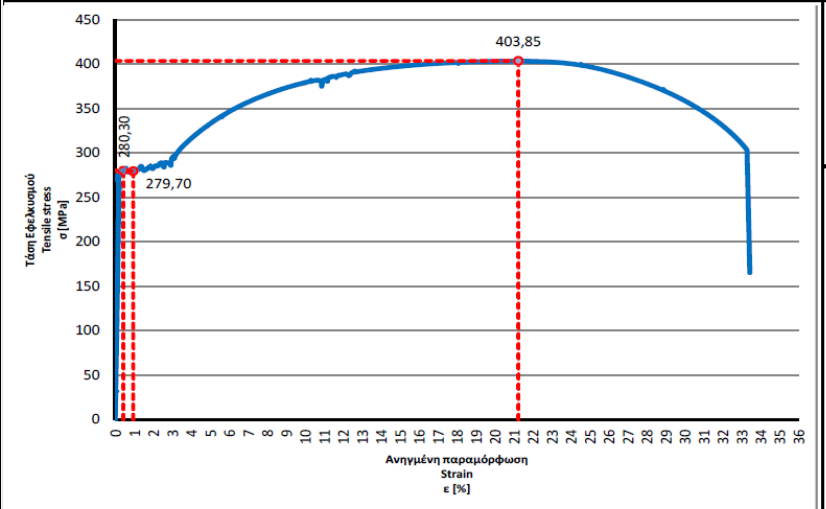

Σχέδιο δοκιμίου σύμφωνα με EN ISO 6892-1
Specimen drawing , in accordance to EN ISO 6892-1

Φωτογραφία αστοχίας δοκιμίου
Photo of specimen failure

Στοιχεία μηχανής δοκιμών / Tensile testing machine	Τύπος Μηχανής δοκιμών / Type of testing machine	Instron 300LX	Τύπος μηκυνσιομέτρου / Type extensometer	*2630-113 clips +50/- B2/0,+70*	Πρότυπο συμμόρφωσης / Reference Standard:	*EN ISO 6892-1*	Υπεύθυνος δοκιμών / Tested by:

Coupon test for section L 40.40.4

Εθνικό Μετσόβιο Πολυτεχνείο
Εργαστήριο Μεταλλικών Κατασκευών
National Technical University of Athens
Institute of Steel Structures

ΔΟΚΙΜΗ ΕΦΕΛΚΥΣΜΟΥ
TENSILE MATERIAL TEST

Εργοδότης / Company: *ANGELHY* | Έργο / Project: *63/2170 ΕΛΕ ΕΜΠ* | Ημερομηνία δοκιμής / Date of testing: 5/11/2019

Κωδικός δοκιμίου / Specimen code	Σχήμα δοκιμίου / Shape of specimen	Πάχος δοκιμίου στα παράλληλα άκρα / Thickness of parallel section			Πλάτος δοκιμίου στα παράλληλα άκρα / Width of parallel section			Μήκος παρά/λων άκρων / Specimen Gage length	Αρχικό εύρος μηκυνσιόμετρου / Gage length extension meter	Θερμ/σια δοκιμής / Testing room temp/re	Σχετική υγρασία χώρου δοκιμής / Relative humidity testing room	Ρυθμός φόρτισης / Stress rate	Δειγ/ψία δεδ/ων / Data sampling frequency	Άνω όριο τάσης διαρροής / Upper tensile stress at yield	Άνω όριο ανηγμένη επιμήκυνση διαρροής / Upper tensile strain at yield	Κάτω όριο τάσης διαρροής / Lower tensile stress at yield	Κάτω όριο ανηγμένη επιμήκυνση διαρροής / Lower tensile strain at yield	Οριακή τάσης / Ultimate tensile stress	Ανηγμένη επιμήκυνση οριακής τάσης / Ultimate tensile strain	Μέτρο Ελαστ/τας / Modulus of Elasticity
		min	max	mean	min	max	mean	L_o	L_e	T	RH	R	f	fy, up	εy, up	$f_{y,Low}$	$\varepsilon_{y,Low}$	f_u	ε_u	E
		[mm]	[mm]	[mm]	[mm]	[mm]	[mm]	[mm]	[mm]	[°C]	[%]	[MPa/s]	[Hz]	[MPa]	[%]	[MPa]	[%]	[MPa]	[%]	[GPa]
L 40.4 1	*Rectangular*	-	-	*4,18*	-	-	*20,34*	*90*	*50*	*22*	*60*	*1,3*	*11,1*	*325,72*	*0,167*	*306,56*	*1,420*	*435,37*	*22,660*	*210*

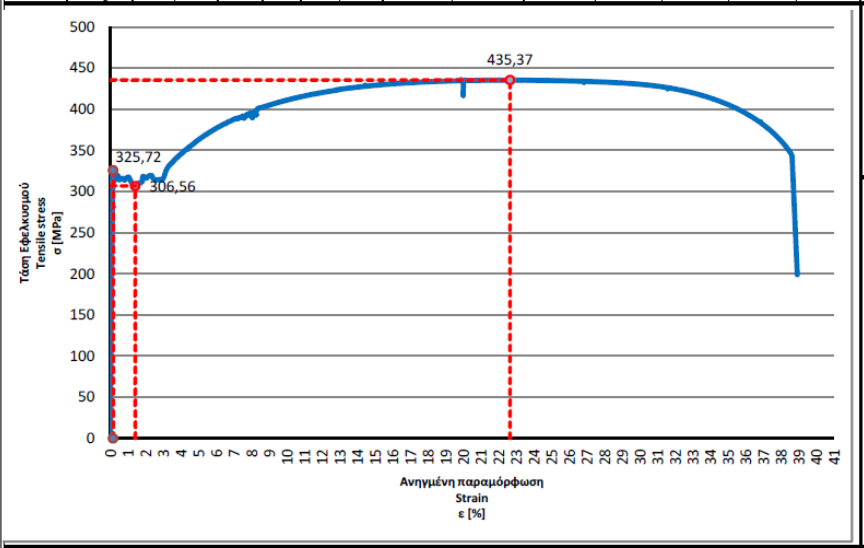

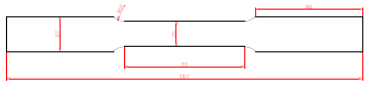

Σχέδιο δοκιμίου σύμφωνα με EN ISO 6892-1
Specimen drawing , in accordance to EN ISO 6892-1

Φωτογραφία αστοχίας δοκιμίου
Photo of specimen failure

Στοιχεία μηχανής δοκιμών / Tensile testing machine	Τύπος Μηχανής δοκιμών / Type of testing machine	Instron 300LX	Τύπος μηκυνσιόμετρου / Type extensometer	*2630-113 clips +50/- B2/0,+70*	Πρότυπο συμμόρφωσης / Reference Standard:	*EN ISO 6892-1*	Υπεύθυνος δοκιμών / Tested by:

Coupon test for section L 45.45.5

Εθνικό Μετσόβιο Πολυτεχνείο
Εργαστήριο Μεταλλικών Κατασκευών
National Technical University of Athens
Institute of Steel Structures

ΔΟΚΙΜΗ ΕΦΕΛΚΥΣΜΟΥ
TENSILE MATERIAL TEST

Εργοδότης / Company: *ANGELHY* | Έργο / Project: *63/2170 ΕΛΕ ΕΜΠ* | Ημερομηνία δοκιμής / Date of testing: 5/11/2019

Κωδικός δοκιμίου / Specimen code	Σχήμα δοκιμίου / Shape of specimen	Πάχος δοκιμίου στα παράλληλα άκρα / Thickness of parallel section			Πλάτος δοκιμίου στα παράλληλα άκρα / Width of parallel section			Μήκος παρά/λων άκρων / Specimen Gage length	Αρχικό εύρος μηκυνσιόμετρου / Gage length extension meter	Θερμ/σια δοκιμής / Testing room temp/re	Σχετική υγρασία χώρου δοκιμής / Relative humidity testing room	Ρυθμός φόρτισης / Stress rate	Δειγ/ψία δεδ/ων / Data sampling frequency	Άνω όριο τάσης διαρροής / Upper tensile stress at yield	Άνω όριο ανηγμένη επιμήκυνση διαρροής / Upper tensile strain at yield	Κάτω όριο τάσης διαρροής / Lower tensile stress at yield	Κάτω όριο ανηγμένη επιμήκυνση διαρροής / Lower tensile strain at yield	Οριακή τάσης / Ultimate tensile stress	Ανηγμένη επιμήκυνση οριακής τάσης / Ultimate tensile strain	Μέτρο Ελαστ/τας / Modulus of Elasticity
		min	max	mean	min	max	mean	L_o	L_e	T	RH	R	f	fy, up	εy, up	$f_{y,Low}$	$\varepsilon_{y,Low}$	f_u	ε_u	E
		[mm]	[mm]	[mm]	[mm]	[mm]	[mm]	[mm]	[mm]	[°C]	[%]	[MPa/s]	[Hz]	[MPa]	[%]	[MPa]	[%]	[MPa]	[%]	[GPa]
L 45.5 1	*Rectangular*	-	-	*4,88*	-	-	*20,28*	*90*	*50*	*22*	*57*	*0,9*	*11,1*	*286,79*	*0,416*	*283,97*	*1,769*	*416,67*	*21,234*	*209*

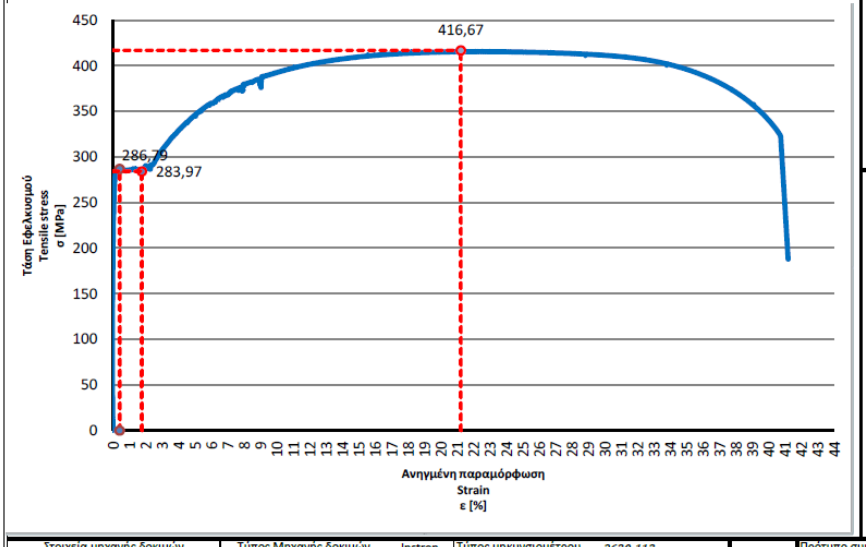

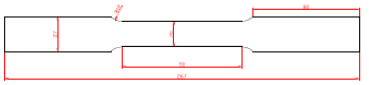

Σχέδιο δοκιμίου σύμφωνα με EN ISO 6892-1
Specimen drawing , in accordance to EN ISO 6892-1

Φωτογραφία αστοχίας δοκιμίου
Photo of specimen failure

Στοιχεία μηχανής δοκιμών / Tensile testing machine	Τύπος Μηχανής δοκιμών / Type of testing machine	Instron 300LX	Τύπος μηκυνσιόμετρου / Type extensometer	*2630-113 clips +50/- B2/0,+70*	Πρότυπο συμμόρφωσης / Reference Standard:	*EN ISO 6892-1*	Υπεύθυνος δοκιμών / Tested by:

Annex D

Measured test results for all towers

TOWER O1

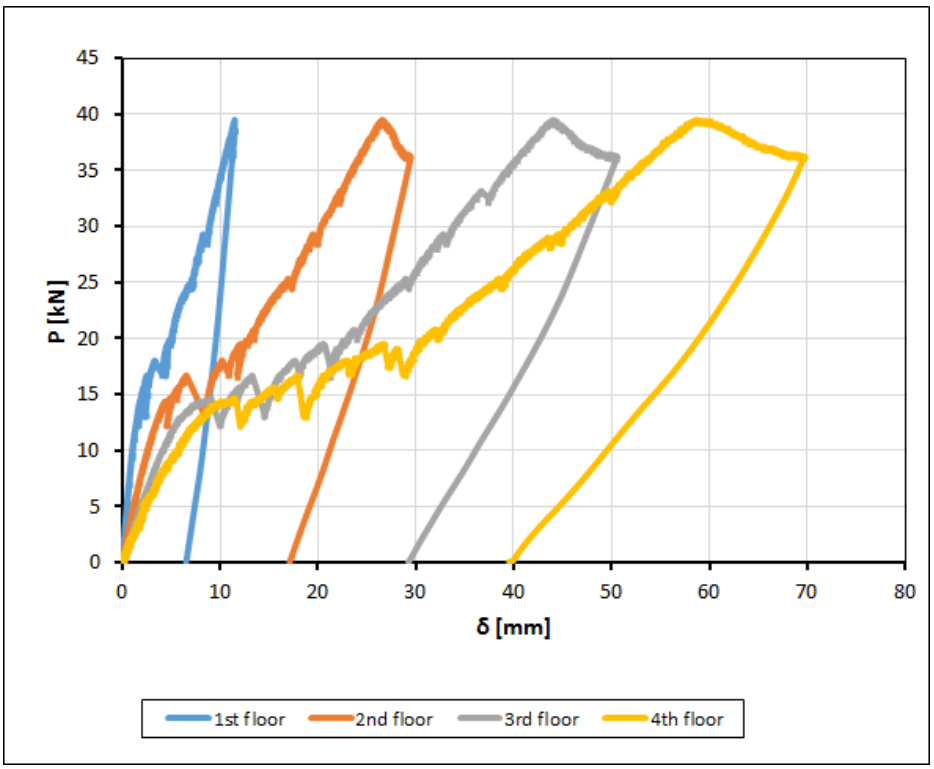

Figure C_O1_1: Load – top displacement curve

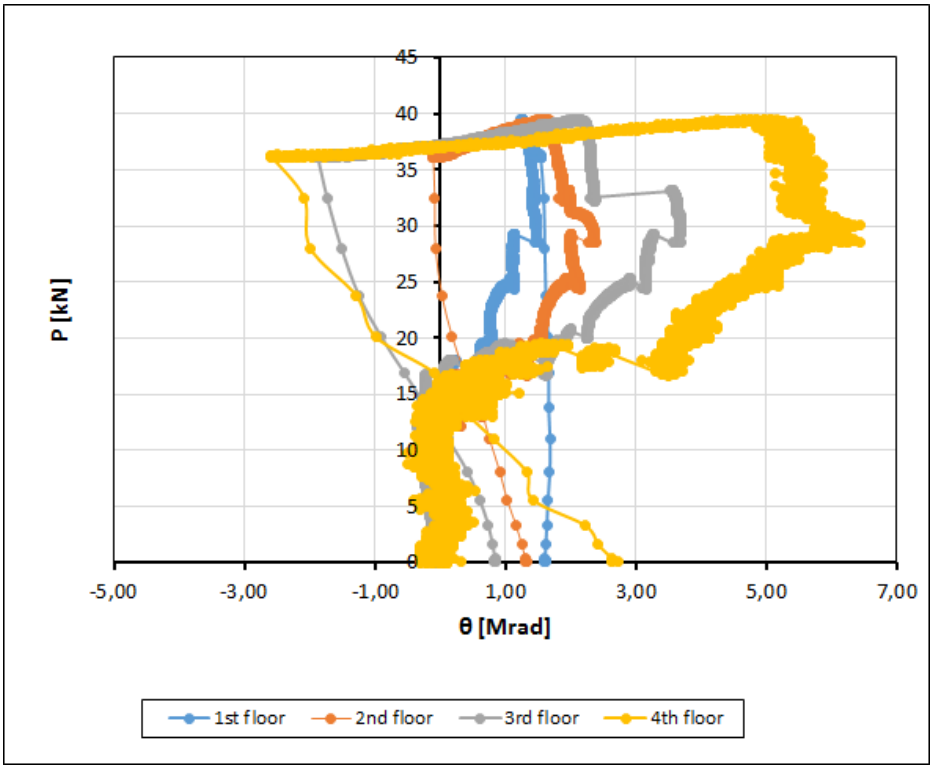

Figure C_O1_2: Load – rotation curve

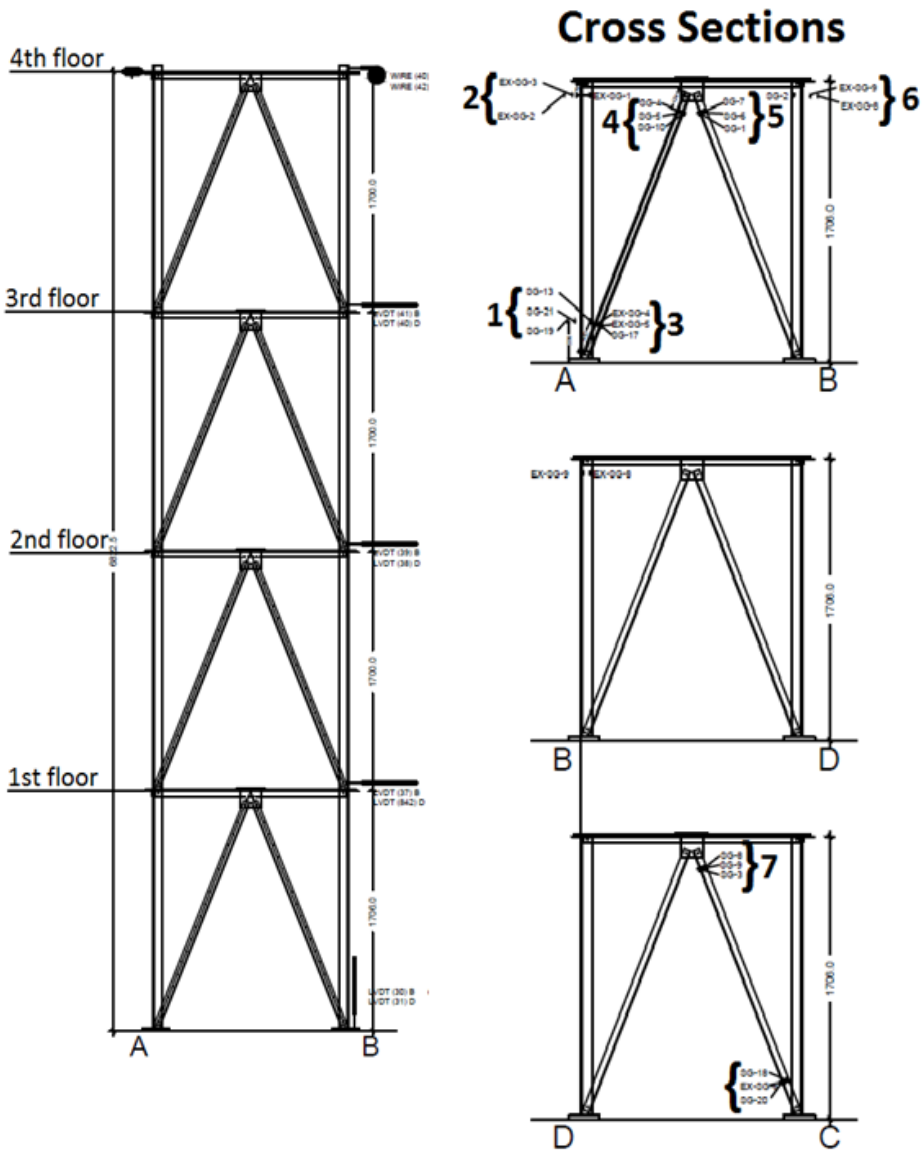

Figure C_O1_3: Cross sections and strain gage numeration

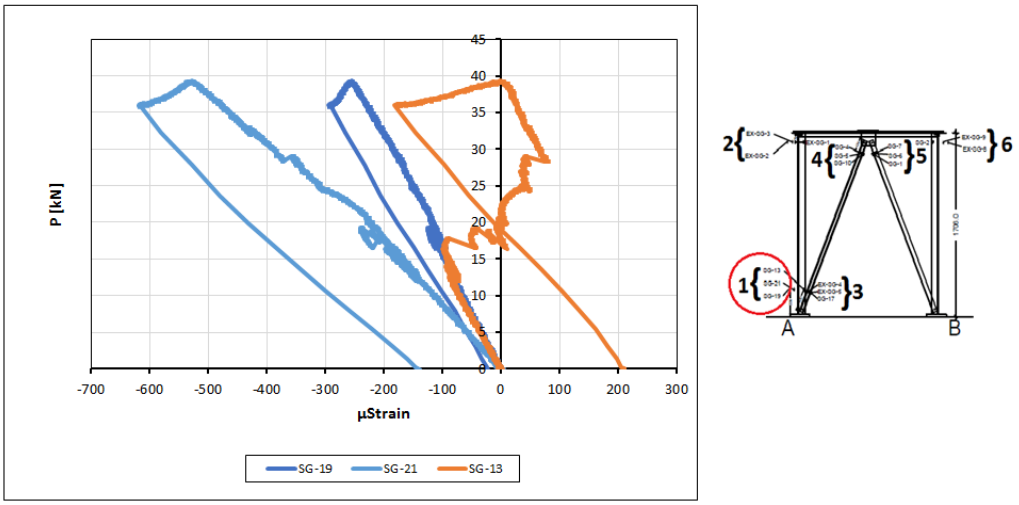

Figure C_O1_4: Strains at cross section 1

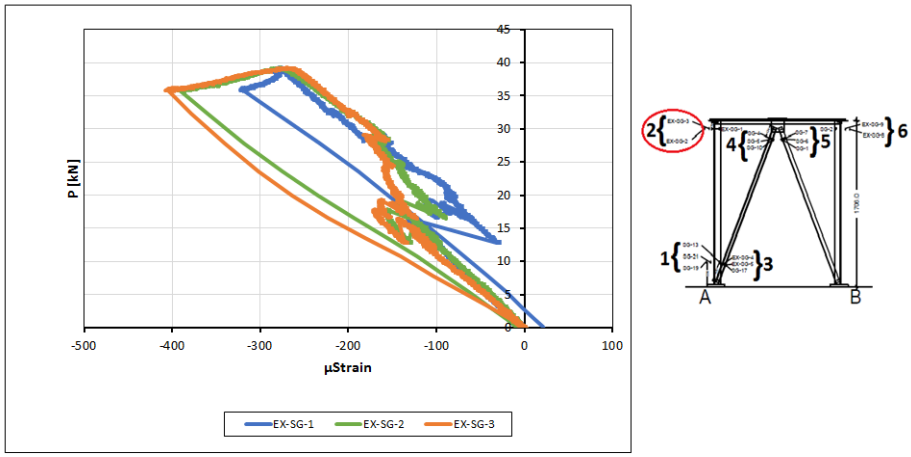

Figure C_O1_5: Strains at cross section 2

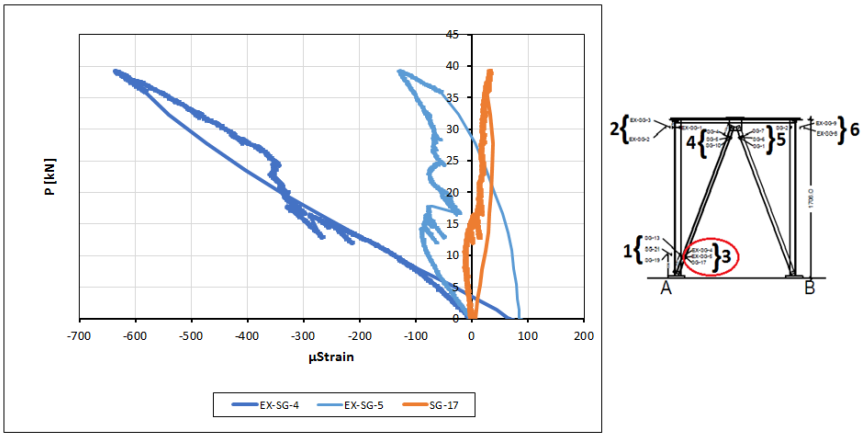

Figure C_O1_6: Strains at cross section 3

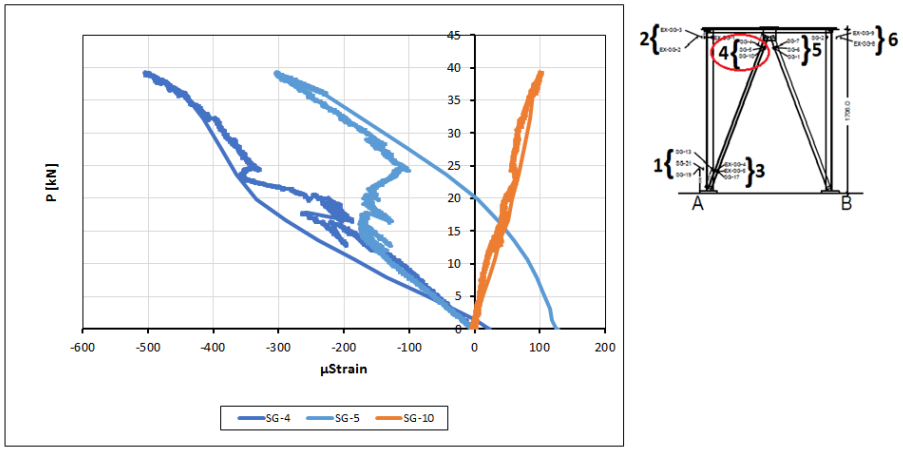

Figure C_O1_7: Strains at cross section 4

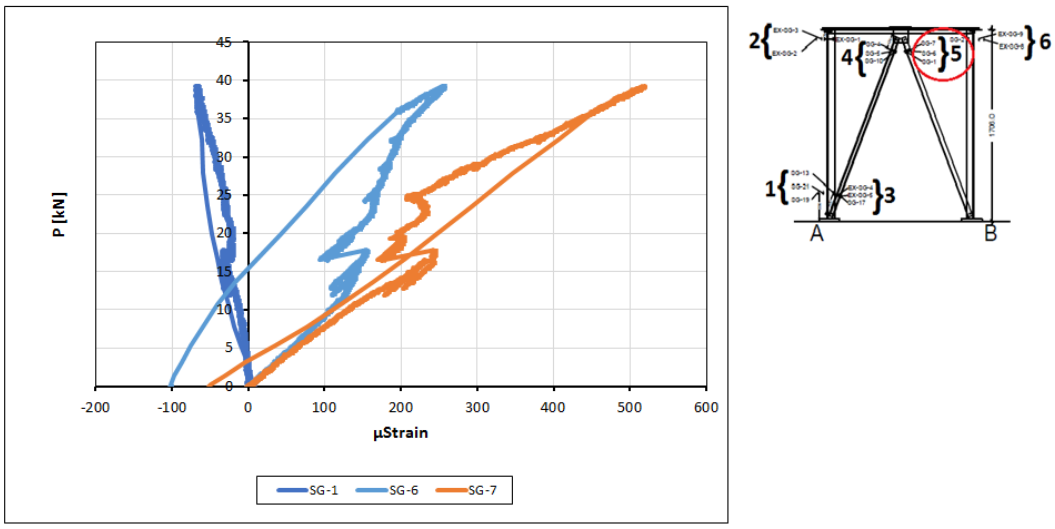

Figure C_O1_8: Strains at cross section 5

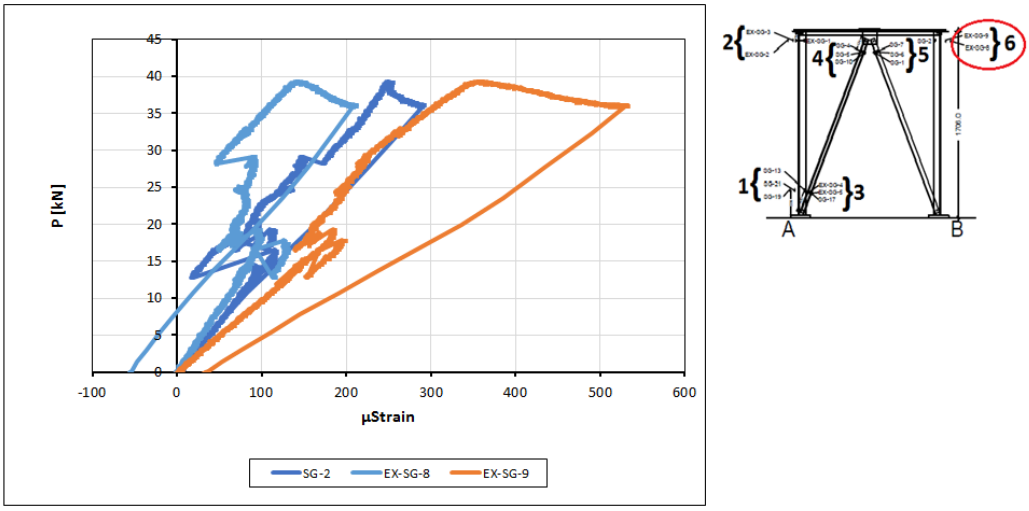

Figure C_O1_9: Strains at cross section 6

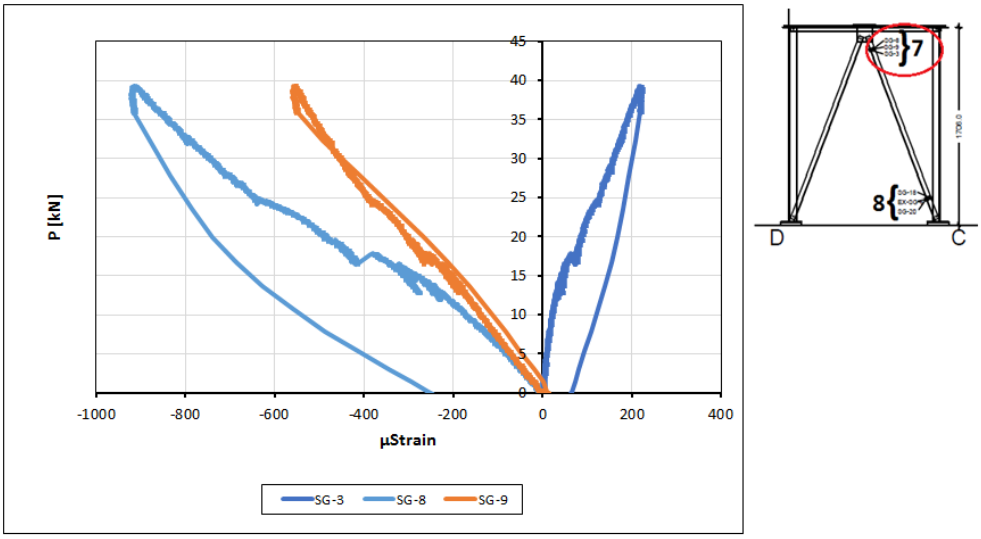

Figure C_O1_10: Strains at cross section 7

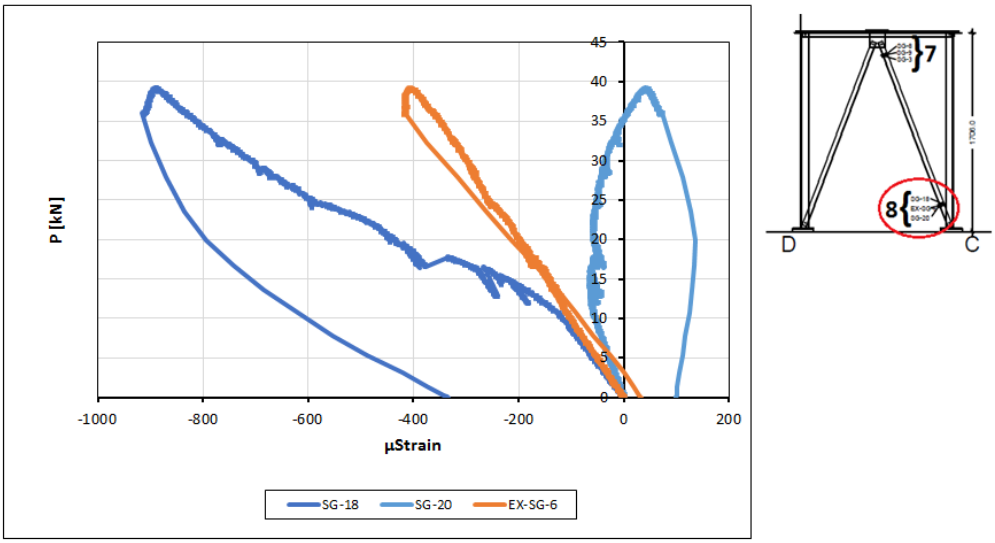

Figure C_O1_11: Strains at cross section 8

TOWER O2

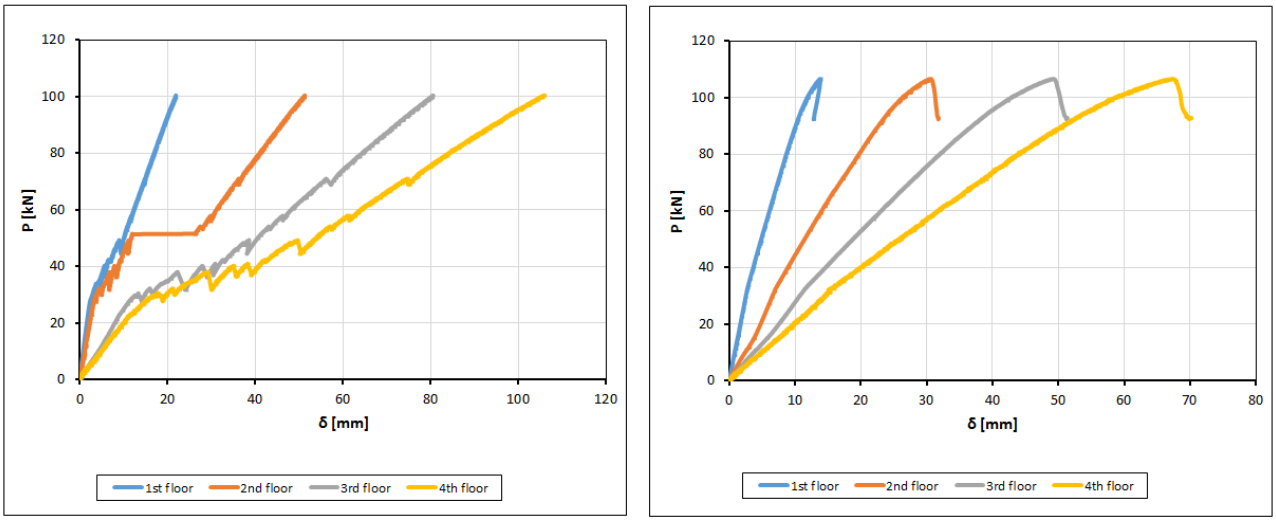

Figure C_O2_1: Load – top displacement curve. Stage 1 – Stage 2

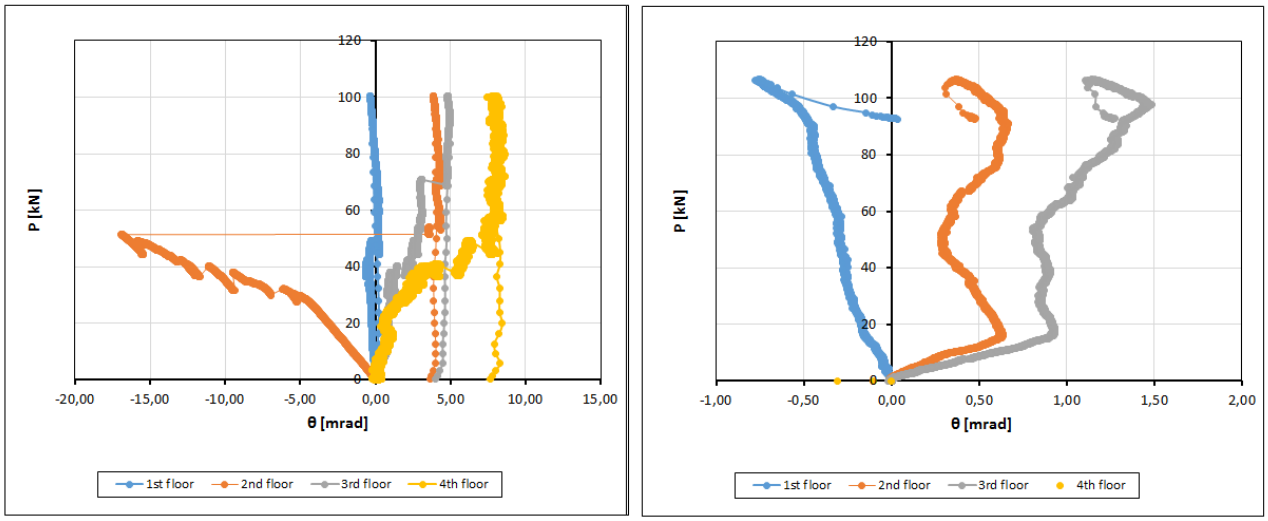

Figure C_O2_2: Load – rotation curve. Stage 1 – Stage 2

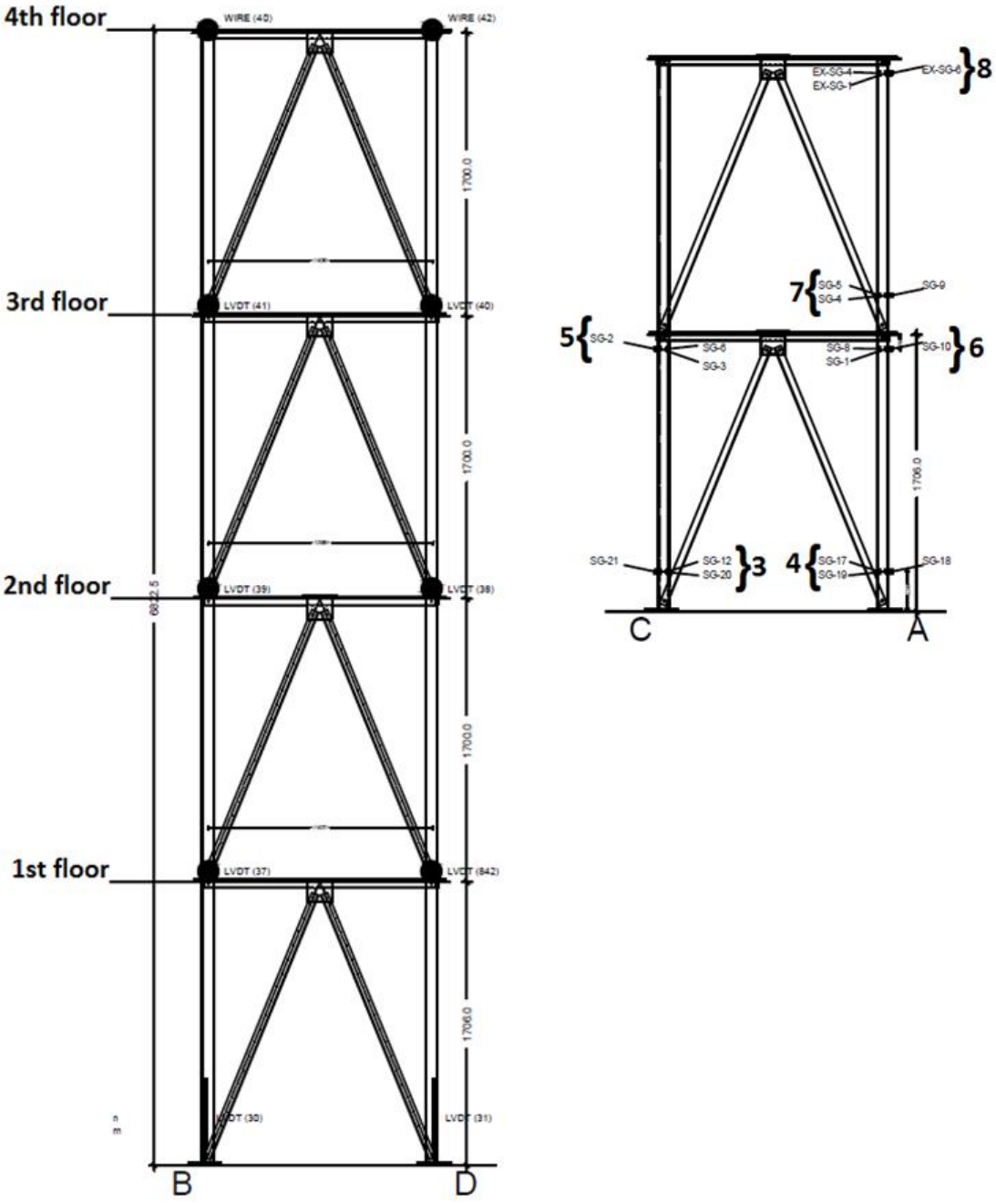

Figure C_O2_3: Cross sections and strain gage numeration

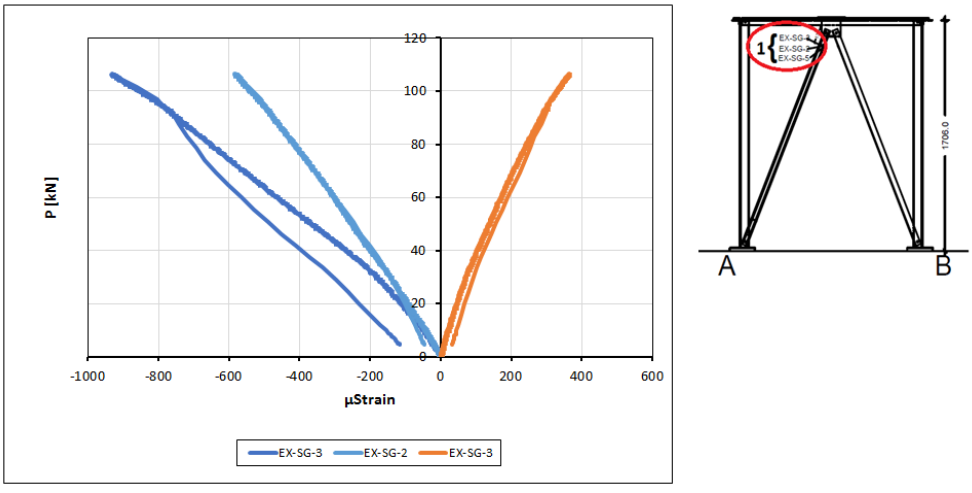

Figure C_O2_4: Strains at cross section 1. Stage 2

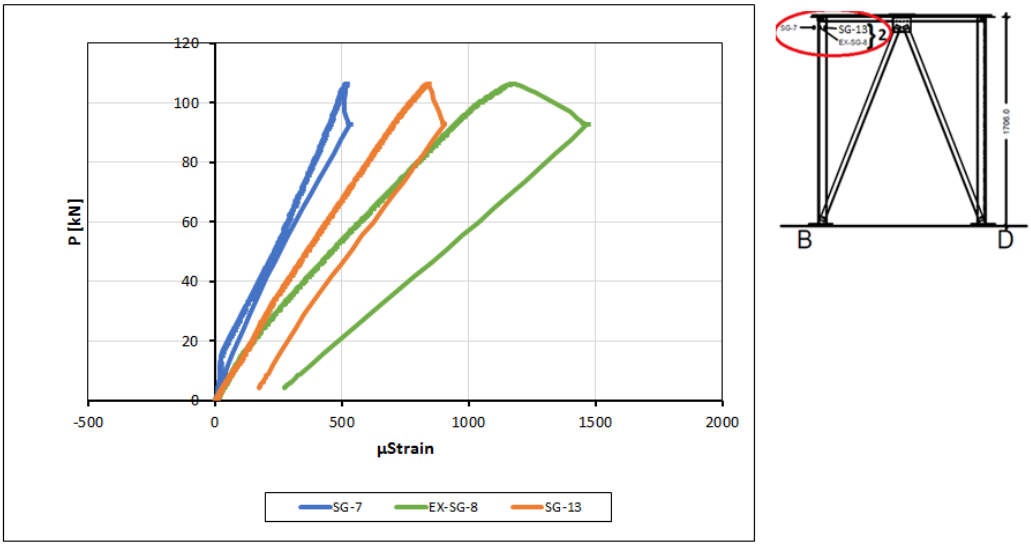

Figure C_O2_5: Strains at cross section 2 Stage 2

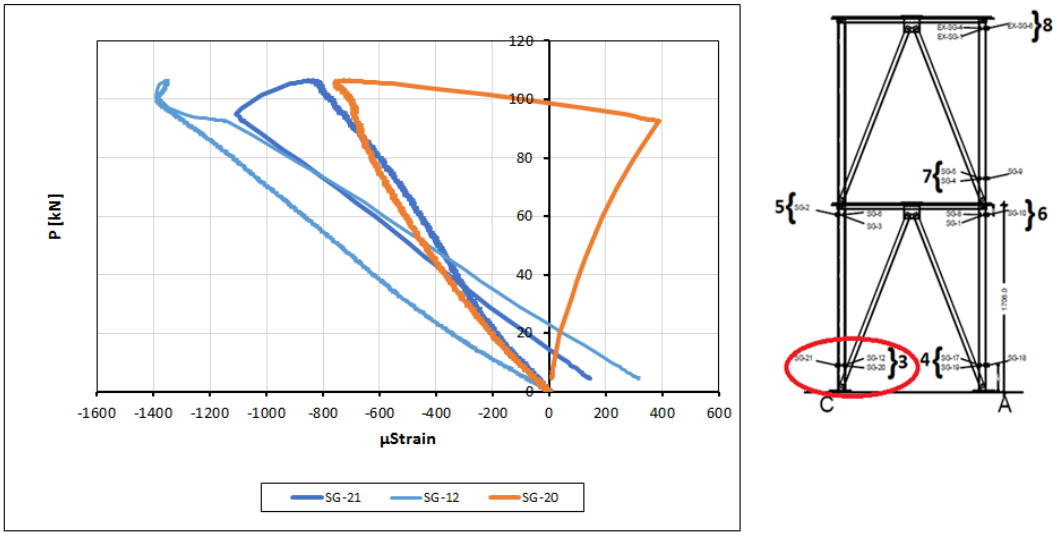

Figure C_O2_6: Strains at cross section 3 Stage 2

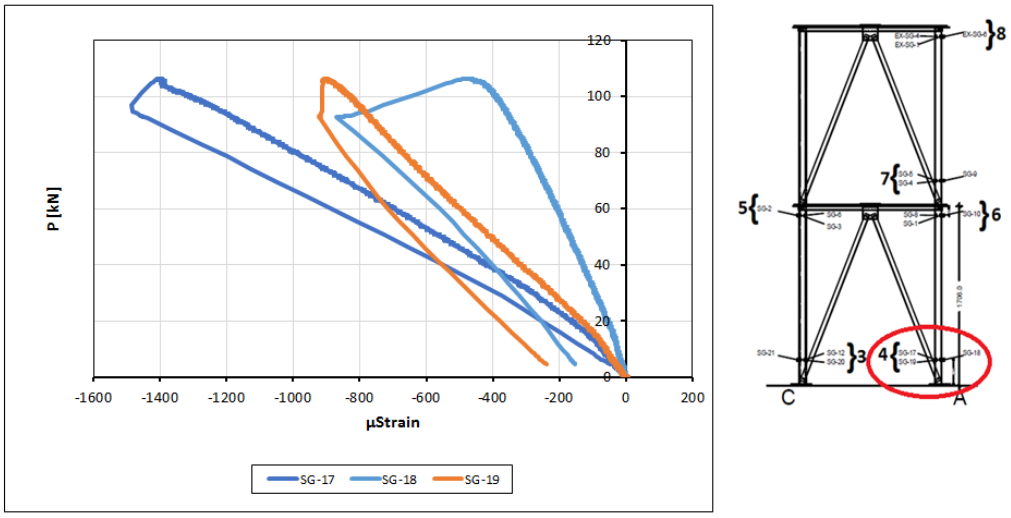

Figure C_O2_7: Strains at cross section 4 Stage 2

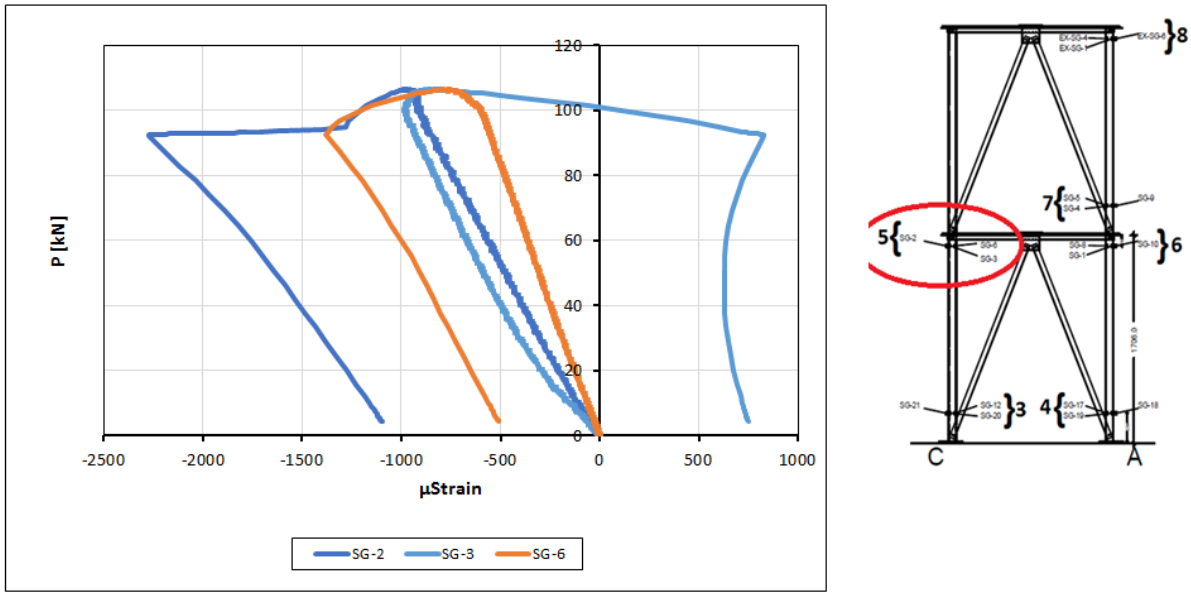

Figure C_O2_8: Strains at cross section 5 Stage 2

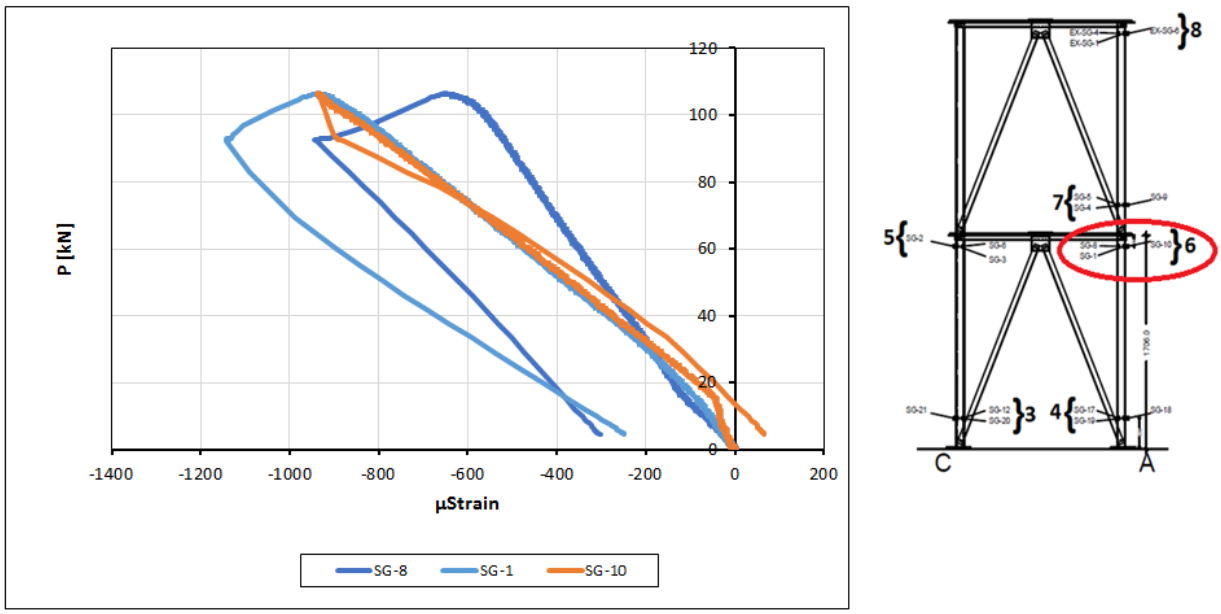

Figure C_O2_9: Strains at cross section 6 Stage 2

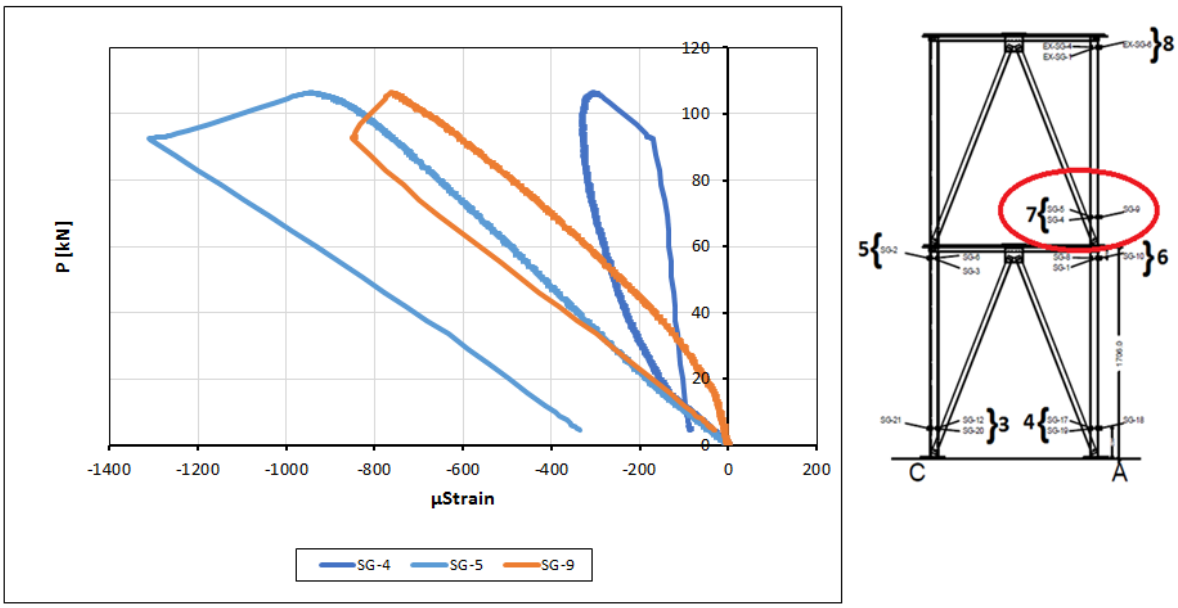

Figure C_O2_10: Strains at cross section 7 Stage 2

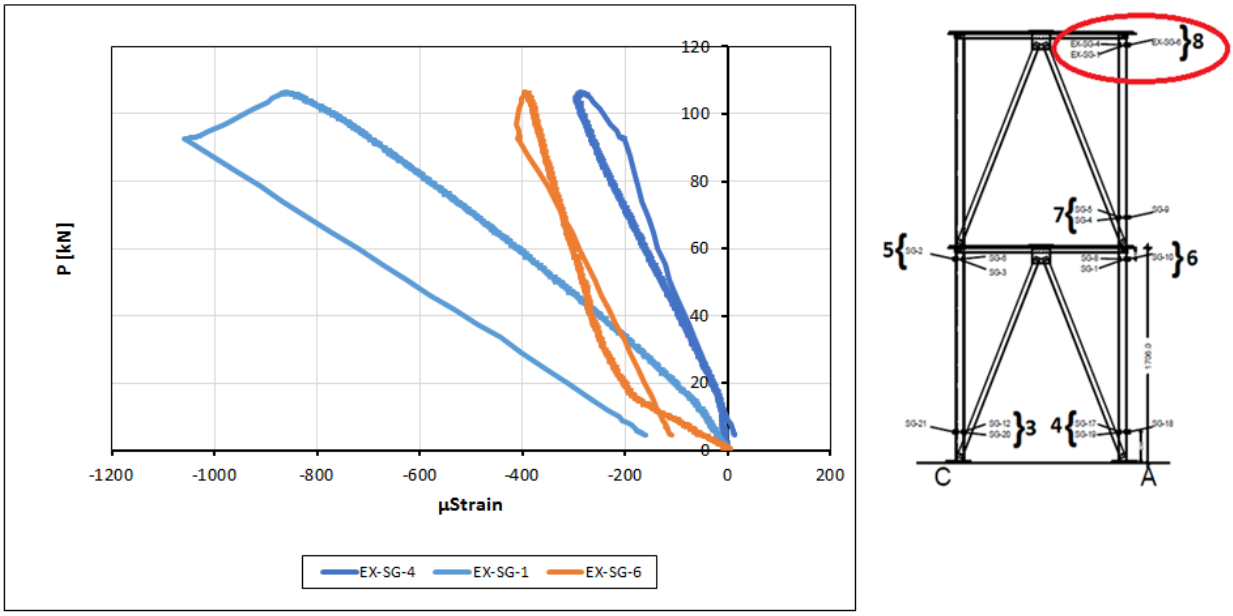

Figure C_O2_11: Strains at cross section 8 Stage 2

TOWER O1S

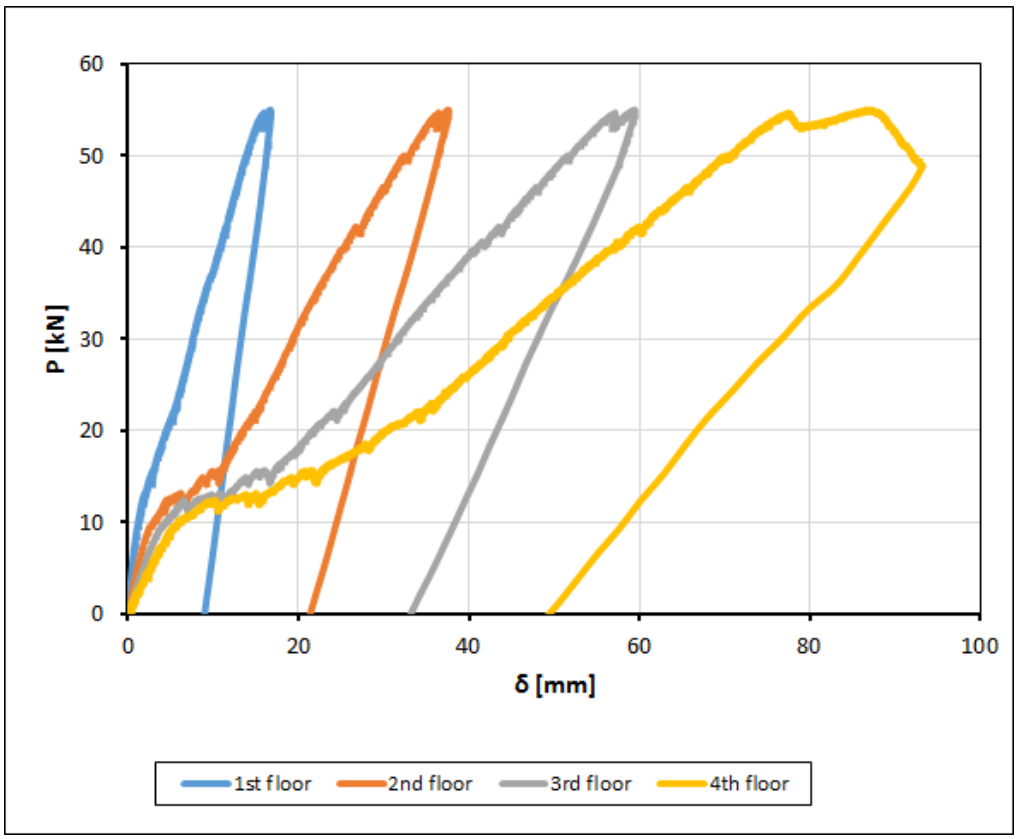

Figure C_O1S_1: Load – top displacement curve

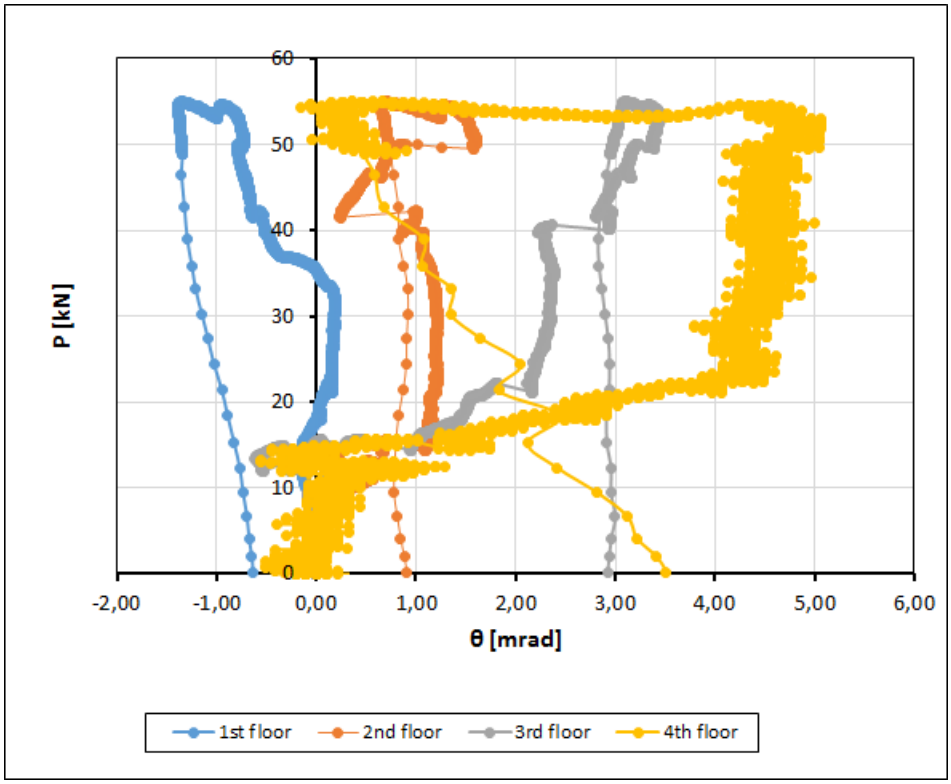

Figure C_O1S_2: Load – rotation curve

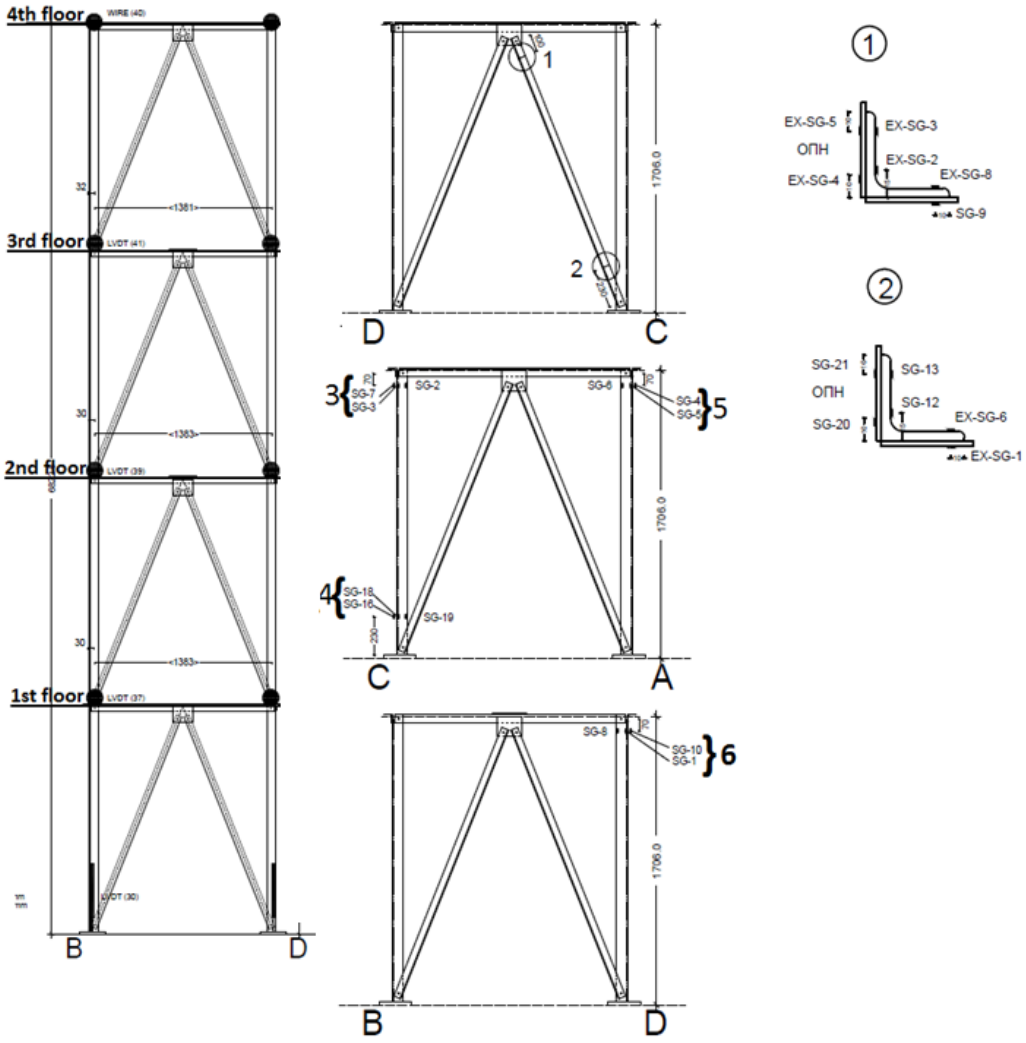

Figure C_O1S_3: Cross sections and strain gage numeration

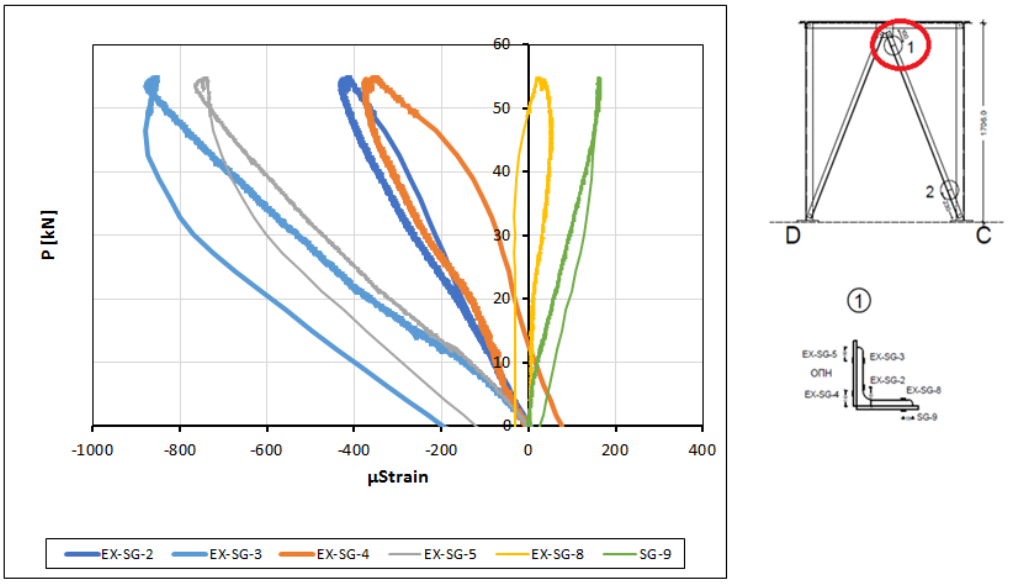

Figure C_O1S_4: Strains at cross section 1

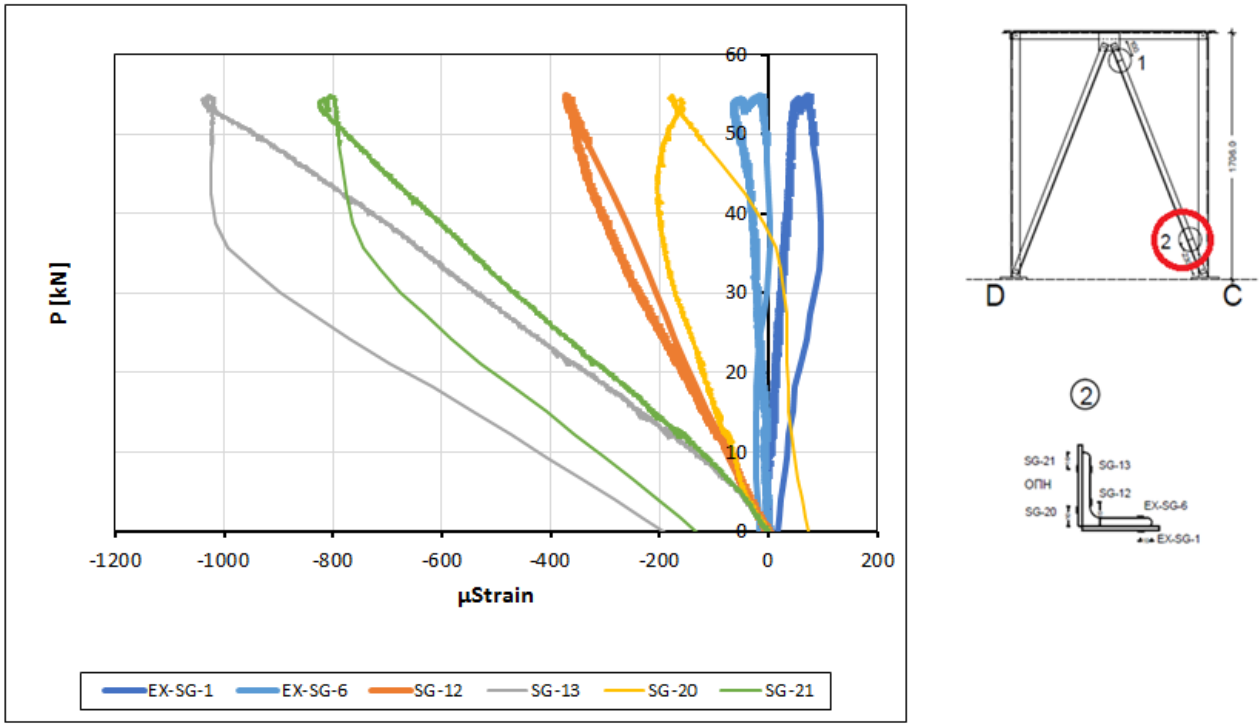

Figure C_O1S_5: Strains at cross section 2

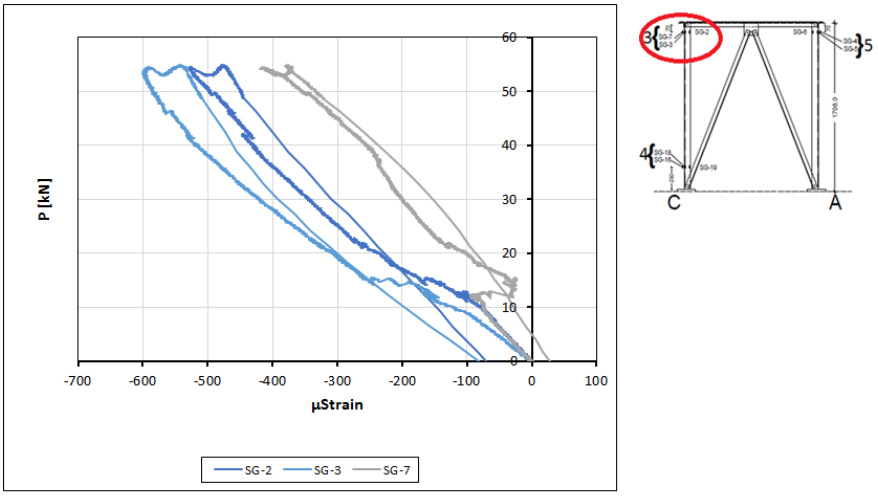

Figure C_O1S_6: Strains at cross section 3

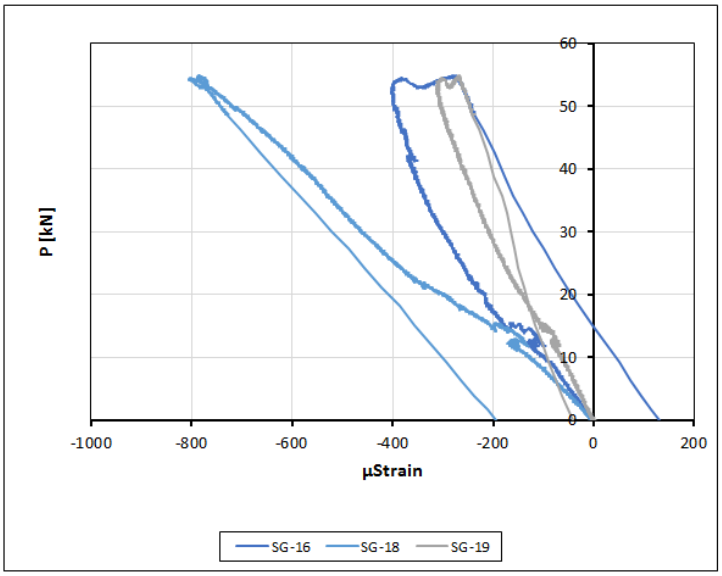

Figure C_O1S_7: Strains at cross section 4

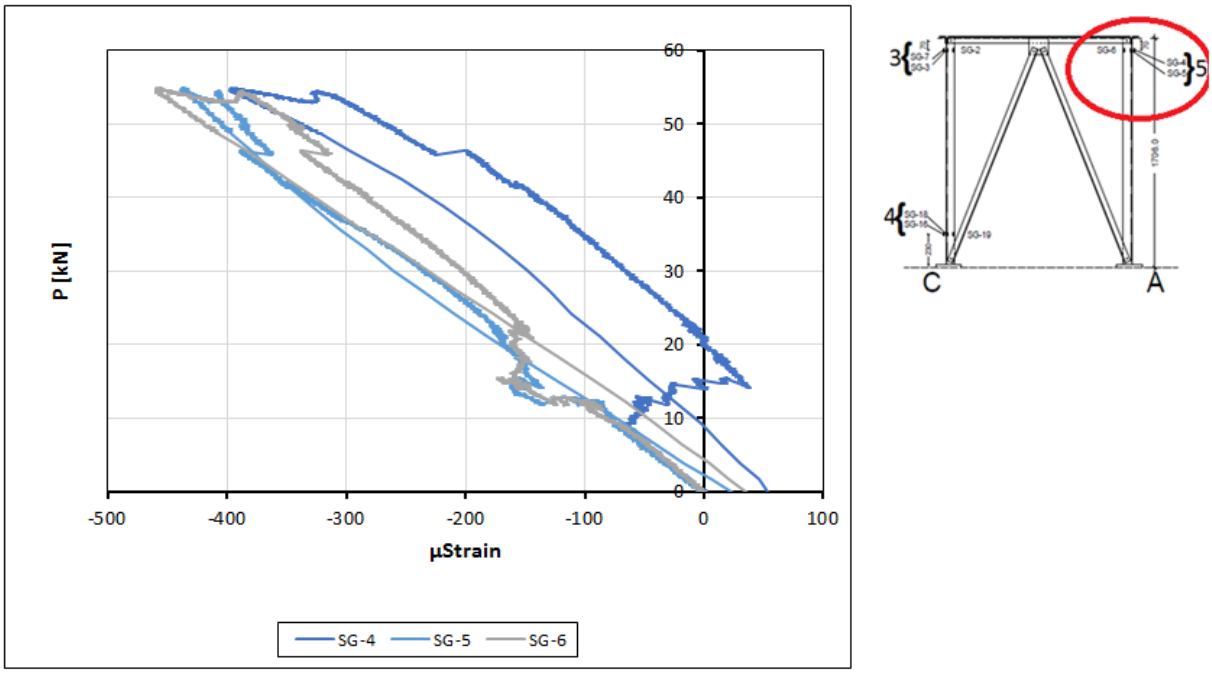

Figure C_O1S_8: Strains at cross section 5

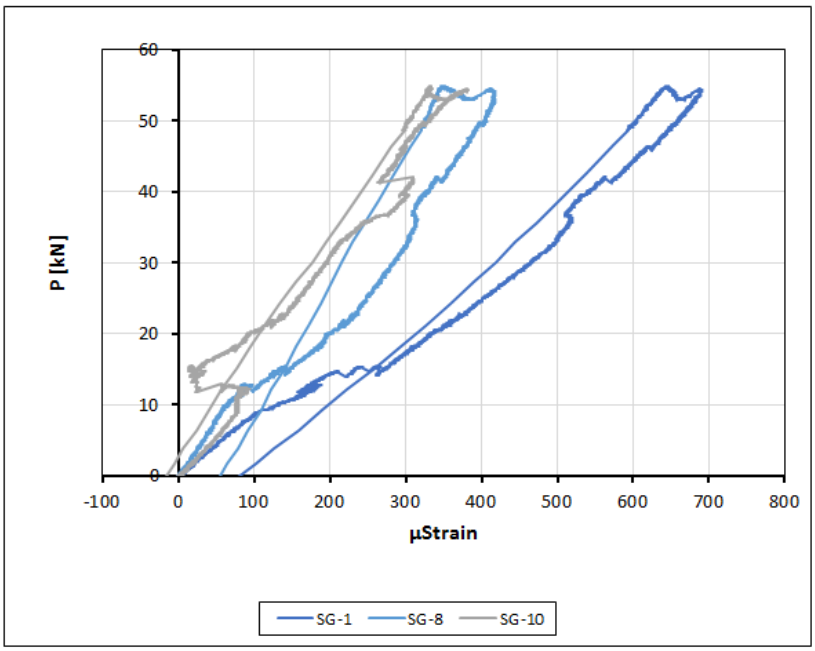

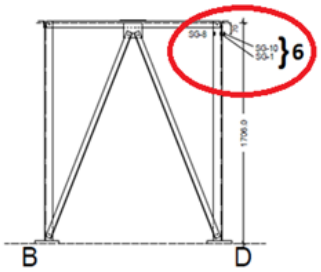

Figure C_O1S_9: Strains at cross section 6

TOWER D1

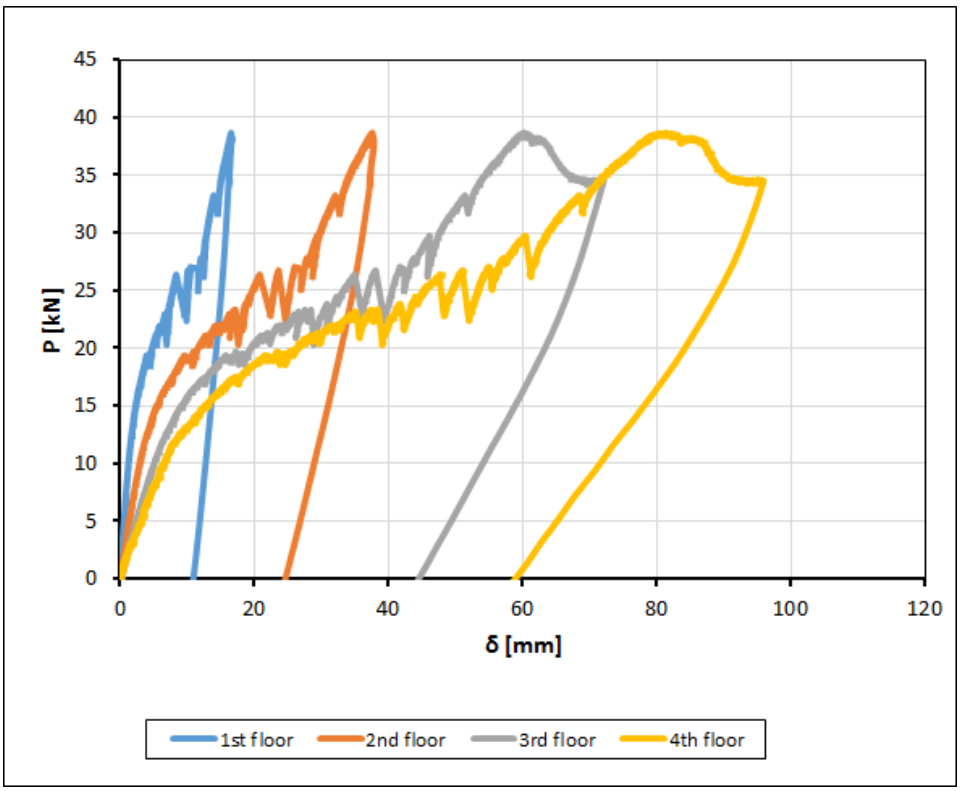

Figure C_D1_1: Load – top displacement curve

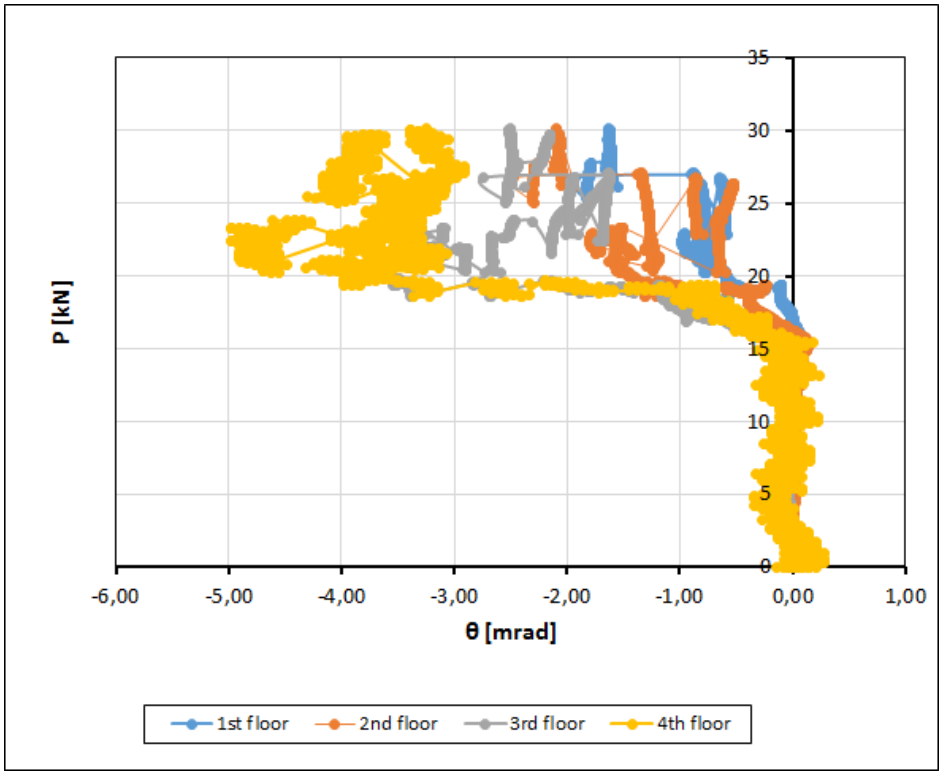

Figure C_D1_2: Load – rotation curve

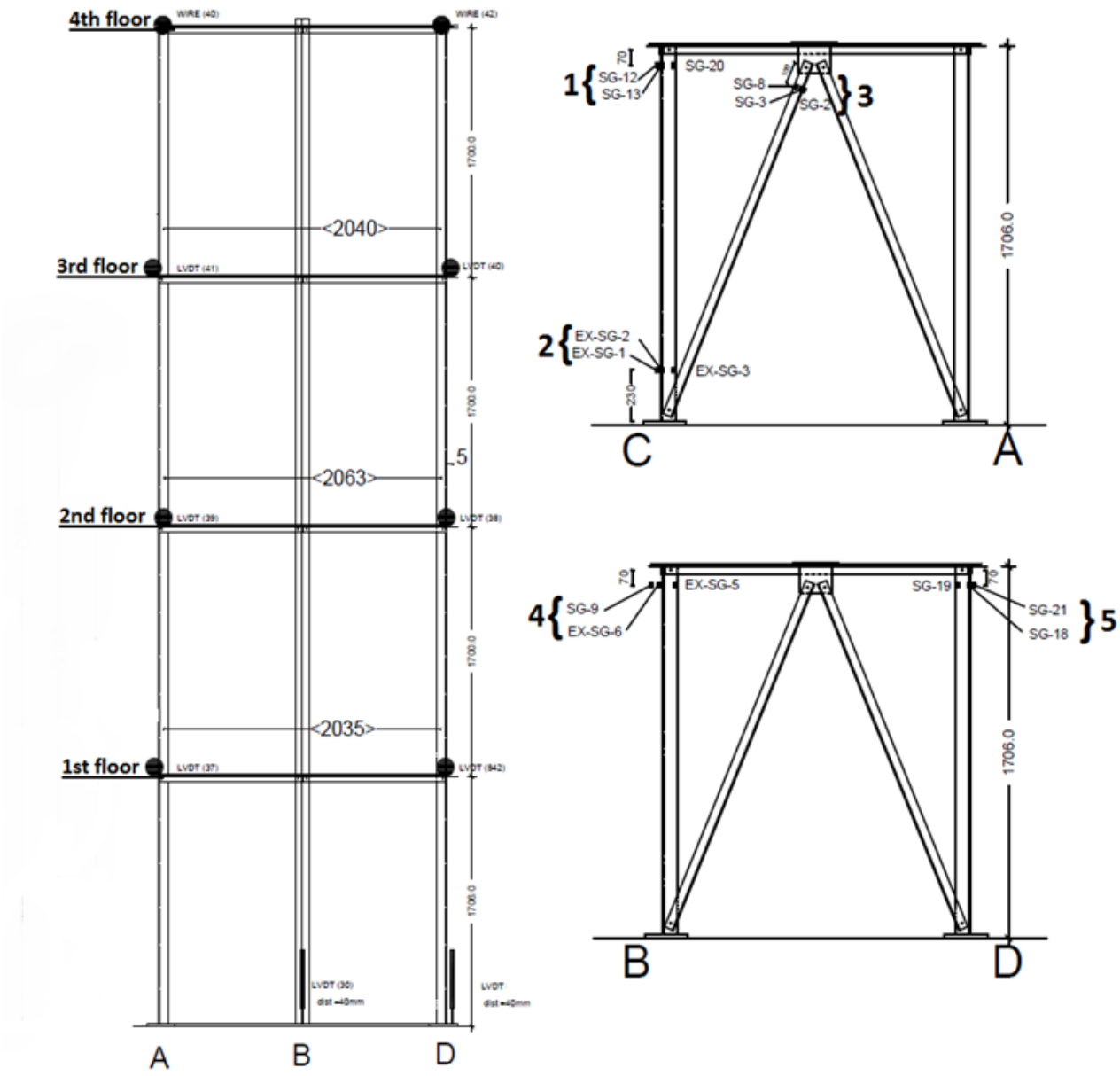

Figure C_D1_3: Cross sections and strain gage numeration

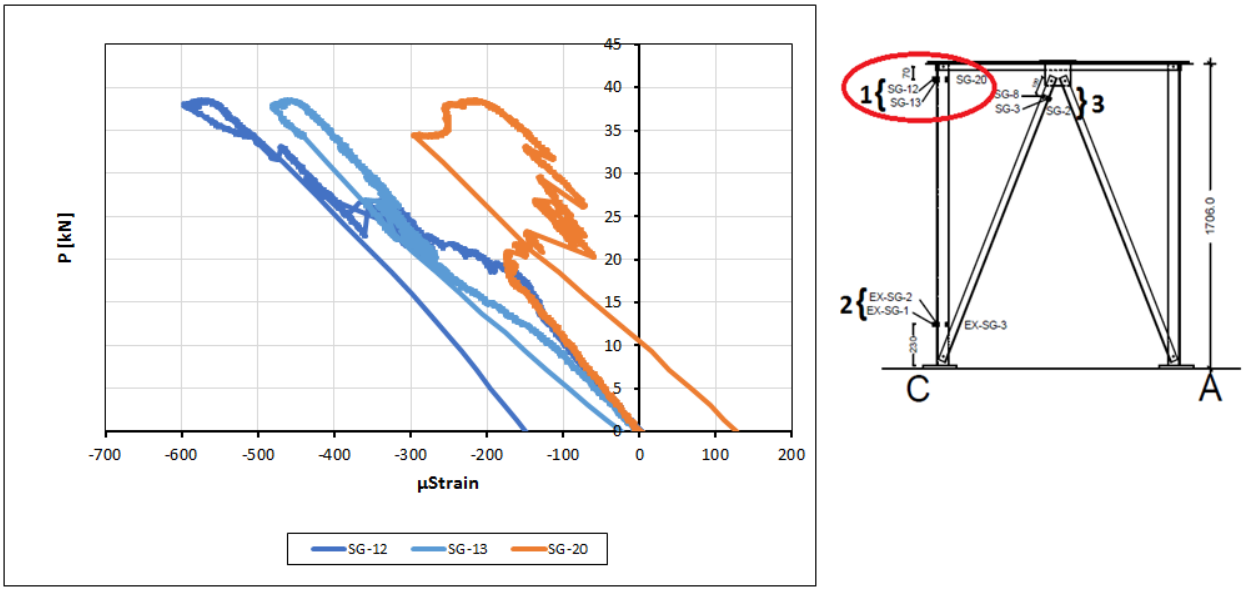

Figure C_D1_4: Strains at cross section 1

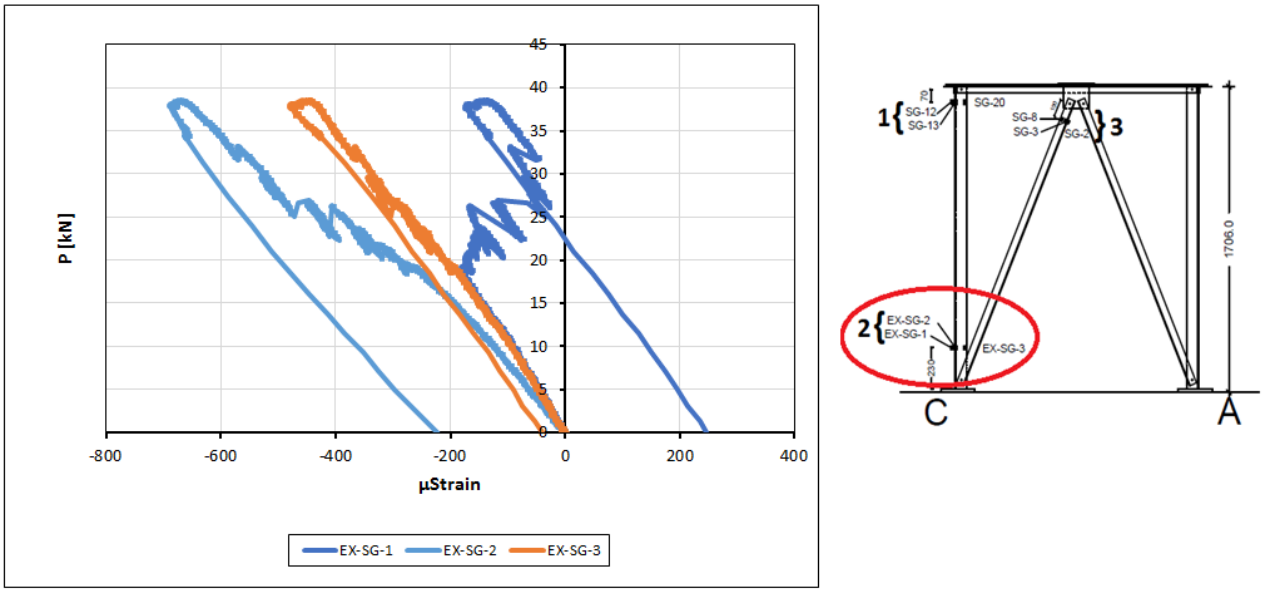

Figure C_D1_5: Strains at cross section 2

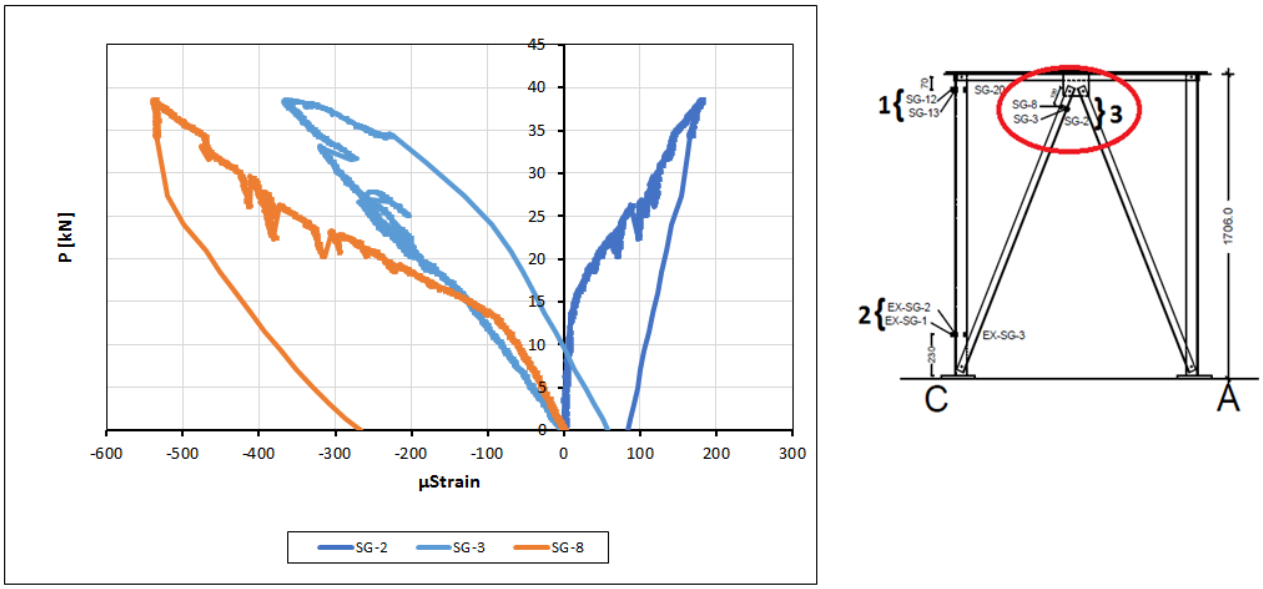

Figure C_D1_6: Strains at cross section 3

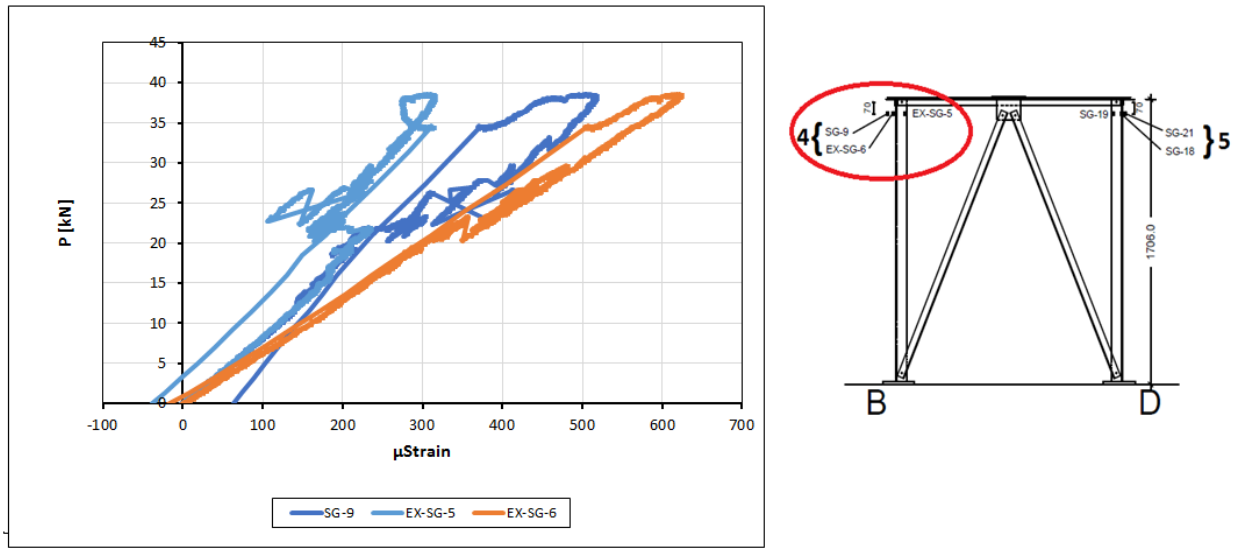

Figure C_D1_7: Strains at cross section 4

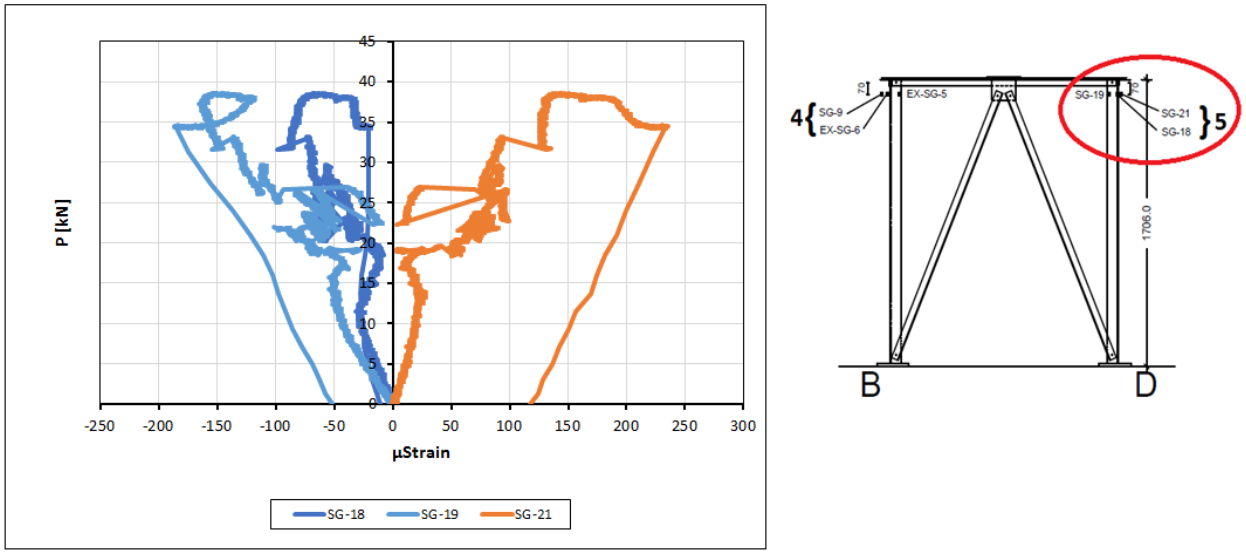

Figure C_D1_8: Strains at cross section 5

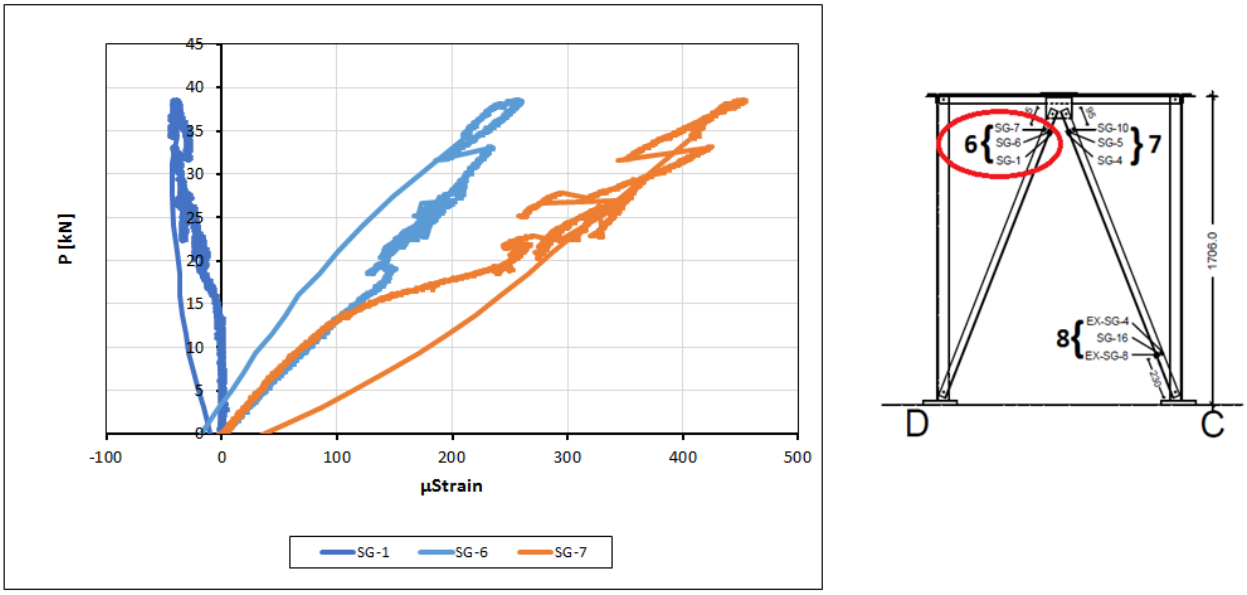

Figure C_D1_9: Strains at cross section 6

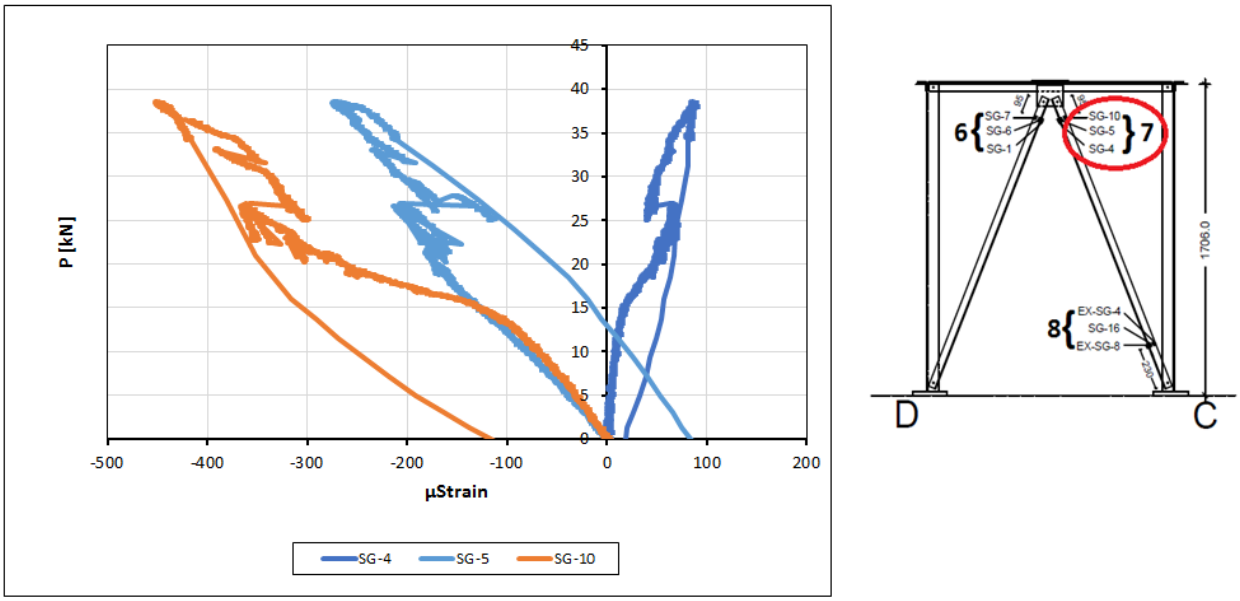

Figure C_D1_10: Strains at cross section 7

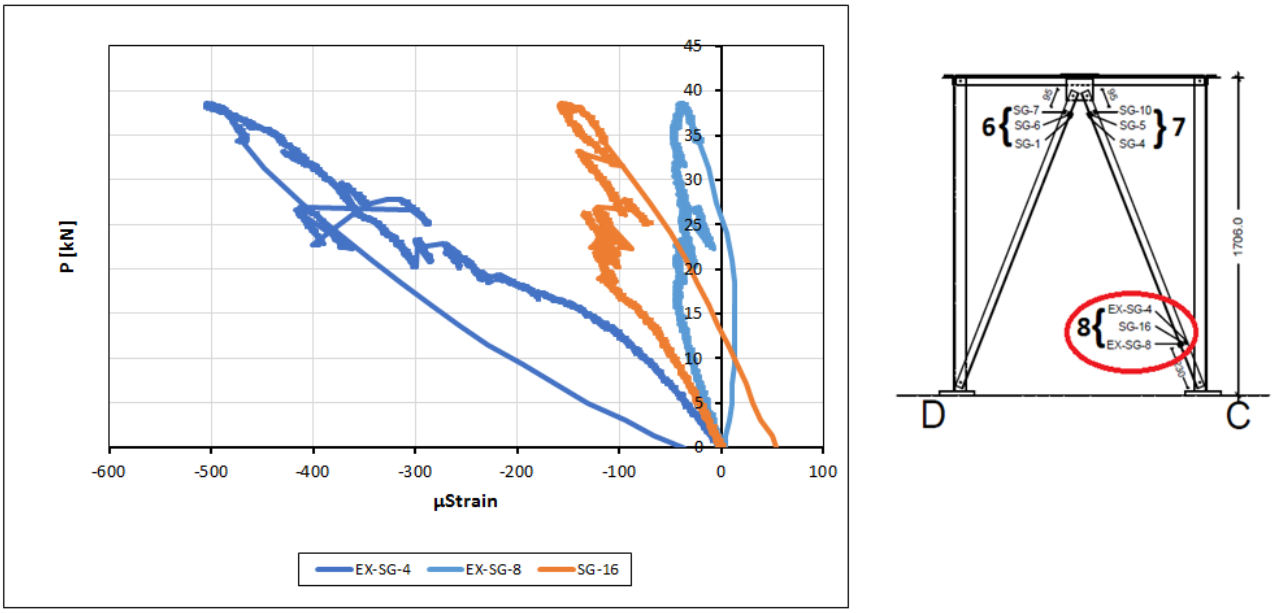

Figure C_D1_11: Strains at cross section 8

TOWER D2

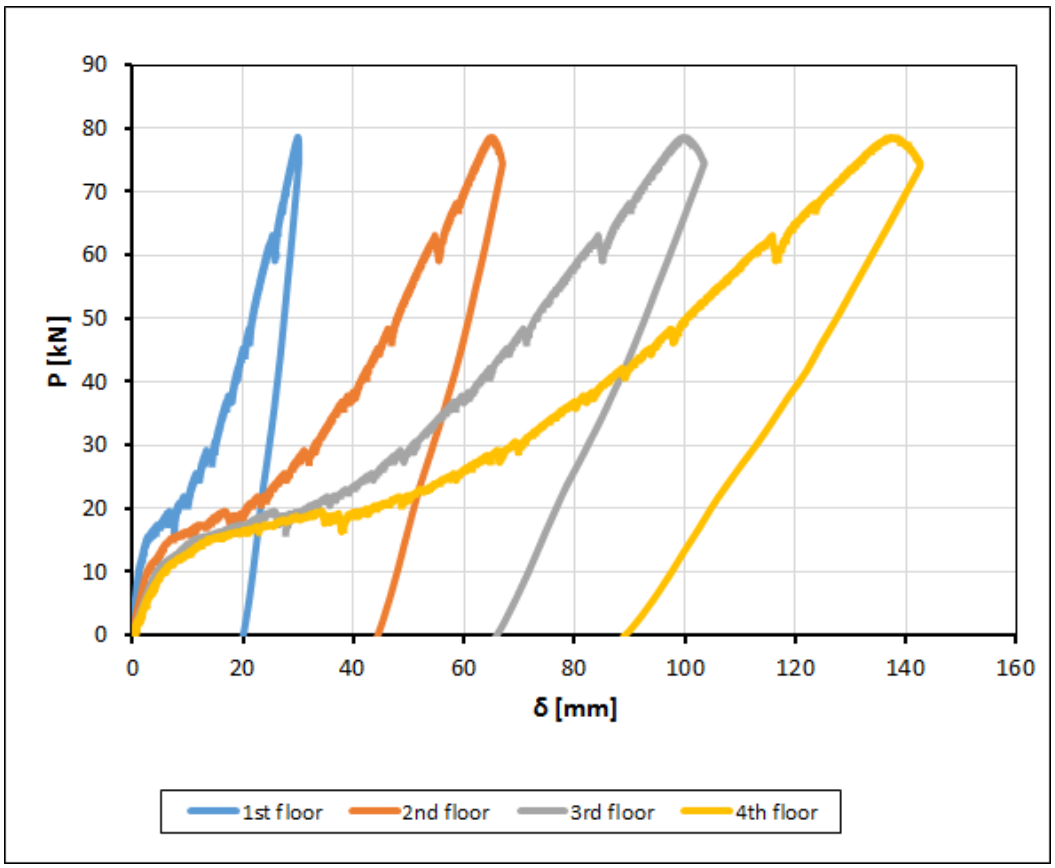

Figure C_D2_1: Load – top displacement curves

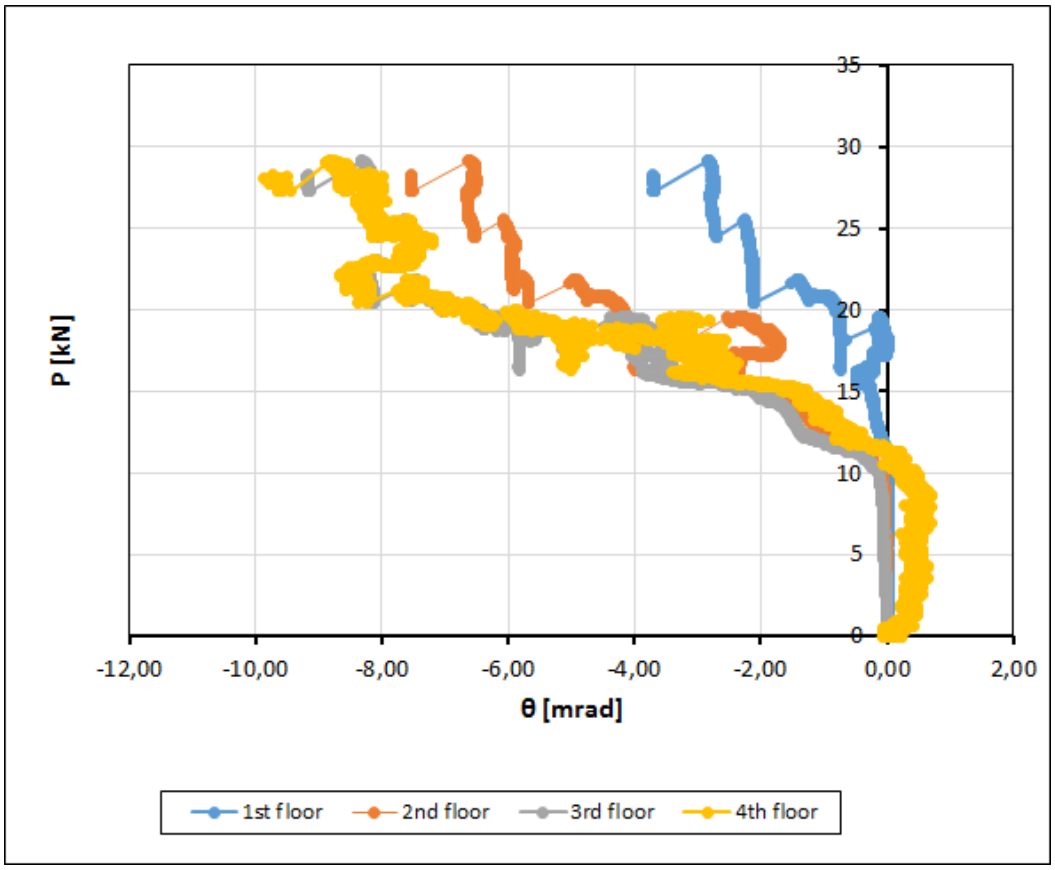

Figure C_D2_2: Load – rotation curves

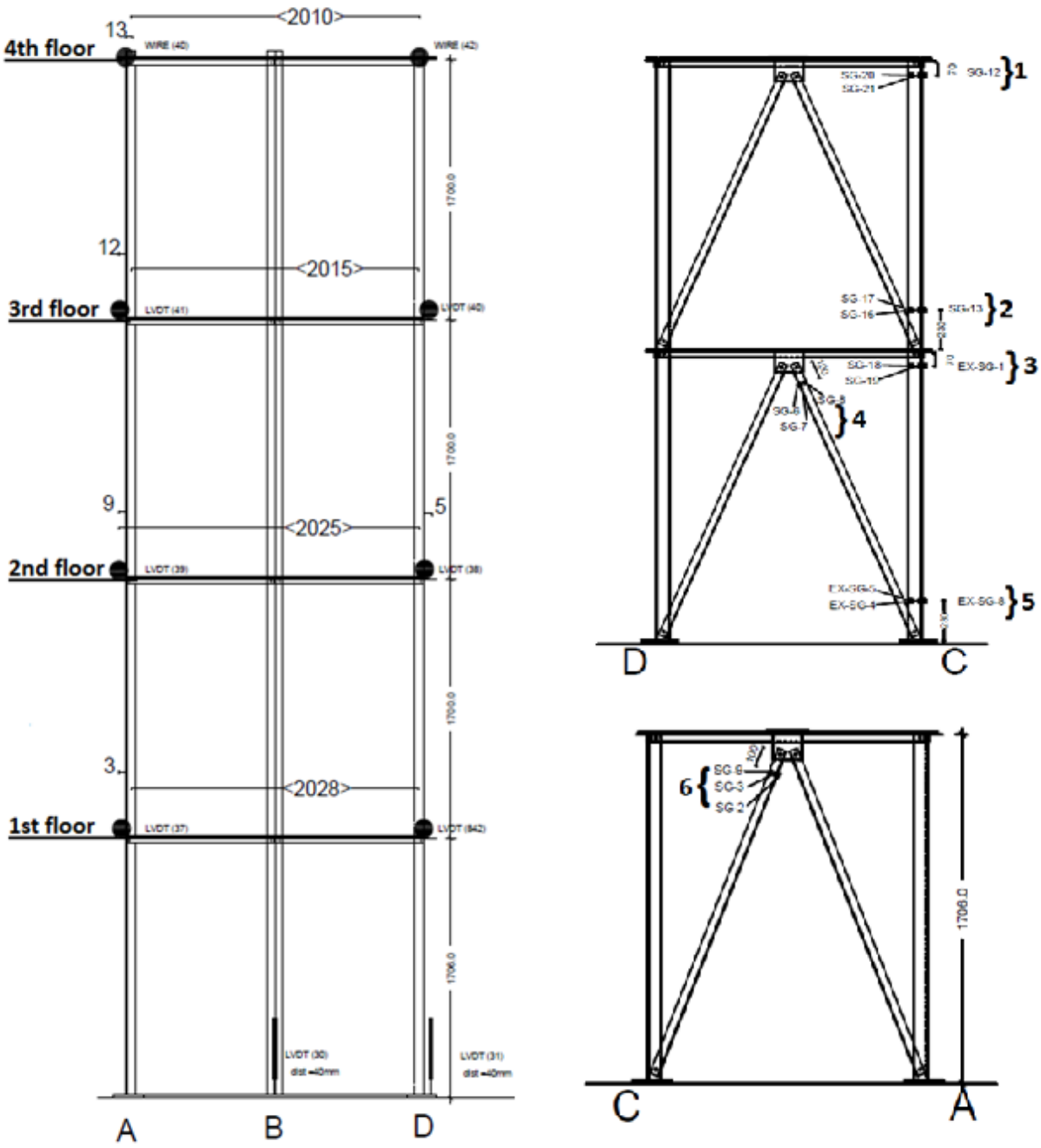

Figure C_D2_3: Cross sections and strain gage numeration

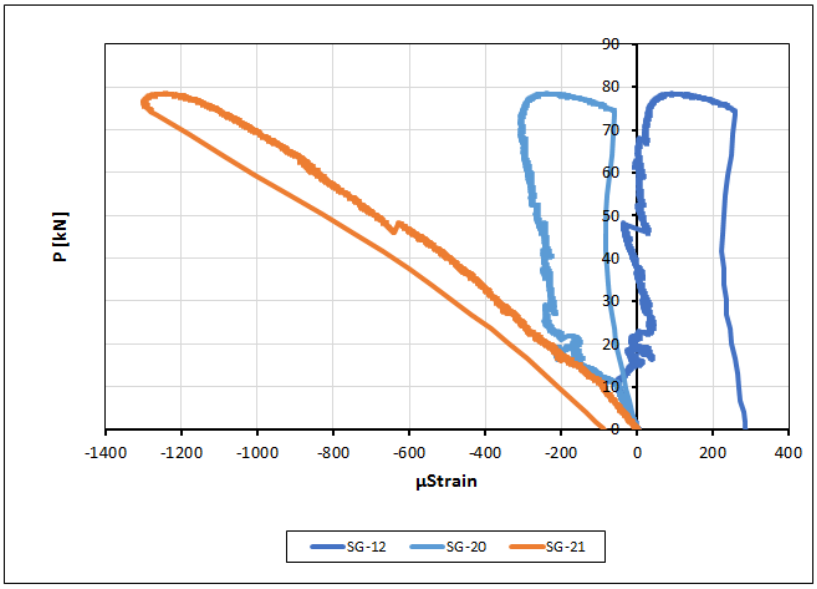

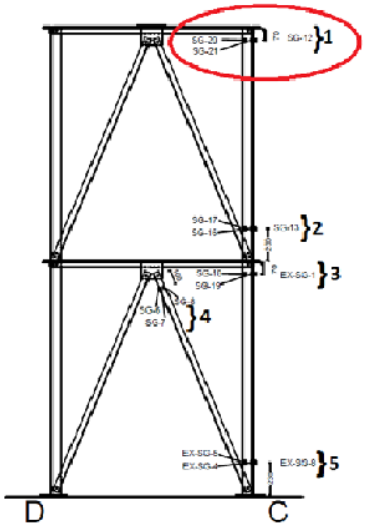

Figure C_D2_4: Strains at cross section 1

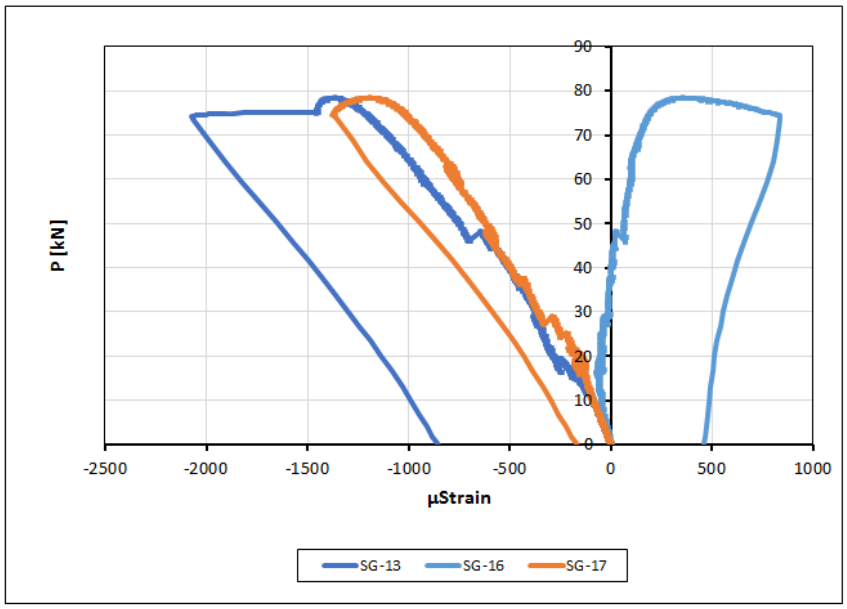

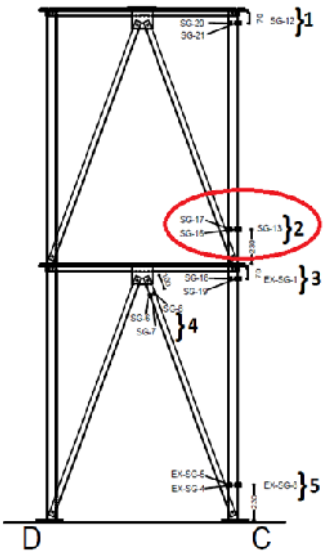

Figure C_D2_5: Strains at cross section 2

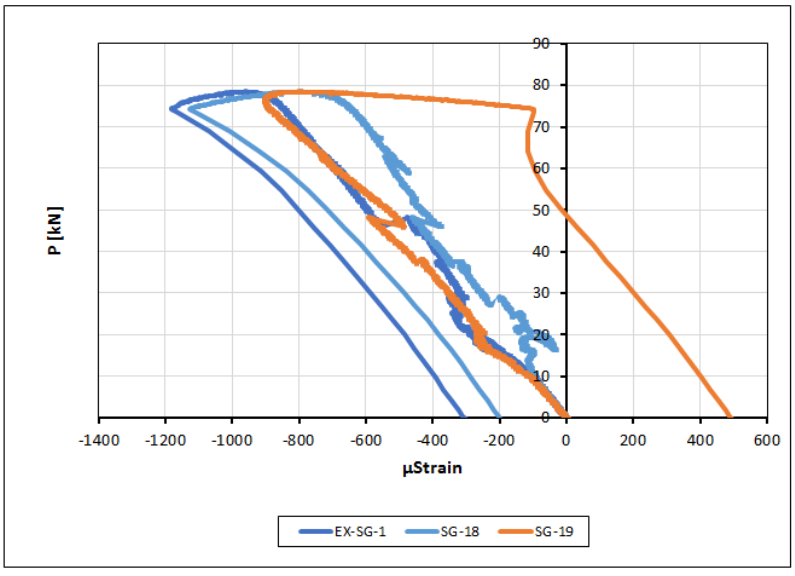

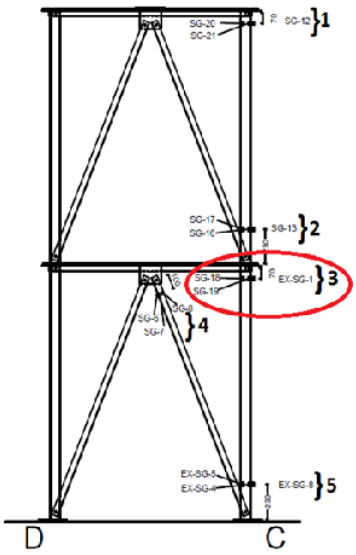

Figure C_D2_6: Strains at cross section 3

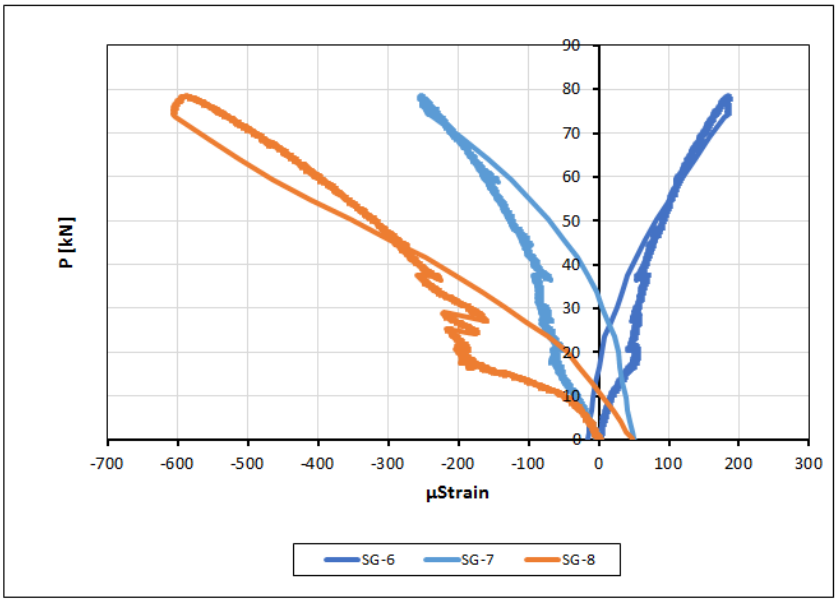

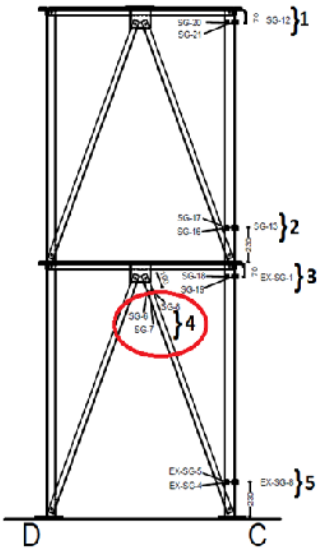

Figure C_D2_7: Strains at cross section 4

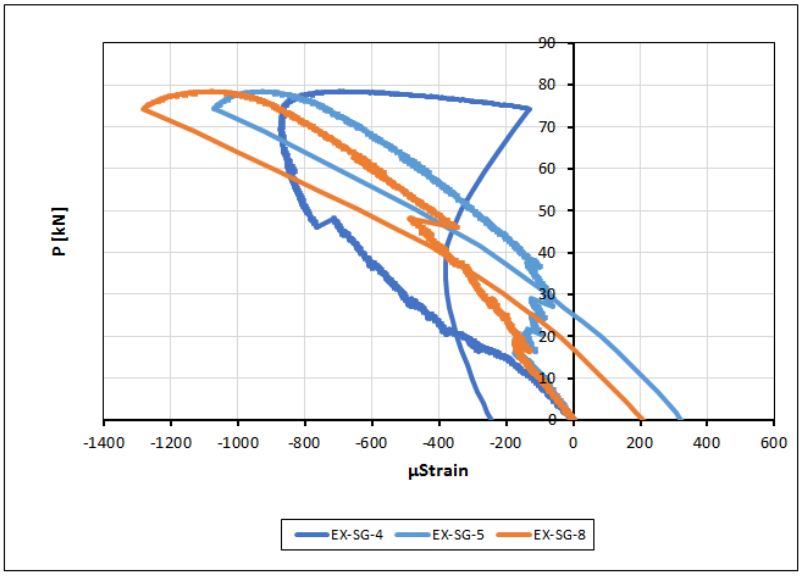

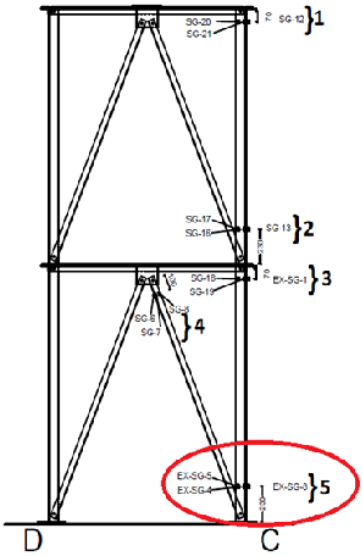

Figure C_D2_8: Strains at cross section 5

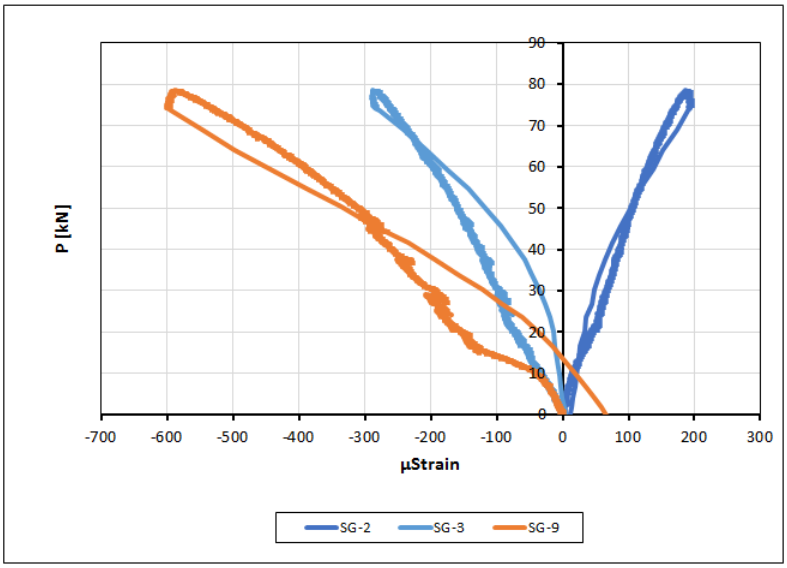

Figure C_D2_9: Strains at cross section 6

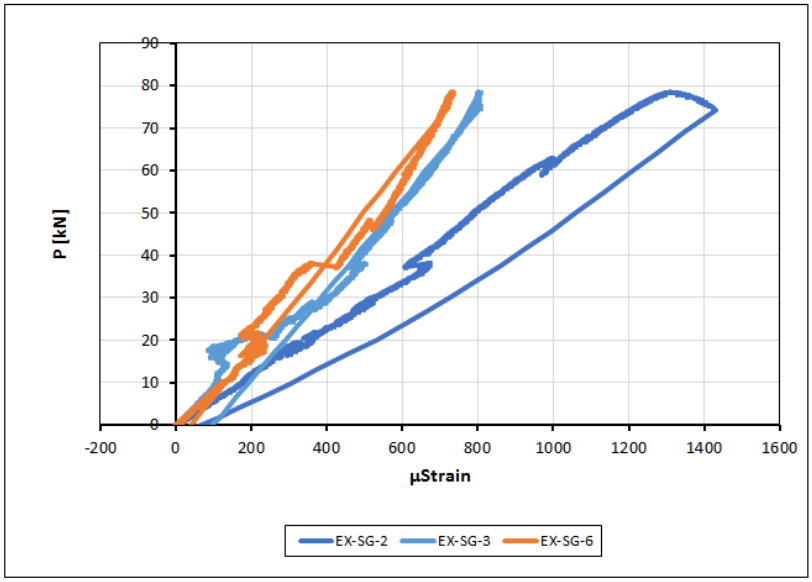

Figure C_D2_10: Strains at cross section 7

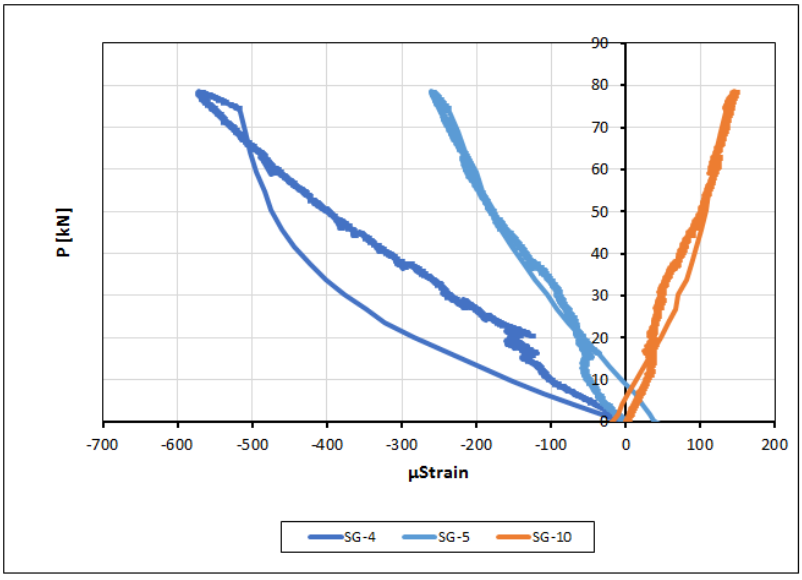

Figure C_D2_11: Strains at cross section 8

TOWER D2S

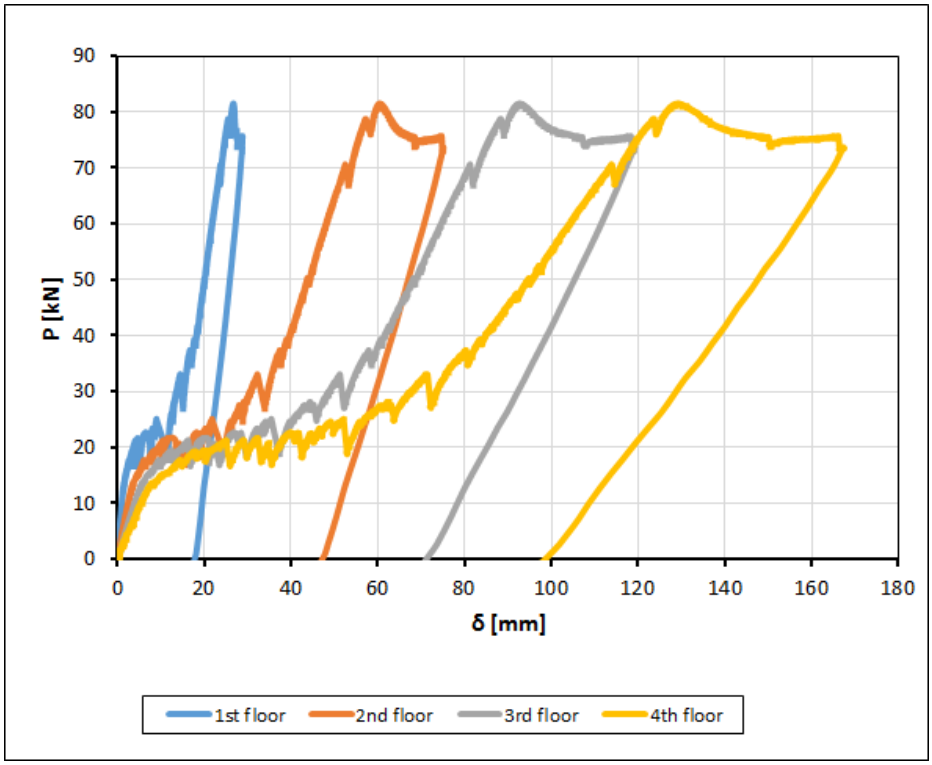

Figure C_D2_1: Load – top displacement curves

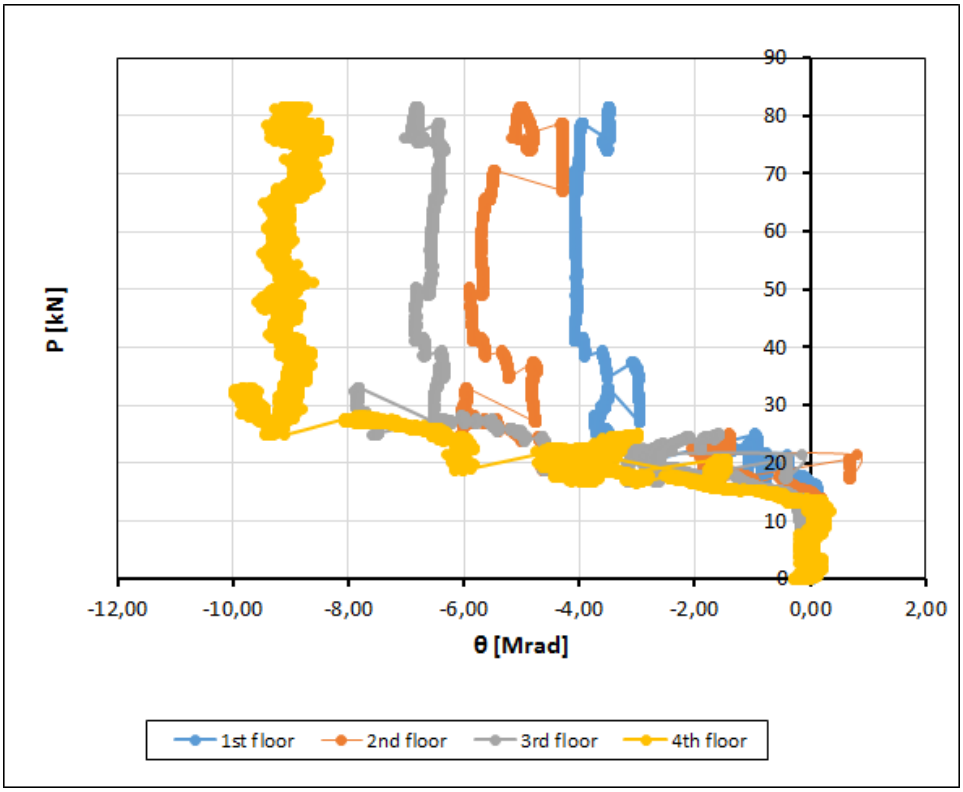

Figure C_D2S_2: Load – rotation curves

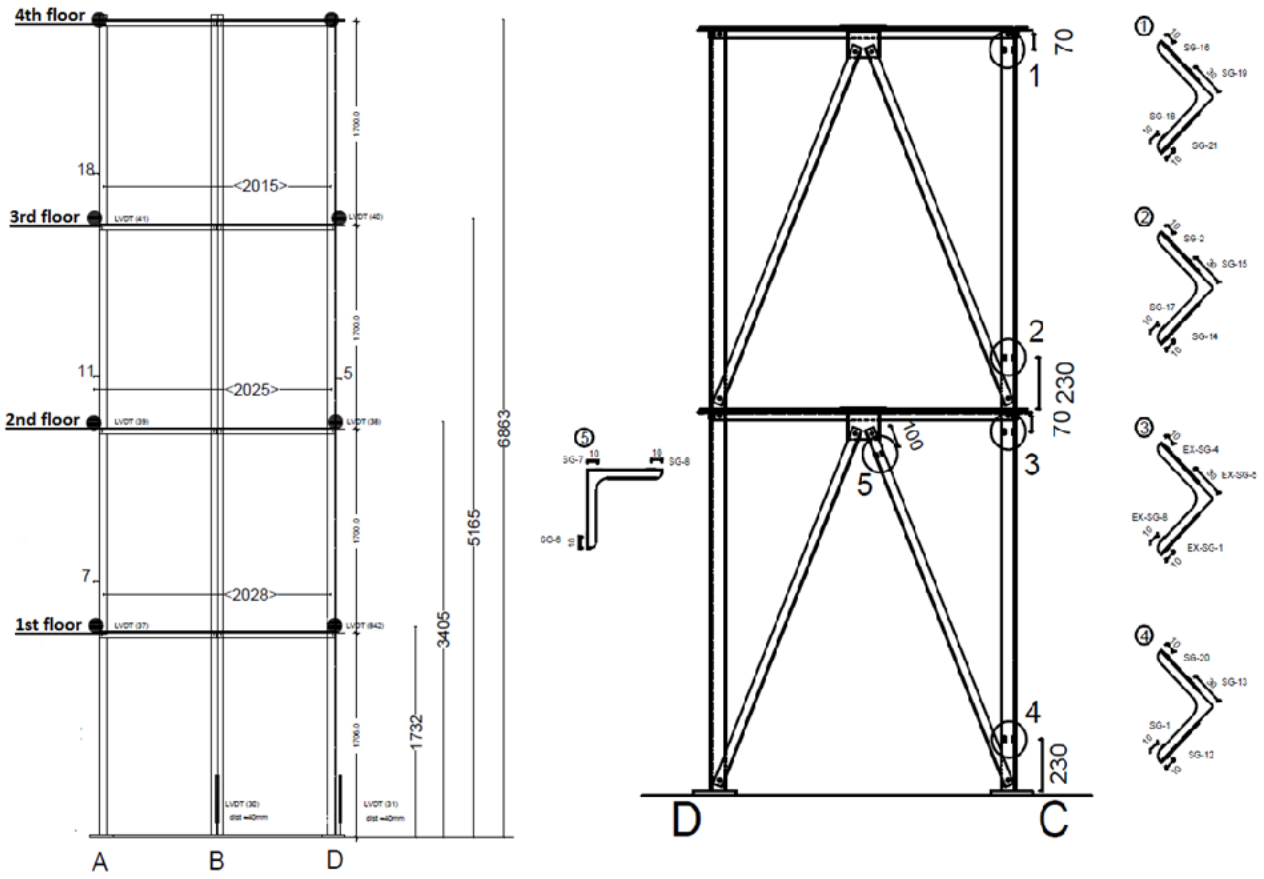

Figure C_D2S_3: Cross sections and strain gage numeration

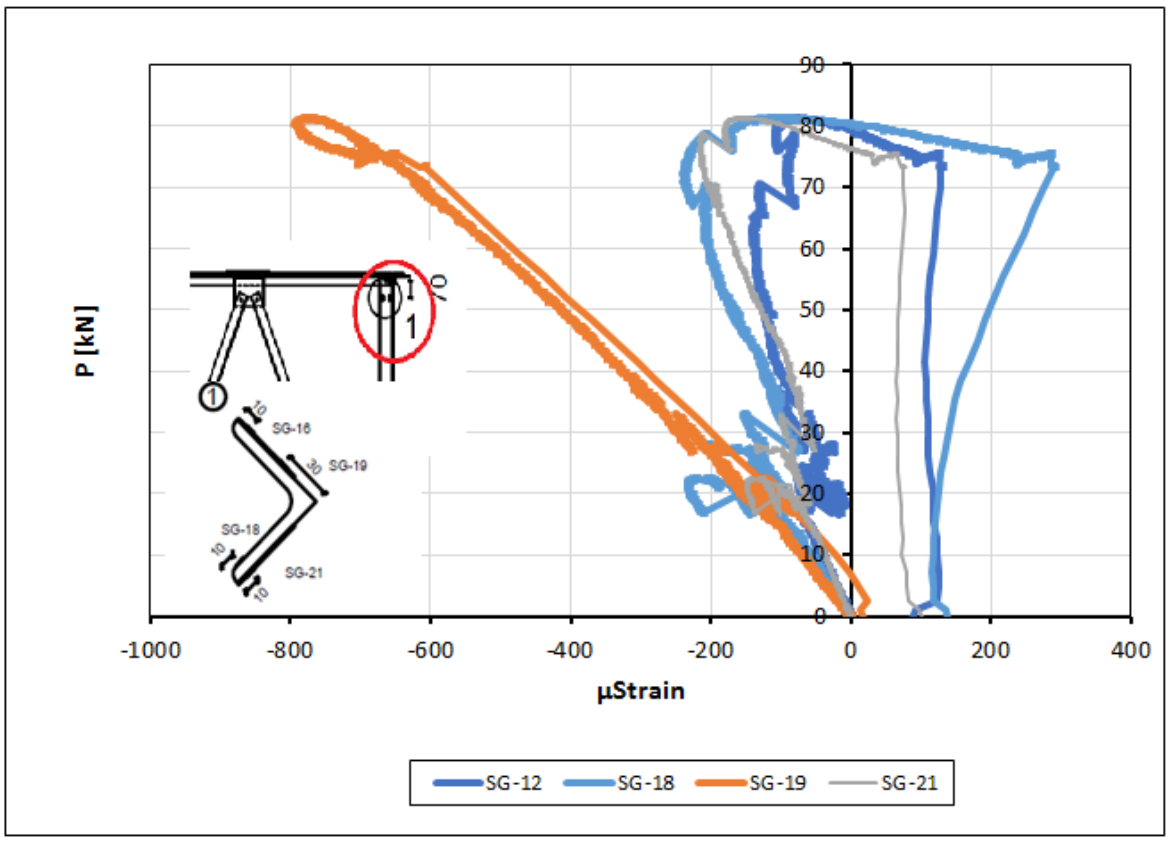

Figure C_D2S_4: Strains at cross section 1

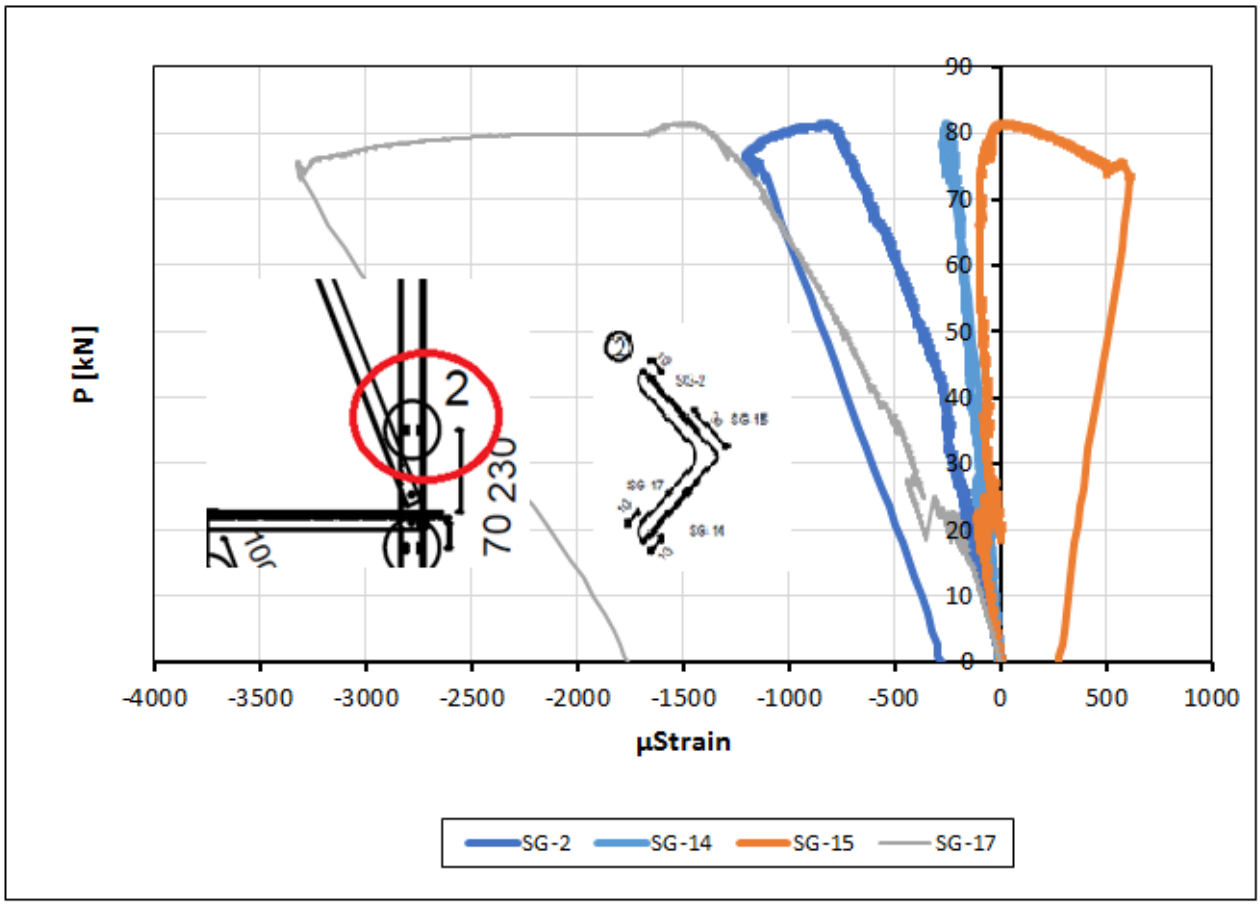

Figure C_D2S_4: Strains at cross section 2

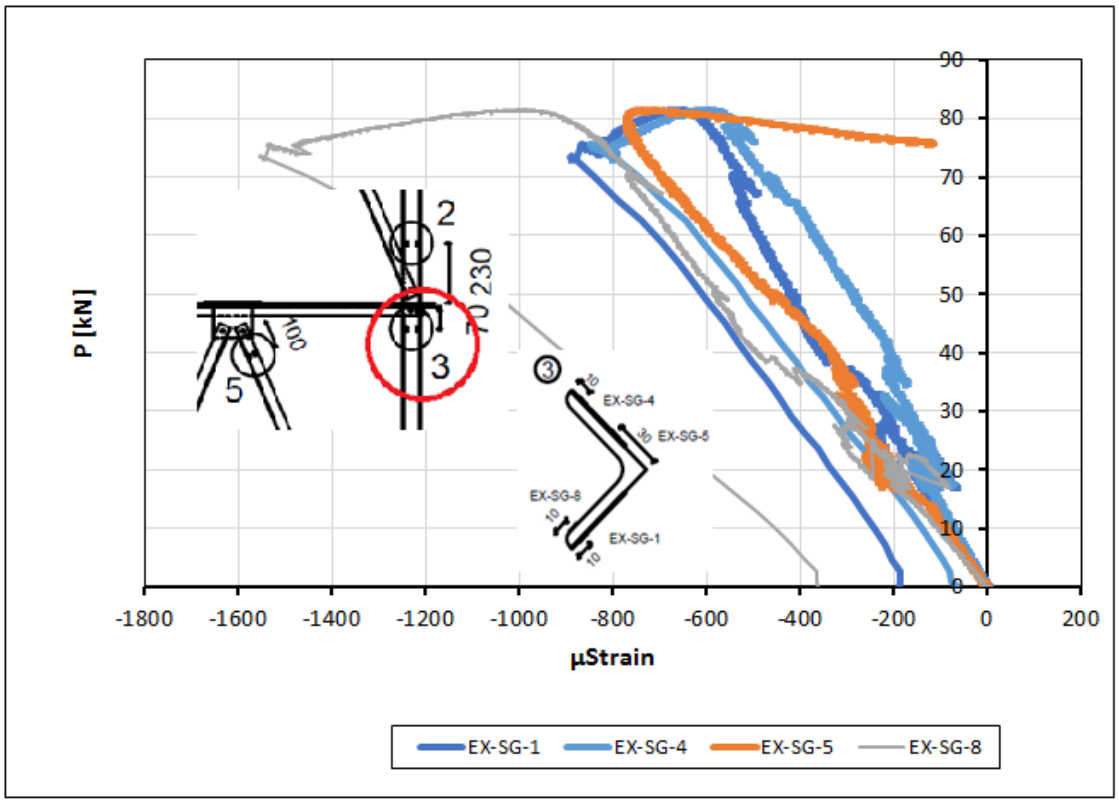

Figure C_D2S_5: Strains at cross section 3

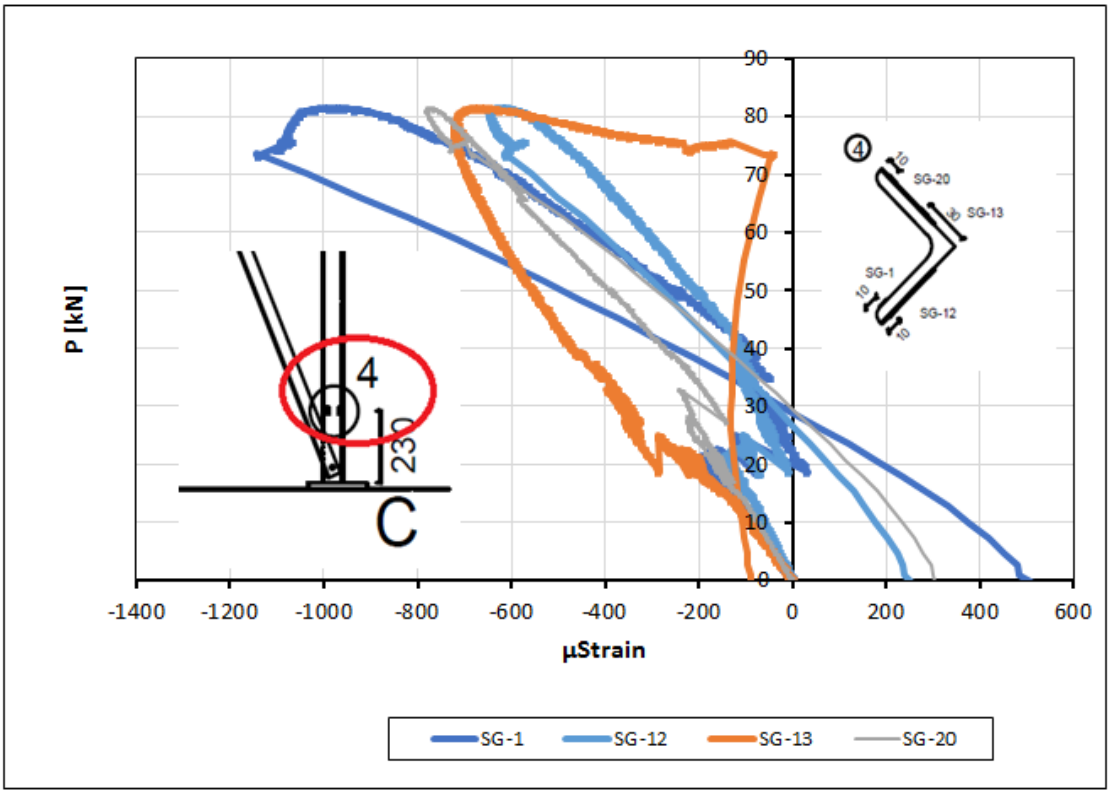

Figure C_D2S_6: Strains at cross section 4

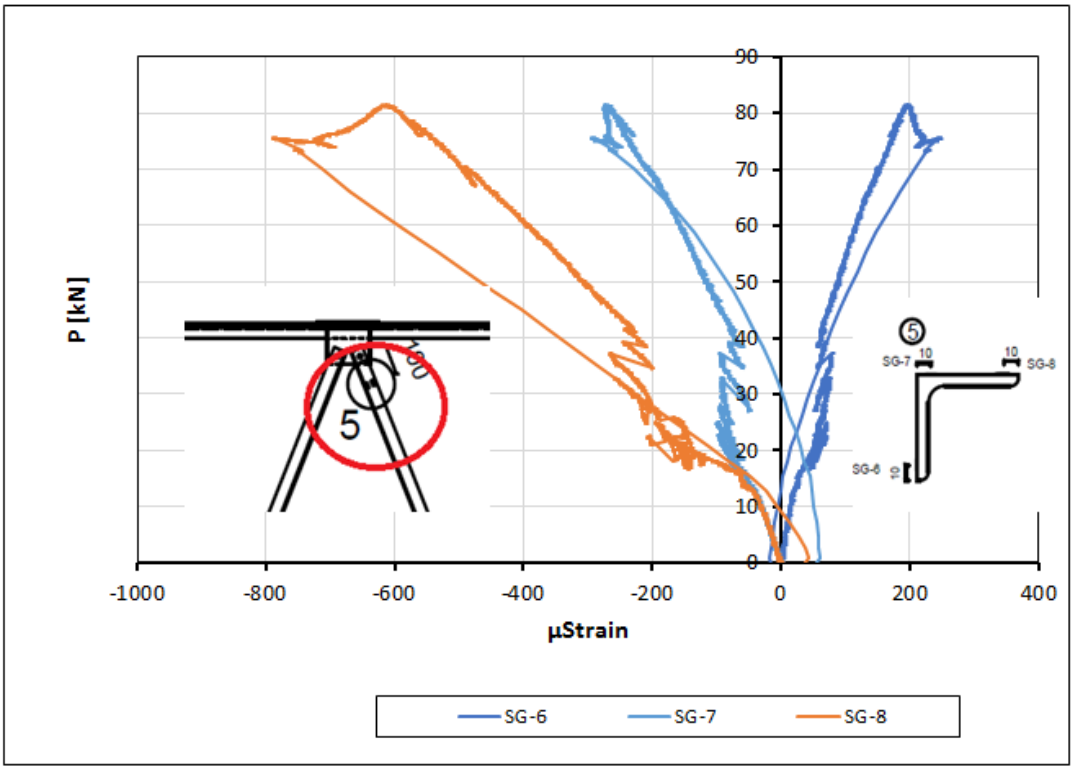

Figure C_D2S_7: Strains at cross section 5

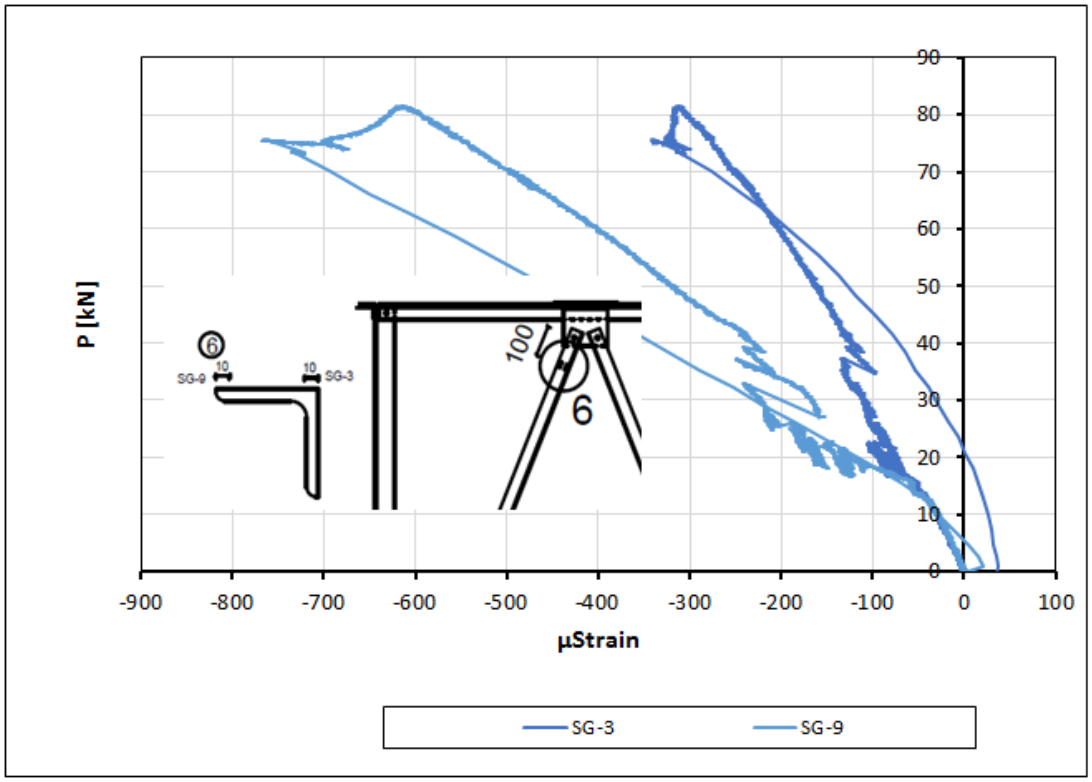

Figure C_D2S_8: Strains at cross section 6

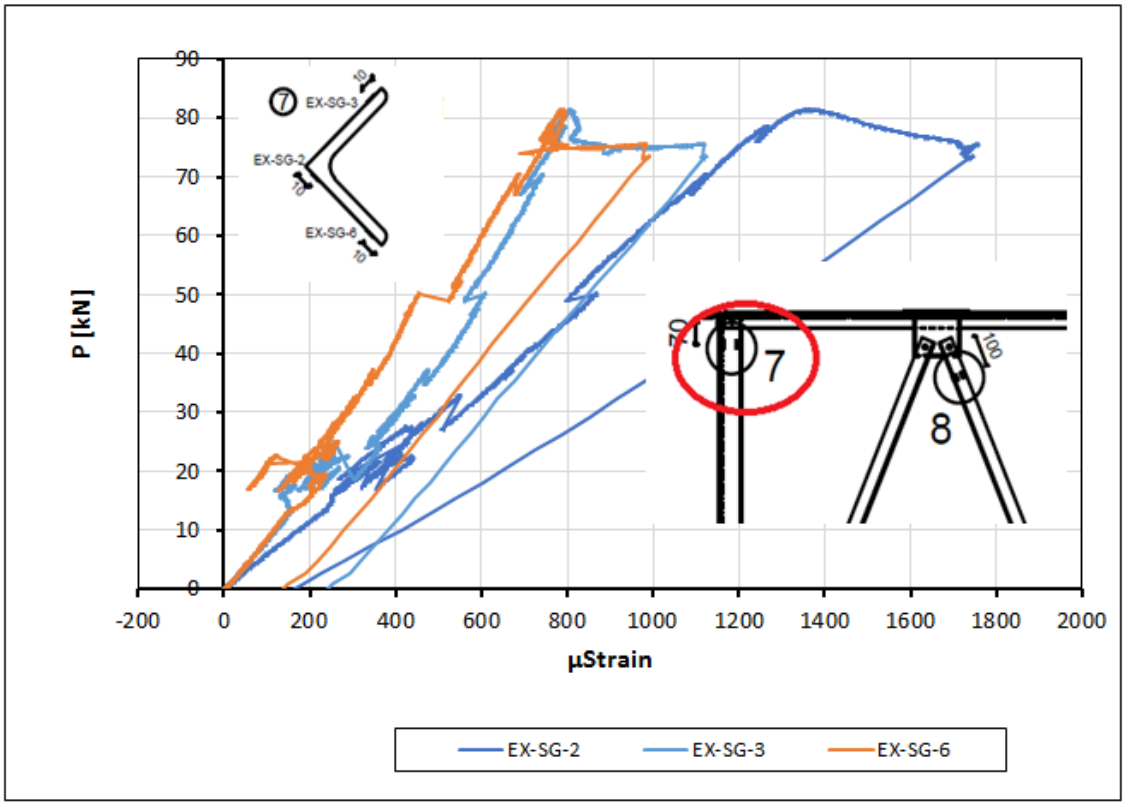

Figure C_D2S_9: Strains at cross section 7

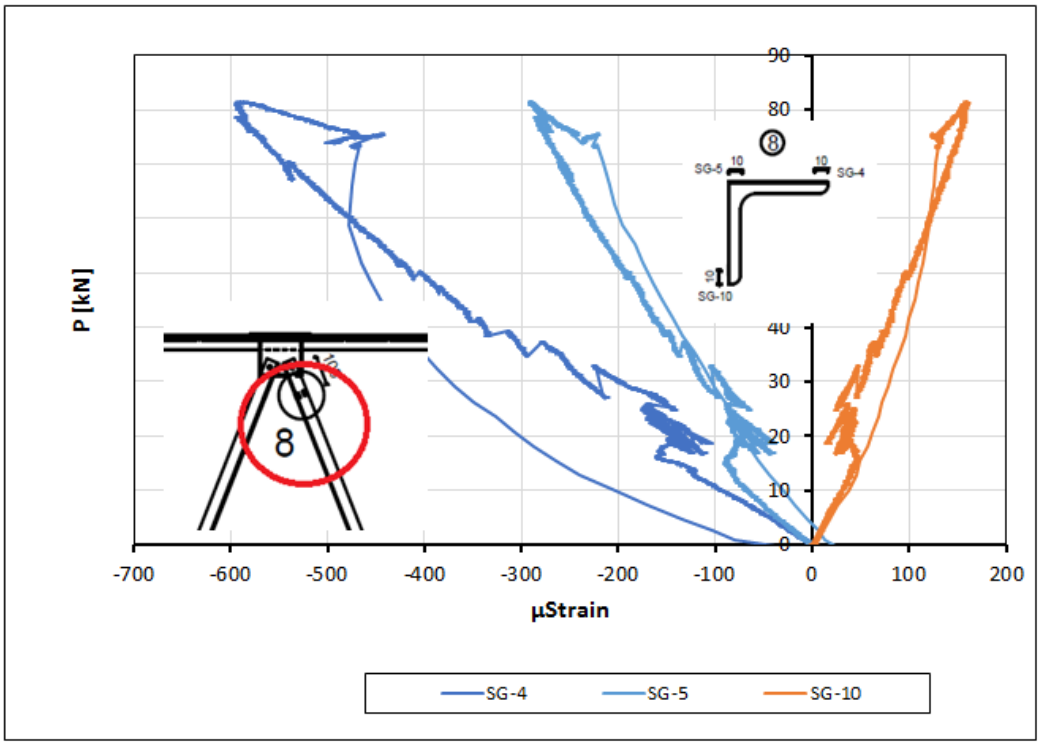

Figure C_D2S_10: Strains at cross section 8